TÉCNICO LISBOA

# Technical and Economic Solutions for Grid-Connected Utility-Scale Solar Photovoltaic Power Plants

Optimization of a 24 $MW_p$ Solar Photovoltaic Power Plant

**Miguel Lima Simões da Silva**

Thesis to obtain the Master of Science Degree in

## Energy Engineering and Management

Supervisor: Prof. Rui Manuel Gameiro de Castro

### Examination Committee

Chairperson: Prof. Luís Filipe Moreira Mendes
Supervisor: Prof. Rui Manuel Gameiro de Castro
Member of the Committee: Prof.ª Cristina Inês Camus

**November 2019**

# Technical and Economic Solutions for Grid-Connected Utility-Scale Solar Photovoltaic Power Plants

Optimization of a 24 $MW_p$ Solar Photovoltaic Power Plant

**Miguel Lima Simões da Silva**

Thesis to obtain the Master of Science Degree in

**Energy Engineering and Management**

Supervisor: Prof. Rui Manuel Gameiro de Castro

**Examination Committee**

Chairperson: Prof. Luís Filipe Moreira Mendes
Supervisor: Prof. Rui Manuel Gameiro de Castro
Member of the Committee: Prof.ª Cristina Inês Camus

**November 2019**

*Dedicated to my grandfather who will always be in our hearts.*

# Acknowledgments

I would first like to thank my supervisor *Prof.* Rui Castro for all the support and availability throughout the development of my thesis. He consistently allowed me to create and follow my own path, but guided me in the right direction whenever he thought I needed it. He made it possible to have regular productive meetings, in which interesting topics were always discussed.

I want to thank Sotécnica for having provided me with crucial data without which I would not have been able to achieve some results. I would also like to acknowledge my industry supervisor *Eng.* Mário Batalha (Engineer at Sotécnica) for having proposed this interesting topic in collaboration with Sotécnica, which allowed me to deepen my knowledge in this field of studies. Additionally, he provided me the contact of *Eng.* Daniele Confente (Engineer at Huawei), whose support was also fundamental to further improve my knowledge regarding string inverters' technical matters.

Last but not least, I want to deeply thank my family for having accompanied me throughout all my journeys. I must utter my gratitude to my parents for always providing me with tireless support and continuous encouragement throughout every stage of my development and for giving me the means to have a successful future. I want to thank my brother for all the unceasing support and, above all, for the example of excellence that I always want to follow. To my grandmother and my grandfather, to whom this work is dedicated to, I want to express my profound gratitude for his unconditional love. He was the only one that saw me growing up but not graduated.

Thank you.

# Resumo

O consumo contínuo de combustíveis fósseis está a gerar elevadas emissões de gases de efeito de estufa, provocando fenómenos preocupantes responsáveis por prejudicar o ambiente e a saúde da população mundial. A energia solar tem demonstrado ser uma fonte renovável de sucesso, pelo que grandes investimentos estão planeados nas próximas décadas. Este estudo visa a maximização da energia a injetar na rede por parte de um parque solar fotovoltaico de larga escala com $24MW_p$ de capacidade instalada. Para tal, foram realizadas sucessivas simulações de forma automática com o software PVSyst para que cada parâmetro pudesse ser estudado individualmente, permitindo perceber a influência destes na variável a maximizar. A melhor combinação de módulo/inversor foi escolhida e dois *string inverters* foram incluídos para que pudessem ser comparados ao inversor central. Os sistemas de *fixed tilt* e *single-axis tracking* (SAT) foram optimizados e o *layout* (AutoCAD) foi realizado para cada caso diferente, o que possibilitou a distribuição dos diferentes aparelhos ao longo da área disponível. Uma análise económica foi também efectuada de forma a que a opção mais viável pudesse ser selecionada. Foi concluído que, com o inversor central e o *string inverter* implementados, o sistema SAT produz 15% e 14.3% mais energia do que o sistema *fixed tilt*, respectivamente. Adicionalmente, os *string inverters* levaram a um ganho de energia 3.5% e 2.7% maior quando implementados no sistema de *fixed tilt* e SAT, respectivamente. A solução mais viável do ponto de vista económico passa pela implementação do sistema SAT em conjunto com um *string inverter* e com a configuração dos módulos em *portrait*.

**Palavras-chave:** Parque solar PV de larga escala, otimização, parâmetros, análise económica

# Abstract

The continuous consumption of fossil fuels is leading to large amounts of greenhouse gases emissions, giving rise to unsettling phenomena responsible for harming the environment as well as world population's health. The solar energy has shown to be a successful renewable source, wherefore large investments are planned in the upcoming decades. This study aims at maximizing the energy to inject into the grid by a solar photovoltaic PV park with $24MW_p$ of installed capacity. Several successive simulations were automatically performed with the PVSyst software, so that each considered parameter could be individually analysed, allowing one to understand their influence on the variable to maximize. The best combination of module/inverter was chosen, and two different string inverters were included to evaluate their efficiency relatively to the central inverter. The fixed tilt and single-axis tracking (SAT) systems were optimized and the layout of each case scenario was undertaken, which enabled the different devices to be distributed over the available area. An economic analysis was carried out so that the most viable solution could be selected. When employing the central inverter and string inverter, the SAT system produces 15% and 14.3% more energy relatively to the fixed tilt one, respectively. Additionally, the string inverters led to 3.5% and 2.7% higher energy yields when employed in the fixed tilt and SAT system, respectively. The most economic viable solution is characterized by the employment of the SAT system together with the string inverters and module portrait configuration.



**Keywords:** Utility-scale solar PV park, optimization, design parameters, economic analysis

# Contents

# List of Tables

# List of Figures

# Nomenclature

| | |
|---|---|
| $\eta$ | Efficiency |
| $\eta_{conv}$ | DC/AC Conversion Efficiency |
| $\eta_{inv}$ | Inverter Efficiency |
| $\eta_{tr}$ | MPPT Tracking Efficiency |
| $A$ | Collector Area ($m^2$) |
| $A_{AC}$ | AC cable cross section ($m^2$) |
| $A_{DC}$ | DC cable cross section ($m^2$) |
| $A_{ground}$ | Total Ground Area ($m^2$) |
| $A_{modules}$ | Modules Sensitive Area ($m^2$) |
| $A_{subarray}$ | Sub-array Area ($m^2$) |
| $A_s$ | String cable cross section ($m^2$) |
| $A_T$ | Annuity (€) |
| $C_F$ | Fixed Cost (€) |
| $C_T$ | Total Cost (€) |
| $C_V$ | Variable Cost (€) |
| $cos(\phi)$ | Power Factor |
| $E_{AC}$ | Produced AC Energy (kWh) |
| $E_a$ | Annual Energy (MWh) |
| $E_{DC}$ | Produced DC Energy (kWh) |
| $E_{grid}$ | Energy injected into the grid (kWh) |
| $FF$ | Fill Factor |
| $G$ | Solar Irradiance Incident on the Solar Cell (W/$m^2$) |

$G_0$ Global Irradiance at STC (W/m$^2$)

$GCR$ Ground Cover Ratio

$H_t$ Total Horizontal Irradiance (W/m$^2$)

$I$ Load Current (Amps)

$I_0$ Initial Investment (€)

$I_{AC}$ Inverter AC nominal current (Amps)

$I_D$ Diode Current (Amps)

$I_{inv,\text{MAX}}$ Inverter Maximum Input Current (Amps)

$I_{mp}$ Maximum Power Point Current (Amps)

$I_n$ Stringbox output current (Amps)

$I_{ph}$ Photoelectric Current (Amp)

$I_{sc}$ Short Circuit Current (Amps)

$IRR$ Internal Rate of Return

$k$ Boltzmann Constant = $8.6173324(78) \times 10^{-5}$ eV/K

$l$ Cable Length (m)

$L_{AC}$ AC Cable Length (m)

$L_c$ Array Collection Losses

$L_{DC}$ DC cable's length (m)

$L_s$ String Cable Length (m)

$LCOE$ Levelized Cost of Energy (€/MWh)

$m$ Modified Ideality Factor/Quality Factor

$N$ Number of strings

$N_{mod}$ Number of modules

$N_{p,\text{MAX}}$ Maximum Number of Modules in Parallel

$N_p$ Number of modules in parallel

$N_{s,\text{MAX}}$ Maximum Number of Modules in Series

$N_{s,\text{MIN}}$ Minimum Number of Modules in Series

$N_{subarrays}$ Number of Sub-arrays

$N_s$ Number of modules in series

$NPV$ Net Present Value

$P$ Pitch (m)

$P_{AC}$ Inverter's nominal AC power (Watts)

$P_{DC}$ Solar park DC peak power (Watts)

$P_{FV}$ String-box Output Power (Watts)

$P_{inv,max,ratio}$ Maximum Inverter Nominal Power Ratio

$P_{inv,min,ratio}$ Minimum Inverter Nominal Power ratio

$P_{inv,ratio}$ DC/AC ratio

$P_{max,inverter}$ Inverter Maximum Power (Watts)

$P_{min,inverter}$ Inverter Minimum Power (Watts)

$P_{mod,\text{STC}}$ Nominal Module Power under Standard Test Conditions (Watts)

$P_{mp}$ Power at Maximum Power Point

$P_{subarray,\text{STC}}$ Nominal Sub-array Power under Standard Test Conditions (Watts)

$P_{syst,\text{STC}}$ Nominal System Power under Standard Test Conditions (Watts)

$P_s$ Line losses (W)

$PR$ Performance Ratio

$q$ Electron Elementary Charge = $1.602 \times 10^{-19}$ (Coulomb)

$r$ Rate of Return

$R_{sh}$ Shunt Resistance ($\Omega$)

$R_s$ Series Resistance ($\Omega$)

$T$ Cell Temperature (Kelvin)

$T_{max}$ Maximum Cell Temperature ($^{\circ}C$)

$T_{min}$ Minimum Cell Temperature ($^{\circ}C$)

$T_{ref,\text{STC}}$ Reference Temperature at Standard Test Conditions = $25^{\circ}C$

$U_N$ Transformer input voltage (Volts)

$U_s$ Maximum Power String Voltage (Volts)

$V$ Load Voltage (Volts)

$V_D$ Diode Voltage (Volts)

$V_{inv,\text{MAX}}$ Inverter Maximum Input Voltage (Volts)

$V_{inv,\text{MIN}}$ Inverter Minimum Input Voltage (Volts)

$V_{mp}$ Maximum Power Point Voltage (Volts)

$V_{oc}$ Open Circuit Voltage (Volts)

$V_T$ Thermal Voltage (Volts)

$W$ Width (m)

$Y_a$ Array Yield (kWh/kW$_p$)

$Y_f$ Final System Yield (kWh/kW$_p$)

$Y_r$ Reference Yield (kWh/m$^2$)

$I_0$ Reverse Bias Diode Saturation Current (Amps)

$G_{on}$ Extraterrestrial Normal Irradiance (W/m$^2$)

$G_{sc}$ Extraterrestrial Irradiance (W/m$^2$)

# Chapter 1

# Introduction

## 1.1 Motivation

Energy is crucial for a wide range of applications in agriculture, transportation, industry and household sectors. The continuous consumption of fossil fuels for power generation is leading to large amounts of greenhouse gas emissions, which consequently heavily harms the environment. Among many consequences stemming from it, the global warming and climate change have been identified as an unsettling phenomena, which requires the mankind to reverse this process at the earliest possible. In this regard, the employment of renewable energies appear to be one of the foremost efficient solutions. Thus, it is required to use cleaner energy sources like solar, wind, hydro and biomass.

In the past few years, solar energy has shown to be a promising solution, since the installation is accessible and it can be extended to any place where there exists abundant sun radiation. The reduction of the investment costs along with the diverse components' efficiency improvements will make the installed power to keep growing in the future, namely through the implementation of large-scale grid connected solar PV parks. Hence, the optimization of solar PV parks turned out to be a crucial topic to be studied since it highly influences the energy output and the project's economic viability in the long term. The solar PV park optimization is a not straight forward problem due to the existence of many variables needed to consider, which might result in controversial parameters' values. For instance, the best combination of parameters aiming at maximizing the grid energy or performance ratio might differ.

Portugal benefits from being the country in Western Europe receiving the highest values of Solar radiation, which is leading to high expectations as well as projects to be undertaken in the near future. Therefore, it is relevant that technical and economical matters relating to the optimization of solar PV parks are carried out to take the most out of this technology.

## 1.2 Objectives

The present dissertation was developed in collaboration with Sotécnica and the objectives to be achieved were initially set. A real case study was provided aiming at enhancing the obtained results

through a different problem approach. This work proposes to develop technical and economical solutions to optimize a utility-scale grid connected solar photovolatic park. More specifically, a solar PV park with an installed capacity of 24 $MW_p$ and a limited land area of approximately fifty hectares will be analyzed, aiming at the maximization of the energy to inject into the grid, finding the most appropriate considered parameters' values. Furthermore, along with the energy yield maximization, an economical study is to be carried out so that the most viable solution can be chosen. The software PVSyst was agreed to be used along the study as a decision support tool. The aforementioned goal is planned to be achieved through the following outlined steps to be developed along the present study:

- Choice of the main equipment (solar modules and inverters);
- Study of the central and string inverter alternatives;
- System sizing;
- Fixed tilt system parameters' optimization;
- Single axis-tracking system parameters' optimization;
- Park layout;
- Economic viability maximization.

## 1.3 Thesis Outline

This section outlines the content of the upcoming chapters throughout the thesis. Chapter two provides an overview regarding previous research undertaken within this field of studies as well as the contribution of the present study. Two different sub-sections are presented (performance assessment and optimization), in which different studies are included in. Chapter three introduces the background and models required to properly develop and understand the project. Firstly, the chapter starts with an overview about the current worldwide energy situation as well as the solar PV, focusing later on the Portuguese status. Later on, the solar geometry, solar PV system components, tracking systems and system sizing are described.

Chapter four provides the general method and followed strategy to approach the problem at stake. Particularly, it starts with the choice of the PV modules and central/string inverters, being followed by a parameters' analysis for both fixed tilt and single-axis tracking systems aiming at the energy yield maximization. Additionally, the layout section proves to be relevant as it describes how certain parameters are correlated between each other. Based on the chosen layout, the diverse cables' lengths as well as their prices are estimated, being relevant for the economic viability study. Lastly, chapter five presents the results stemming from PVSyst simulations for both fixed tilt and single-axis tracking systems, in which different parameters are analyzed always envisioning the energy maximization. Later on this chapter, an economic viability comparing each different combination (differing on the modules configuration, type of system and inverter) is carried out, having the most suitable option been chosen.

# Chapter 2

# State of the Art

Throughout time, several studies concerning performance assessment of solar PV parks have been carried out aiming at the attainment of greater values of performance ratio and energy yield. Furthermore, research in the field of solar PV power plants optimization has been undertaken as this represents a multi-variable problem involving several parameters that need to be considered. The optimization domain is a crucial matter that has been gaining particular importance in the past few years, since PV technology prices have been decreasing and large-scale parks have been built, where just few improvements may lead to important yield performance differences. Thereafter, the main reviewed literature deemed relevant regarding PV parks performance assessment and optimization will be described.

Relatively to what is described in the articles presented in this section, the present study aims at approaching this multi-variable problem employing a generic method to optimize the parameters deemed relevant in both fixed and single-axis tracking PV utility-scale installations. Initially, simulations were carried out aiming at finding the module/inverter combination leading to the greater energy output, so that the pair with the best performance could be selected. Different central and string inverters were included in the study so that their performance could be assessed and compared in both technical and economical terms.

## 2.1 Performance Assessment and Design

C. Kandasamy, P. Prabu and K. Niruba [8] simulated a grid-connected solar PV power plant to assess its performance making use of PVSyst software. Performance ratio and various types of power losses data were obtained and from it, the viability of installing a 1MW solar PV power plant in four different areas was discussed. The solar modules' tilt angle was adjusted accordingly to the site latitude and both the modules and inverter assumed throughout the study were initially chosen, having been the only option considered. Based on the derived performance ratio, energy yield and losses for all the four studied sites, the one performing better was chosen.

Ashish Raj, Manoj Gupta, Sampurna Panda [4] carried out a design simulation, performance assessment yield and loss forecasting for a 100 $kW_p$ grid connected solar PV System. Throughout

the study, an equivalent mathematical model was developed and the performance parameters were obtained with the help of PVSyst design tool. Additionally, the forecast yield was compared with real data measured over one month, which is always useful to perceive the tolerance and errors that might stem from forecasting tools.

Priya Yadav, Nitin Kumar, S.S Chandel [32] aimed at the design and simulation of a solar PV system power plant having 1kW of installed capacity using PVSyst software. The energy generated by the system and incurred losses were computed and analyzed. As it does not represent a large-scale system, the modules tilt angle was simulated as being varied seasonally accordingly to the "optimal angle" provided by the software. As in [8], both module and inverter type were initially chosen. B. Shiva Kumar, K. Sudhakar [5] presents a similar study to Priya Yadav, Nitin Kumar, S.S Chandel [32], evaluating the performance of a 10MW PV power plant to be installed in a given area of fifty acres, while also considering seasonal tilt angle variation.

Irfan Jamil, Jinquan Zhao, Li Zhang, Rehan Jamil, Syed Furqan Rafique3 [18] presents a study of a 150MW grid-connected utility-scale solar PV plant to be installed within a 750 acres land. The analysis was mainly focused in the preliminary design of the case project such as the feasibility study and PV solar design aspects, which were underpinned by an energy yield assessment simulation study performed using PVSyst software. Both Meteonorm and Solar GIS data base were used as resources to get a reliable estimate of the solar radiation and temperature information at the considered site. The authors considered a fixed tilt system due to the more convenient installation lower costs. The fixed tilt angle was also set accordingly to the site coordinates.

Alberto Dolara, Francesco Grimaccia, Sonia Leva, Marco Mussetta, Roberto Faranda, Moris Gualdoni [2] performed an analysis of a photovoltaic single-axis tracking system installed in a 800kW solar PV park based on experimental data collected throughout one year. The authors rested on the transposition factor (amount of captured irradiation by the collector plane with respect to a fixed panel) rather than only on the performance ratio, mentioning that the latter one is not sufficient to estimate the solar park energy behaviour while using a tracking system. Hence, this comparative study showed that the transposition factor index properly represents the energy increase of a tracking system relatively to a fixed one.

Basha [6] proposed eight different locations in India aiming at analyzing the difference between fixed tilt (adjusted according to each location latitude) and horizontal single axis tracker solar PV system. The author concluded that the horizontal single axis tracker generates annually 17% more energy than the fixed tilt system. A lower performance ratio was obtained with the single axis tracker system when compared to the fixed tilt system, explained through variations caused by factors as the IAM losses, DC cable losses, plant availability, auxiliary consumption and temperature losses.

Verma and Singhal [41] carried out a research study where several performance parameters (PR, cumulative utilization factor) and factors contributing to the performance of solar power plants (climate conditions, design parameters) are covered, which is essential in the extent that it helps when one is trying to optimize the energy generation and the PV park overall performance. Additionally, the research study also covers a real case in which a 20MW solar PV park is analyzed with the aid of PVSyst software.

## 2.2 Optimization

An overview regarding PV parks performance assessment using PVSyst was presented in the last section for both fixed tilt and single-axis tracking systems. However, all the reviewed articles in the last section do not focus on a detailed optimization but rather on an evaluation of the performance through the analysis of the already mentioned parameters. In the present section, four articles regarding the optimization of PV solar parks will be introduced as they cover some of the relevant topics to be addressed along this study. These studies, however, have used different approaches since some were carried out employing the PVSyst software (as in the present study) while others are underpinned by optimization algorithms.

Mermoud [25] presented an analysis of the mutual shading effect in rows arrangement using PVSyst software, which plays a major role in a fixed tilt solar PV park optimization. A deep analysis of the different components' shading effects (beam, diffuse, albedo and mismatch electrical effects) was carried out and it was concluded that the diffuse and albedo losses are dominating. Additionally, it was shown that the electrical effects are essentially important with one only string in the width of rows.

Mermoud [26] introduced a tool to optimize the layout of ground-based PV solar systems considering economic boundary conditions. Besides the optimization aiming at maximizing the installation yield performance, economic boundary conditions as the investment and maintenance costs, surface availability and feed-in tariff have also a relevant impact on the design choices. As so, the optimization tool addresses the mentioned problem by finding the ground cover ratio and module tilt angle capable of optimizing the economic benefit. The employed software tools to carry out this study was still not made available in the latest software version.

Muhammad Z. B. Rosselan, Shahril Irwan Sulaiman, Ismail Musirin [29] developed a cuckoo search-based algorithm aiming at the sizing optimization of a 5MW large-scale grid connected photovoltaic system. Over this study, the algorithm was used to select the optimal combination of the system components (PV module and inverter) so that the performance ratio (PR) was maximized. Tamas Kerekes, Eftichis Koutroulis, Dezso Sera, Remus Teodorescu, Markos Katsanevakis [38] provides a method through the employment of a genetic algorithm for the calculation of the optimal configuration of large PV plants aiming at minimizing the levelized cost of energy (LCOE). The design optimization was carried out considering the number of components and their arrangement within the field as well as the lifetime cost and energy production. The design results allowed to conclude that the proposed optimization method leads to a reduction of the energy cost generated by the PV plant, enabling the economic benefit maximization.

# Chapter 3

# Background and Models

Throughout this chapter, a theoretical overview will cover technical subjects, aiming at providing several insights deemed relevant to perceive the main topics addressed along the present study. Hence, the various main components that constitute a PV solar system will be considered as well as a more in-depth focus about each component's function. Additionally, vital aspects to count with while designing a PV park will be discussed as the shading, orientation, tracking systems and system losses. The models related with solar geometry, incident irradiation, solar cell and system sizing will be described, as they are employed by PVSyst. Besides the technical background, as one of the main goals of the current study is the optimization of a utility-scale solar PV park, one must introduce the different type of project's assessment indicators that will be used later on. Consequently, energy yield indicators (performance ratio and specific energy yield) and financial performance indicators (levelized cost of energy, NPV and internal rate of return) will be addressed as well.

## 3.1 Energy and PV Solar Energy

This section presents an overview concerning the currently used energy sources as well as PV solar systems' evolution and its importance among the diverse existing renewable energy sources. Additionally, a brief introduction regarding utility-scale solar PV parks is presented, as the study is focused on this fast growing segment. Firstly, an outline regarding the worldwide evolution and current situation will be briefly described as well as the prospects for the future. Ahead in the present chapter, as the current project aims at the optimization of a utility-scale PV park in Portugal, a review about this country's promising growth and relevance of this type of renewable energy will also be presented.

### 3.1.1 World Energy

World population has been always increasing and it is foreseen for this trend to remain in the future, albeit with a slower rate than in the past decades. In 2016, 7.4 billions of people were registered and nowadays, a growth of 1.10% has been registered, yielding an additionally 83 million people annually [9], which in turn makes the forecasts to point towards an estimation of 9.8 billion people in 2050. The

population growth together with multiple advances in technology make up one of the reasons from which an increase in the world energy consumption stem from. Consequently, a proper management of the different available types of energy is required for the demand to be satisfied.

Between 1971 and 2016, the world total primary energy supply (TPES) increased from 5523 Mtoe to 13 761 Mtoe, as presented in figure 3.1 (a) [16]. Although the coal is still presented as the dominant source for power generation (due to China high consumption), its share has been decreasing. Natural gas share has been growing (figure 3.1 (a)), and renewables have also contributed for a large portion of the electricity generation, which initially was dominated by hydro power, but over the past few years has come from the development of wind and solar PV energy [16].

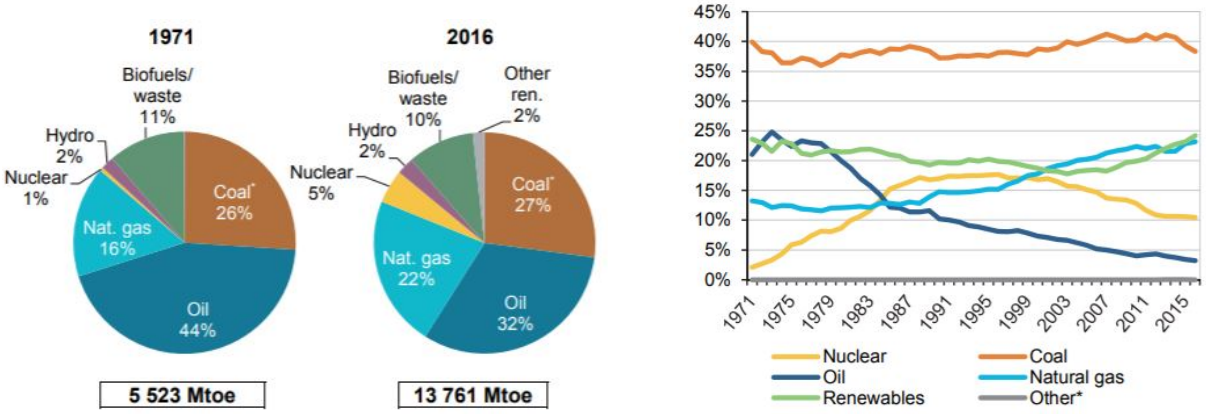


(a) Primary Energy Supply

(b) World Electricity Generation Mix

Figure 3.1: Total Primary Energy Supply and World Electricity Generation [16]

As stated above, world total primary energy supply reached 13 761 Mtoe in 2016, among which 13.7% was produced from renewable sources, as shown in figure 3.2 [15]. Biofuels still represent the largest used renewable source, accounting for 62.4% of global renewable supply, followed by hydro power with a share of 2.5% of world TPES and 18.6% within the renewables' portion. Although solar PV still does not represent a predominant energy source as the already mentioned, it has been growing at an average annual rate of 37.3% (fig 3.2 b) from 1990 on [15], which makes it a relevant energy source with high prospects for the future.

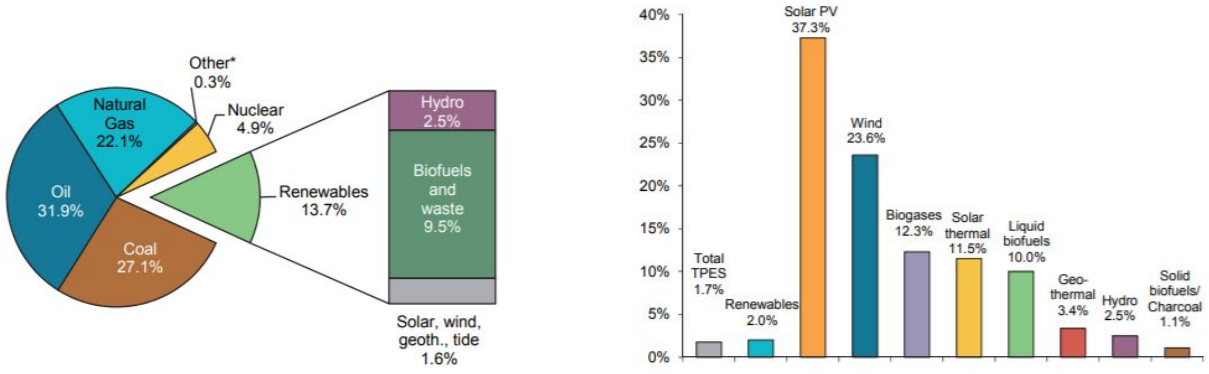


(a) Fuel Shares in TPES in 2016

(b) Annual Growth Rates of Renewables Supply (1990-2016)

Figure 3.2: Renewable sources in the World [15]

### 3.1.2 World PV Solar Energy

Over the past few decades, solar photovoltaic energy has started to play a steadily increasing role within the field of renewables, stemming from higher efficiencies and competitive prices driven mainly by technological breakthroughs and economies of scale. Although this type of technology still makes up only a small percentage of the total global power generation, it has been growing at a fast pace for both utility-scale and distributed power generation [14]. In 2017, according to the International Energy Agency (figure 3.3), the total solar PV installed capacity achieved almost 398 GW and generated over 460 TWh (2% of the global power output). Utility-scale power plants account for 60% of the total solar installed capacity, being the rest fulfilled with distributed applications as residential, commercial and off-grid. Furthermore, a favorable future is expected concerning the development of this type of renewable energy. Over the period between 2018 and 2023, IEA predicts a growth by over 1 TW in the main case forecast (counting with the prevailing market and policy framework) [14]. The global PV installed capacity as well as the yearly energy generated over the world can be seen in figure 3.3.

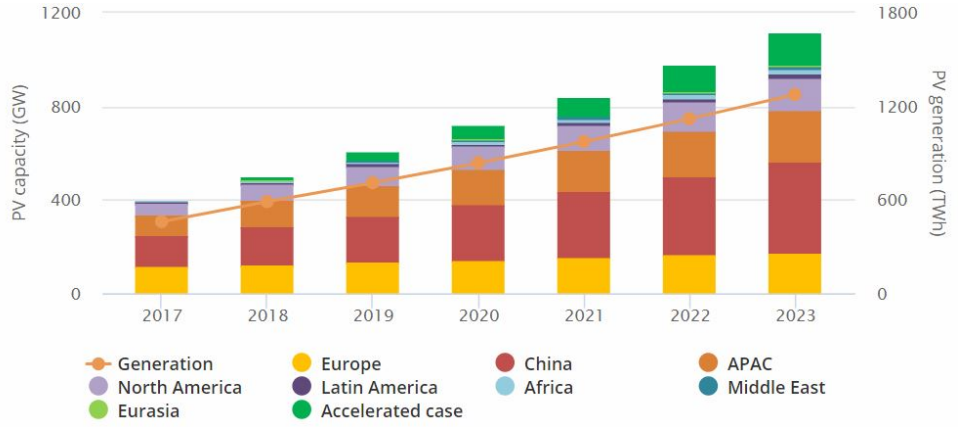


Figure 3.3: Solar PV Generation and Cumulative Capacity by region (2017-2023)[*Source: IEA*]

### 3.1.3 Utility-Scale PV Systems

As solar PV is a modular technology, it might be employed either in small or big scale projects, covering a wide range of applications from off-grid parks up to utility-scale power generation facilities. There exist several perspectives regarding the size from which a solar PV park is considered a utility-scale facility, ranging from 5MW to 50MW. However, apart from the PV park installed capacity, the functionalities and ways of operation represent also a manner to identify this type of solar power plants. A utility-scale solar facility generates solar power to feed into the grid, supplying energy to a utility, since the majority of the end-customers do not hold the load to support this power amount [27]. Thus, every utility-scale solar power plant has a Power Purchase Agreement (PPA) with a utility, making sure that there will be a market for its energy for a fixed time period [31]. Therefore, what mainly differentiates a utility-scale solar from distributed generation is the project size and the fact that the energy is sold not directly to the end-consumers but to the wholesale utility buyers.

### 3.1.4 Energy in Portugal

As presented in figure 3.4 (PORDATA/DGEG), a decrease in the oil consumption has been noticed during the past years similarly to what has been occurring worldwide. In contrast to the world level, primary energy consumption from coal represents a smaller share when compared with both natural gas and renewables.

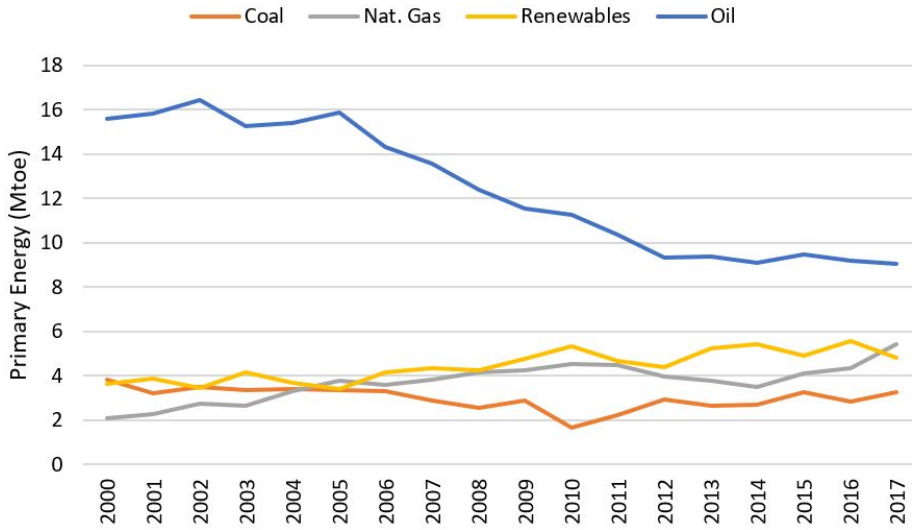


Figure 3.4: Primary energy consumption in Portugal [*Source: DGEG*]

National Renewable Energy Action Plan (NREAP) projects a PV contribution of 670 MW of installed capacity and 1039 GWh of generated electricity for 2020, in which solar energy is expected to represent an important contribution to the increase of decentralized energy production [17]. In 2017, the increase of installed capacity came mainly from self-production systems, accounting for 46 MW. On the other hand, 11 MW of new utility-scale power plants were added, making up a total new installed capacity of 57 MW in 2017, leading to a cumulative installed PV power of 566,4 MW [17]. The total value of produced PV energy accounted for 970 GWh (2% of total energy consumption). It is interesting to notice that this year (2019) it was already registered a solar PV installed capacity of 784MW (REN), which already surpassed some predictions. In figure 3.5, ancillary information regarding the electricity generation in Portugal (from January until September 2018) is shown. Renewable energy sources have contributed with a share of 53.2 % to the overall electricity production among which the highest share stemmed from hydro power (25.7%).

This year, an auction of 1.15GW took place in the Portugal solar photovoltaic market, which has been identified as a way of increasing the competitiveness between developers, resulting in new improvements and developments in this field. It is important to refer that, together with the development of many solar PV parks aiming at reaching the aforementioned installed capacity, there comes another challenge, related with the actual grid reception capacity. Thus, investments should be made so that the grid is prepared to withstand the planned power to install.

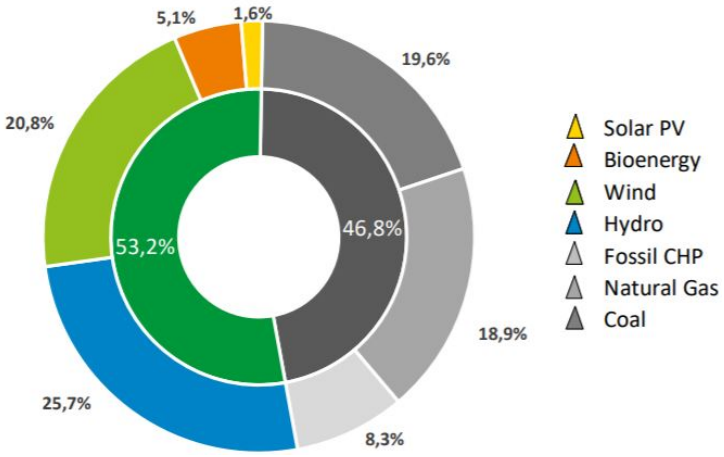


Figure 3.5: Electricity generation by energy sources (Jan-Sep 2018) [*Source: APREN*]

## 3.2 Solar Geometry and Incident Irradiation

Solar rays are the source of energy harnessed by the photovoltaic panels for electricity to be produced. However, before the photons reach the panels, radiation intensity is modified due to several phenomena caused by the atmosphere as reflections, dispersions and absorptions. Irradiance is defined as the flux of radiant energy per unit area ($kW/m^2$), while insolation denotes the cumulative sum of the energy striking the surface for a certain time interval ($kW.h/m^2$). Before reaching the atmosphere, solar radiation intensity is nearly constant, varying 3.3% due to the eccentricity of the earth's orbit. The extraterrestrial irradiance $G_{sc}$ is the average solar irradiance at normal incidence outside the earth's atmosphere and accordingly to the World Radiation Center, it has a value of 1367 $W/m^2$. As the distance between the Earth and Sun in constantly varying, the extraterrestrial normal irradiance ($G_{on}$) is dependent on the $n^{th}$ day of the year, accordingly to:

$$G_{on} = G_{sc}\left[1 + 0.033cos\left(\frac{360°}{365}n\right)\right] \tag{3.1}$$

The irradiance strength hitting the solar panel hinges on the direction the collector is facing. The angle between the normal to the collector plane and the solar rays is referred to as the incidence angle ($\theta$), which depends on the latitude ($\varphi$), Sun azimuth angle ($\gamma_{sun}$), declination ($\delta$) surface tilt ($\beta$), plane azimuth angle ($\gamma_{plane}$), zenith angle ($\phi$) and Sun height ($90-\phi$), as shown in figure 3.6 a. The expression to compute the incidence angle is given by:

$$cos(\theta) = cos(\gamma_{sun} - \gamma_{plane})cos(90 - \phi)sin(\beta) + sin(90 - \phi)cos(\beta) \tag{3.2}$$

where the Sun's height and azimuth are given as represented in equations 3.3 and 3.4, respectively. The $h$ term refers to the hour angle, being the angle between the meridian of the collector plane and the meridian line on which the Sun is.

$$sin(90 - \phi) = sin(\varphi)sin(\delta) + cos(\varphi)cos(\delta)cos(h) \tag{3.3}$$

$$\gamma_{sun} = sin(h) \left| arccos\left( \frac{cos(\phi)sin(\varphi) - sin(\delta)}{sin(\phi)cos(\varphi)} \right) \right| \tag{3.4}$$

The solar radiation can be direct, diffuse or reflected depending on solar rays' path before reaching the solar panels (figure 3.6 b). Direct radiation (also known as beam radiation) describes the portion coming directly from the Sun, while diffuse radiation refers to the part of the sunlight scattered by particles in the atmosphere. The reflected one (also known as albedo) comes from the radiation hitting the ground before reaching the solar panels, which may vary depending on the type of ground material.

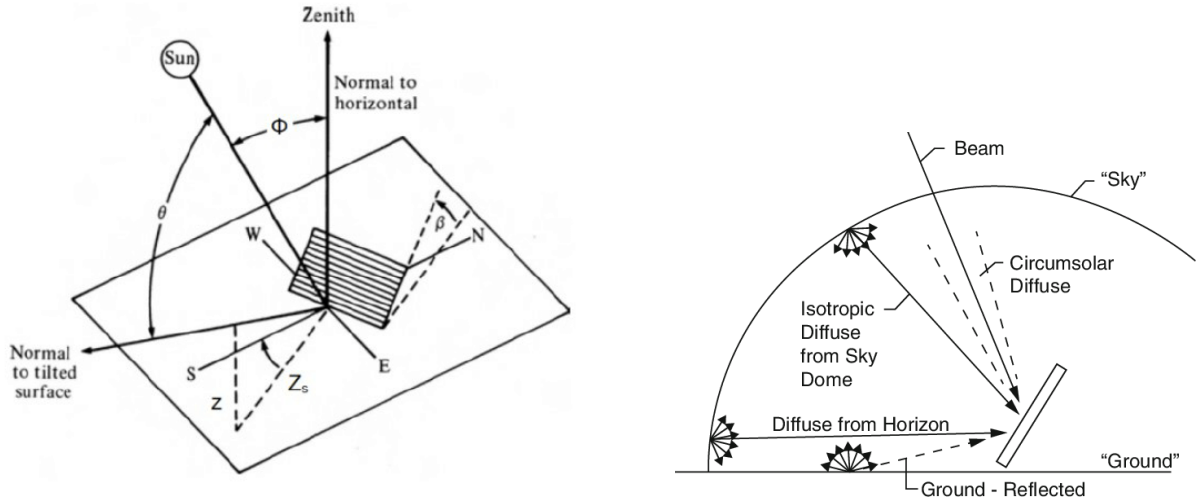


(a) Collector Orientation Angles [1]

(b) Beam, Diffuse and Reflected Radiation [11]

Figure 3.6: Collector Orientation and Radiation Types

PVSyst software simulations are based on meteorological data (section 4), which must provide horizontal irradiance (including both diffuse and beam components), as given in the equation 3.5. Thereafter, a transposition model is employed to compute the total available irradiance on the tilted plane (solar panel plane).The beam component includes a purely geometrical calculation, which might be presented through the equation 3.2. Concerning the diffuse component, PVSyst provides both Hay's and Perez transposition models, being the latter one used in the simulations, as it was proved to be more sophisticated. Hay's model considers the diffuse irradiance to be isotropic (uniform over all the sky dome), whereas Perez model divides the sky into sectors and parametrizes the transformations of the circumsolar and the horizon band according to correlations established on empirical data from several sites distributed all over the world [35]. The albedo component is similarly calculated by both models, being given as a fraction of the global irradiance. These three mentioned components are related as given in equation 3.6.

$$G_{hor} = B_{hor} + D_{hor} \tag{3.5}$$

$$G_{plane} = B_{plane} + D_{plane} + A_{plane} \tag{3.6}$$

After the transposition model has been applied, the near shading losses are taken into account

through a model described in section 3.6.2.1, as well as IAM (array incidence loss) and soiling losses (3.6.2.1), which allows the effective irradiance ($G_{eff}$) to be obtained.

## 3.3 Solar PV System Components

This section presents a description on the main components' features forming a solar PV power system. The insights specified below are crucial as they are the basis for the selection and sizing of the system components. Firstly, the different types of materials employed to produce solar cells will be described. Furthermore, a brief explanation about the functioning of the solar cell will be outlined as well as the mathematical model (one-diode standard model) used in PVSyst software to describe the cell's electronic behaviour.

### 3.3.1 Solar Cell

The solar cell is responsible to convert the energy transported by radiation into electricity. Silicon Crystalline and Thin Film (CdTe) technology are the two main different types of solar photovoltaic cell and both their classification and installed capacity (GW) evolution can be seen in figure 3.7(a) and 3.7(b), respectively. The method of manufacturing of the two different types of crystalline solar cell and the process to convert radiation into electricity will be briefly explained ahead. As noticeable through the chart, crystalline solar cell type is dominant compared to thin-film model, inflicted by the differences concerning both efficiency and cost as one will better understand through more detailed descriptions presented next.

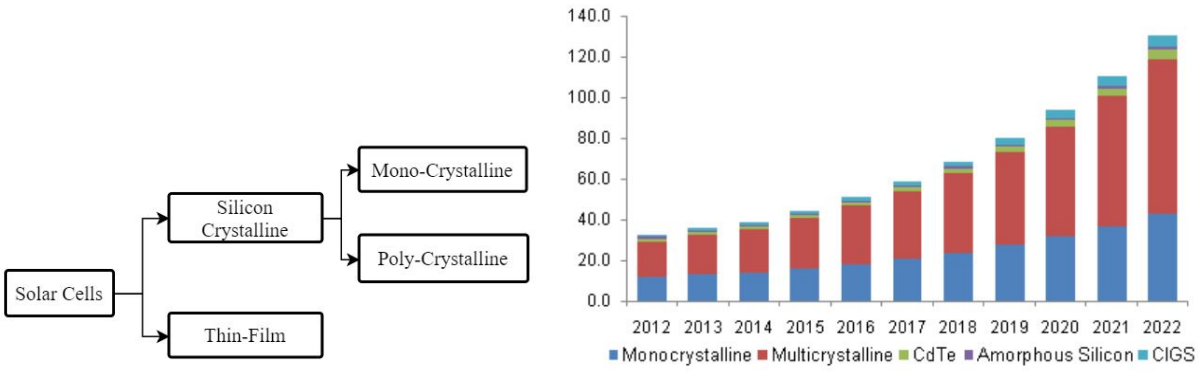


(a) Solar Cell Types

(b) Solar Cell Installed Capacity [34]

Figure 3.7: Solar Cell Types and Installed Capacity

***Crystalline***

Crystalline cell type makes up 90% of grid connected photovoltaic systems worldwide [12]. This type of solar cells is more expensive than thin-film technology, requiring a larger investment cost. On the other hand, crystalline solar cells are generally more efficient and have longer performance warranties. Silicon Crystalline family include mono-crystalline and poly-crystalline photovoltaic cells. Both types of

silicon cells have a layer doped with Boron and a layer doped with Phosphorous, responsible for creating p-type and n-type regions, respectively. These two mentioned doped layers create an intermediate depletion zone between them, resulting in an electric field (fig. 3.8). Photons present in the solar radiation transfer their energy to the electrons firstly present in the valence band, which in turn gain mobility and are transported towards the conduction band. Hence, the electrons move from the p-type layer to the n-type layer and the holes (+ sign in the figure) move in the opposite direction in the depletion zone, which makes a current start flowing if a load is connected [42]. The p-type and n-type layers possess different thicknesses, which is correlated to the mobility, lifetime and diffusion of minority carriers. The n-type layer is often thinner than the p-type layer, since the electrons have higher mobility and diffusion length (average length a carrier moves between generation and recombination) than holes. Therefore, when irradiation hits the solar cell, electrons present in the depletion zone (minority on the p-side) absorb energy generating an electron-hole pair with lower probability of recombination.

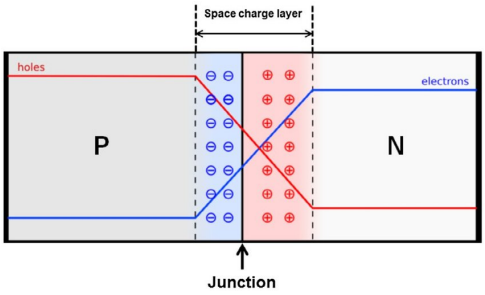


Figure 3.8: PN Juntion [37]

Mono-Crystalline PV cell technology has been the most commonly used technology both in utility-scale and stand-alone applications. The mono-crystalline manufacturing process (known as Czochralski) is a method of crystal growth from a seed, used to obtain single crystals of semiconductors [40]. This process, in spite of producing higher efficiency cells, causes the manufacturing costs to increase. On the other hand, in spite of having a lower efficiency compared to the aforementioned material, poly-crystalline cell turned out to be a suitable material to reduce the cost of developing a PV module [40]. Poly-crystalline is produced by melting silicon and solidifying it to orient crystals in a fixed direction producing a rectangular ingot of poly-crystalline silicon, which is followed by the block slicing to produce thin wafers [40].

***Thin-Film***

Thin-Film solar cells appeared in the market aiming at decreasing the cost of PV array by lowering material and manufacturing costs without hindering the cell life-time [22], contributing for the possibility to make the projects economically viable. The advantage of this type of technology compared to crystalline solar cells lies in the fact that the thickness of the deposited layers are much thinner, which if placed on stainless steel sheets, provide the PV modules with a flexible structure [22]. However, thinner layers result also in a decrease of photovoltaic material to absorb income radiation, which results in a lower efficiency when compared with crystalline type of solar cells [22]. There exist several different types of thin-film solar cells, among which the most known are the amorphous silicon (a-Si), cadmium telluride

(CdTe) and copper indium gallium selenide (CIS/CIGS). CdTe thin-film cell type has proved to be one of the most promising ones, having relative good efficiencies at a low manufacturing cost. This type of thin-film solar cell has an ideal band-gap (distance between valence and conduction band through which the electrons have to pass when they absorb energy from the photons) of 1.45eV, having been already employed in utility-scale PV systems [22].

#### 3.3.1.1 The One Diode Model

A solar cell consisting of a p-doped and n-doped material has identical electronic features when compared with a diode, whose equivalent electronic circuit is presented in figure 3.9. As so, it is possible to correlate them and describe the former one using the single diode equation, given by:

$$I = -I_D = -I_0 \left[ \exp\left(\frac{V}{m' V_T}\right) - 1 \right] \tag{3.7a}$$

where $I$, $I_o$ and $V$ represent the load current, reverse saturation current and load voltage, respectively. The ideality factor $m'$, thermal voltage $V_T$ (dependent on temperature) and diode current $I_D$ are dependent on each other as follows:

$$m' = N_s m \tag{3.7b}$$

$$V_T = \frac{kT}{q} \tag{3.7c}$$

In the equation 3.7c, k, T and q represent the Boltzmann constant, temperature and electron elementary charge, respectively. As $N_s$ stands for the number of PV cells in series and one is considering only one solar cell in the following expressions ($N_s = 1$), the ideality factor $m$ will be adopted rather than $m'$. When light hits the solar cell, the energy coming from the photons generate free charge carriers. Hence, a power source responsible for producing a photoelectric current $(I_{ph})$, which depends on the level of Irradiance $G$, is also included in the equivalent system.

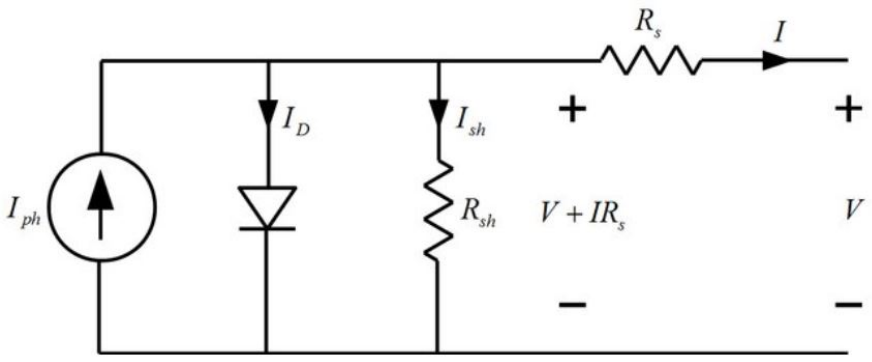


Figure 3.9: Single Diode Equivalent Circuit [23]

Different equivalent mathematical models may be considered to analyze the solar cell electrical behaviour. In the present study, the one-diode standard model with five unknowns $(I_0, I_{ph}, R_s, R_{sh}, m)$

will be considered, since the used software (PVSyst) also employs this model to perform the simulations. These five parameters are based solely on the manufacturer's data sheets, whose information provide $V_{oc}$, $I_{sc}$, $V_{mp}$, $I_{mp}$, $\alpha_{I_{sc}}$ and $\alpha_{V_{oc}}$ [36]. The equivalent circuit of this module is shown in figure 3.9 and, as one can notice, two different types of resistances are present: series resistance $R_s$ and shunt resistance $R_{sh}$. Series resistance comprises all the cell series resistances, connection strips as well as soldered joints [12] and it has a high influence on efficiency at high irradiance. On the other hand, shunt resistance refers to the emergence of a leakage current that bypasses the load, leading to power losses mainly at low irradiance [12].

Applying Kirchhoff's Current Law, one can deduce the one diode-model current, which is given by:

$$I = I_{ph} - I_D - I_{sh} = I_{ph} - I_0\left(\exp\left(\frac{V + R_s I}{mV_T}\right) - 1\right) - \frac{V + R_s I}{R_{sh}} \tag{3.8}$$

$$\text{which, if} \qquad \exp\left(\frac{V + R_s I}{mV_T}\right) >> 1,$$

$$\text{(3.8) can be written as} \qquad I = I_{ph} - I_0 \exp\left(\frac{V + R_s I}{mV_T}\right) - \frac{V + R_s I}{R_{sh}} \tag{3.9}$$

Considering the five already mentioned unknowns, one may compute the numerical solutions through the derivation of non-linear equations [28]. At first, equation 3.9 is considered at three different points of the IV curve (red line in fig. 3.10): short circuit $(0, I_{sc})$, open circuit $(V_{oc}, 0)$ and maximum power point $(V_{mp}, I_{mp})$, given by the equations (3.10), (3.11) and (3.12), respectively. The maximum current (3.12), given when $\frac{dP}{dV}$ equals zero, corresponds to the maximum power point (blue curve in figure 3.10).

$$I_{sc} = I_{ph} - I_0 \exp\left(\frac{R_s I_{sc}}{mV_T}\right) - \frac{R_s}{R_{sh}} I_{sc} \tag{3.10}$$

$$0 = I_{ph} - I_0 \exp\left(\frac{V_{oc}}{mV_T}\right) - \frac{V_{oc}}{R_{sh}} \tag{3.11}$$

$$I_{mp} = I_{ph} - I_0 \exp\left(\frac{V_{mp} + R_s I_{mp}}{mV_T}\right) - \frac{V_{mp} + R_s I_{mp}}{R_{sh}} \tag{3.12}$$

Through the equations 3.10 and 3.11 one can express the two unknowns ($I_0$ and $I_{ph}$) as function of the remaining three (m, $R_s$ and $R_{sh}$). If one replaces the result from equations 3.10 and 3.11 in the maximum power point (equation 3.12) [36], the following equation representing the the maximum current can be written:

$$I_{mp} = I_{sc} - \left(I_{sc} - \frac{V_{oc} - R_s I_{sc}}{R_{sh}}\right) \exp\left(\frac{V_{mp} + R_s I_{mp} - V_{oc}}{mV_T}\right) - \frac{V_{mp} + R_s I_{mp} - R_s I_{sc}}{R_{sh}} \tag{3.13}$$

It is important to point out that the STC (Standard Test Condition) parameters are obtained from the solar panel data sheet. STC is an industry standard to indicate the PV modules performance, being characterized by a cell temperature of 25° and an irradiance of 1000$W/m^2$ with an air mass of 1.5 (AM1.5). From the previous equations the aforementioned unknowns $m$, $R_s$ and $R_{sh}$ can be found and based on them, the diode reverse saturation current ($I_0$) and the photoelectric current ($I_{ph}$) can also be computed:

$$I_0 = \left(I_{sc} - \frac{V_{oc} - R_s I_{sc}}{R_{sh}}\right) \exp\left(-\frac{V_{oc}}{mV_T}\right) \tag{3.14}$$

$$I_{ph} = I_{sc} - \left(\frac{R_s I_{sc}}{R_{sh}}\right) \tag{3.15}$$

Furthermore, it is important to refer the dependence of the five model parameters on the irradiance and module temperature. In this model the unknowns m, $R_s$ and $R_{sh}$ are considered as constant values. However, the short circuit current ($I_{sc}$) and open circuit voltage ($V_{oc}$) are dependent on the irradiance ($G$) and module temperature ($T$). Both $I_{sc}$ and $V_{oc}$ vary with the module temperature, depending on the temperature coefficients ($\alpha_{I_{sc}}$ and $\alpha_{V_{oc}}$) provided in the data sheets [36], as follows:

$$I_{sc}(G,T) = I_{sc}(G)\left[1 + \alpha_{I_{sc}}(T - T^r)\right] \tag{3.16}$$

$$V_{oc}(G,T) = V_{oc}(G)\left[1 + \alpha_{V_{oc}}(T - T^r)\right] \tag{3.17}$$

where $T$ and $T^r$ represent the instantaneous module temperature and the reference module temperature (25°C at STC), respectively. The dependence of the short circuit current $I_{sc}$ with the irradiance $G$ is assumed as a linear variation:

$$I_{sc}(G) = \frac{G}{G^r} I_{sc}^r \tag{3.18}$$

where $G$ and $G^r$ represent the instantaneous irradiance and reference irradiance (1000 $W/m^2$ at STC), respectively. Regarding the dependence of the open circuit voltage with the irradiance, equation 3.8 is written at the open circuit point, which results in the following equation:

$$V_{oc}(G) = mV_T ln\left(\frac{\frac{G}{G^r} I_{ph} R_{sh} - V_{oc}(G)}{I_0 R_{sh}}\right) \tag{3.19}$$

The parameters $I_0$ and $I_{ph}$ (equations 3.14 and 3.15) depend on the irradiance G and temperature T according to:

$$I_0(G,T) = \left(I_{sc}(G,T) - \frac{V_{oc}(G,T) - R_s I_{sc}(G,T)}{R_{sh}}\right) \exp\left(\frac{-V_{oc}(G,T)}{mV_T(T)}\right) \tag{3.20}$$

$$I_{ph}(G,T) = I_0(G,T)\exp\left(\frac{V_{oc}(G,T)}{mV_T(T)}\right) + \frac{V_{oc}(G,T)}{R_{sh}} \tag{3.21}$$

The classic PV cell IV curve is plotted as shown in red in figure 3.10. This curve is obtained through the diode curve, which then assumes a different position in the IV graph when receiving radiation. The solar cell IV curve is obtained by the overlapping of the solar cell diode IV curve in the dark with the light generated current, which makes the curve to shift downwards towards the fourth quadrant. Since the cell is generating power the convection is to invert the current axis, switching the curve for the first quadrant, obtaining the IV solar cell curve represented in red (fig. 3.10).

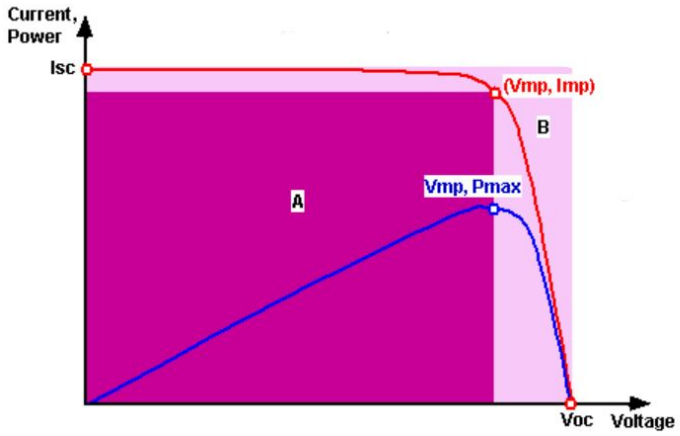


Figure 3.10: Solar Cell IV and Power Curves *[Source: PVEducation]*

The key-elements shown on the IV curve depicted in fig. 3.10 are:

- **Short Circuit Current ($I_{sc}$)** - Maximum current the cell/module can produce when the voltage across it is zero. It is the highest current that can be drawn from a solar cell/module and it is related with the collection of light-generated carriers. For a solar cell with moderate resistive losses, it can be considered equal to the light generated current ($I_{ph}$).
- **Open Circuit Voltage ($V_{oc}$)** - Maximum voltage of the cell/module as it was connected to an infinite resistance with no current flowing.
- **Maximum Power Point ($V_{mp}, I_{mp}$)** - Corresponds to the point where $\frac{dP}{dV}$ equals zero. The output power corresponds to the area "A" in the fig. 3.10.
- **Maximum Power Point Current ($I_{mp}$)** - Current at maximum power point.
- **Maximum Power Point Voltage ($V_{mp}$)** - Voltage at maximum power point.

As aforementioned, the $I_{sc}$ and $V_{oc}$ are the maximum current and maximum possible voltage drawn by the solar cell/module. However, since the output power is given as $P = VI$, its derivative turns out to be null at these specific points. The fill factor (FF) denotes the ratio of areas considering the cell

operating in both cases $(I_{sc}, V_{oc})$ and $(I_{mp}, V_{mp})$. This parameter is influenced by the quality of PV cell junction and its resistances. In the fig. 3.10 it is represented by the ratio between areas "A" and "B", being written as:

$$FF = \frac{A}{B} = \frac{I_{mp} \times V_{mp}}{I_{sc} \times V_{oc}} \tag{3.22}$$

On the other hand, the efficiency depends on the irradiance, cell/module area and maximum power point power. As the power in the maximum power point is related with the fill factor, the efficiency can be written in function of the latter one, as:

$$\eta = \frac{P_{mp}}{G \times A} = \frac{FF \times I_{sc} \times V_{oc}}{G \times A} \tag{3.23}$$

### 3.3.2 Solar Modules and Arrays

A PV module is composed of several solar cells electrically connected together to attain a higher voltage and consequently, a higher power output. A typical solar cell provides a voltage of approximately 0.5 Volts (depending on external factors as temperature and irradiance) and a solar module is commonly composed of either 60 or 72 cells connected in series. In order to form an array, modules are similarly connected together. They can be connected in series to form a string, which in turn can be connected in parallel with another string to attain higher current values. Series connected modules add up the voltage whereas parallel connected modules (or strings of modules) add up the current (figure 3.11), which is an essential point to outline since it has a significant impact on the components' organization, influencing the final PV plant layout.

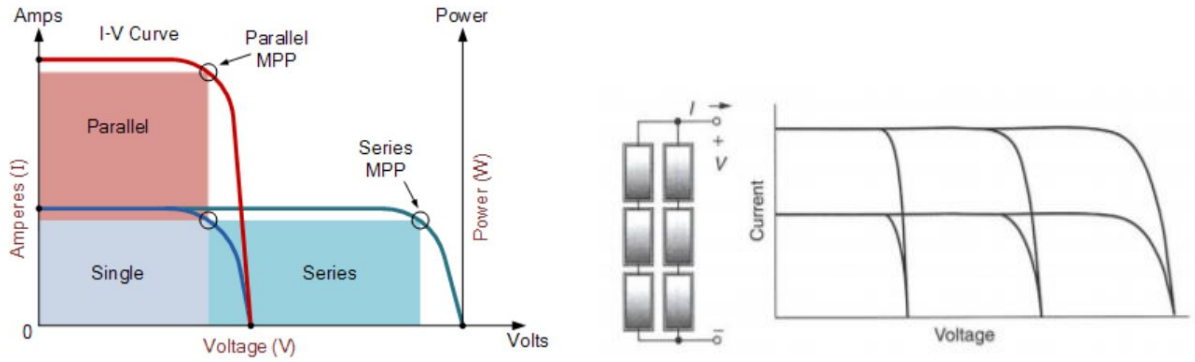


(a) Series and Parallel Connection [39]

(b) Array connection and correspondent IV curve

Figure 3.11: Influence of Modules Series and Parallel Connections in the IV curve [39]

### 3.3.3 Inverter and MPPT

Solar PV modules produce DC current, which before being injected into the grid, must be converted into AC current through an inverter. Inverters, besides converting DC current to AC current, also have built-in maximum power point trackers (MPPT), responsible for searching for the point in the IV curve where the power is maximum, as this curve is always changing its shape according to various

external factors. Therefore, in order to attain the maximum array performance, the inverter varies the current drawn from the module, which controls the module voltage and makes it operate at the IV curve maximum power point [12]. There exist different PV inverters classified in different groups [33], which influence the type of possible connections to be made between the PV modules themselves. Inverters can be classified as:

- Module integrated inverters - operate typically in the 50-400W range for a single solar panel.
- String inverters - operate typically between 0.4kW and 2kW range for a single string of PV modules, suiting small roof-top PV power plants. This type of inverters started to be recently used in utility-scale PV parks as well, being able to stand higher power values.
- Multi-string inverters - operate in the 1.5kW to 6kW range for medium roof-top PV power plants with solar panels composed in one to two strings.
- Mini central inverters - operate typically at a power higher than 6kW with three-phase topology and modular design for larger roof-tops or smaller power plants in the range of 100kW
- Central inverters - operate in the 100kW to 1MW range with three-phase topology and modular design for larger power plants ranging to tens of MW.

Initially, a central inverter will be considered, as it is the most common one used for this type of application, being capable of standing high amounts of power arising from a utility scale PV park. However, string inverters have recently started to be introduced on this type of PV parks as well. As so, two different string inverters manufactured by Huawei will be included in this study to conclude about its capability of increasing the energy yield when compared to a central inverter. The use of a string inverter may result in some advantages. One clear advantage of employing this type of inverter is the redundancy factor, since if one inverter gets damaged, only a few strings will be affected rather then one entire sub-array which wouldn't be able to inject energy in the grid, resulting in large yield losses. Additionally, replacing a string inverter is much simpler when compared with a central inverter, as it doesn't require specialist personnel and spare inverters can be kept on site prepared to be used. Thereby, a fast replacement diminishes the amount of time a string is inoperable. On the other hand, the employment of this type of configuration will lead to a large number of inverters, as utility-scale systems might be composed by thousands of module strings. In figure 3.12 a simplified scheme with these two main inverter types is depicted. As one can notice, the central inverter (3.12 a) is connected to two different strings connected in parallel between each other, while each one of the string inverters (3.12 b) is connected to a module string, which afterwards are connected in parallel. In a real case scenario, hundreds and tens of strings might be connected to a central and string inverters, respectively.

For the power conversion to be performed at maximum efficiency, it is crucial to know both the peak power produced by the PV array as well as the maximum AC power that the inverter is able to deliver. The DC to AC ratio or the oversizing ratio is known as the ratio of the solar park peak power $P_{DC}$ to the inverter's nominal AC power output $P_{AC}$ [21], being given by the equation 3.24.

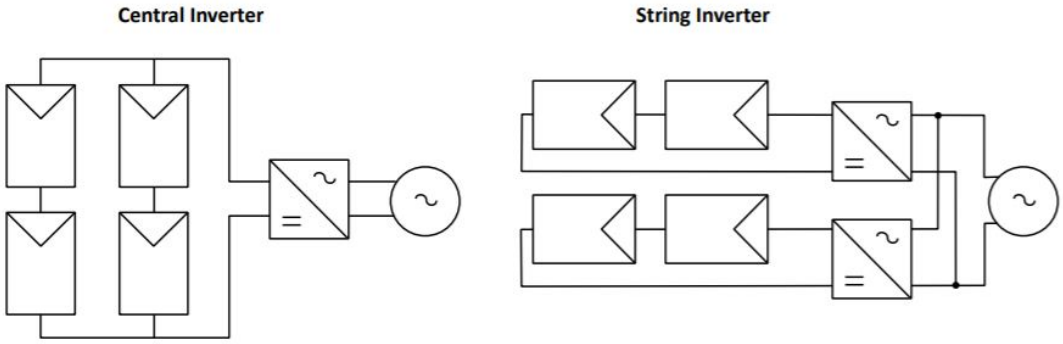


Figure 3.12: Inverter Types [13]

$$P_{inv,ratio} = \frac{P_{DC}}{P_{AC}} \tag{3.24}$$

Since full standard test conditions are rare, the solar PV array doesn't work at its peak power during most of the time, wherefore an oversizing of the PV array in relation to the inverter's AC power rating has shown to be advantageous. Additionally, temperature losses reduce the high power even further, since the modules normally operate at a higher temperature than $25°C$ (STC). In figure 3.13, the purple line depicts the case where the array power doesn't reach the inverter's AC rated power (DC/AC ratio of approximately 1), whereas the green line illustrates the case where the power of the PV array overcomes the inverter AC rated power during a certain amount of time, causing an increase in the inverter AC final power output (reflected in the increase of the area shown in the figure). However, as one can notice, when the PV array is working at its peak power (curve peak), the excess of power attained besides the one corresponding to the inverter AC rated power is clipped. As so, it is important to take these two factors into account when designing a system, particularly in areas where the irradiance might lead to higher DC power output [21]. As values between 1.1 and 1.3 of DC/AC ratio were shown to be beneficial for a higher energy harvesting [19], ahead in the present study these values will be considered when choosing the different modules and inverters.

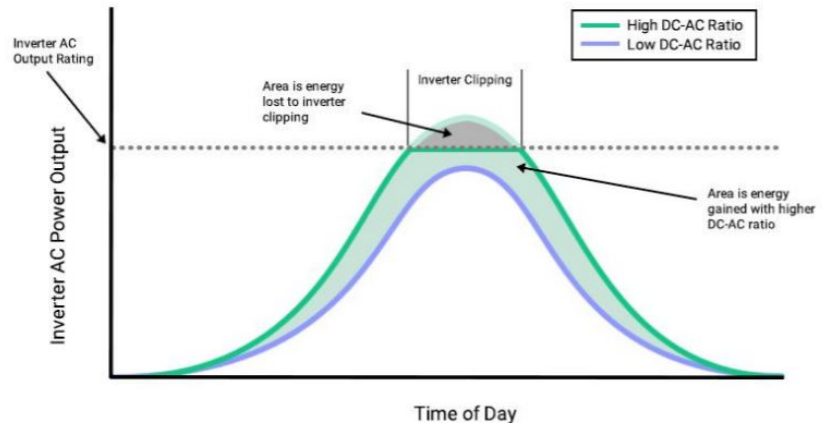


Figure 3.13: Comparison between low and high DC-AC ratio [21]

## 3.4 Tracking Systems

PV modules must be incorporated within a structure to keep them oriented in the right direction and to provide them with structural support and protection from dirt and adverse weather conditions which might lead to a decrease in the efficiency performance. For the solar panel plane to be faced towards the most favorable direction aiming at reducing the incidence angle ($\theta$), different system types might be employed. The mounting structures systems may be either fixed or tracking (fig. 3.14). The choice between the mentioned systems influence both the initial investment and the $O\&M$ costs. The study of both fixed system and horizontal single-axis tracker will be carried out aiming at maximizing the energy yield. Furthermore, an economic analysis will be also undertaken for these two different systems, mainly through the attainment of the levelized cost of energy.

Fixed systems (fig. 3.14, left) keep the modules at a fixed tilt angle ($\beta$) to maximize the annual irradiation they receive. As it will be referred, the "optimum angle" varies depending on what is to be maximized. Since this type of system doesn't have any moving part, PV modules also face a fixed orientation angle, known as azimuth ($\gamma$) as specified in section 3.2. When in the north hemisphere, the solar panels are chosen to be facing south, as this direction provides a larger amount of irradiation to be harnessed. Fixed tilt systems are simpler and cheaper as there are no moving parts, which in turn incurs in a lower investment and maintenance costs.

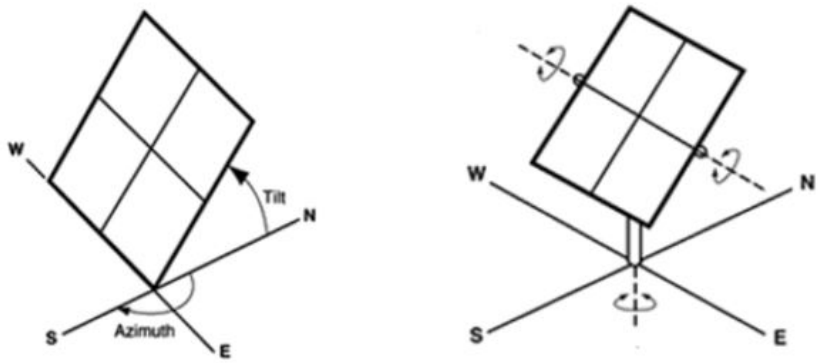


Figure 3.14: Fixed and tracking systems *[Source: Adapted from EIA]*

Tracking systems (fig. 3.14, right), on the other hand, are able to follow the sun and decrease the incidence angle on the collector plane, so that more beam irradiation is harnessed. Depending on the number of degrees of freedom, tracking systems might be of two different types (single-axis tracker or dual-axis tracker). Single-axis trackers are able to rotate around one axis, which in turn might be horizontal (North-South or East-West) or vertical, depending on the angle to vary. The azimuth and tilt angle can be varied through the use of a vertical and a horizontal single-axis system, respectively. The latter one (approached in the study) rotates from east to west on an axis parallel to the ground. On the other hand, a dual-axis tracking system is able to vary both tilt and azimuth angles, providing a more accurate way to follow the sun. As one can expect, this type of system incurs in larger costs (of both investment and maintenance) due to its complexity and moving parts. However, horizontal single-axis trackers make up the most used type of installed capacity worldwide [6].

Horizontal single-axis tracking systems (HSAT) often employ a backtracking strategy, responsible for reducing the beam shading effect coming from adjacent rows when the sun is lower in the sky (sunrise and sunset). Hence, the strategy makes the solar panel plane to be oriented with a lower tilt angle (as shown in figure 3.15 b, which makes the solar modules not to be shaded, in contrast to the case with no backtracking (figure 3.15 a). On the other hand, when employing this strategy, the plane is not directly facing the solar rays (causing an increase of the incidence angle), which in turn results in a decrease on the received beam component. The difference while using or not backtracking will be studied ahead as well.

(a) HSAT with no backtracking

(b) HSAT with backtracking

Figure 3.15: No-Backtracking vs Backtracking [7]

## 3.5 System Sizing

In an early stage of a project, the PV solar park must be sized according to initial given data so that it is capable of meeting the required demand. Sizing a PV system is the basis for the electrical design and allows one to establish the major components sizes and ratings needed to meet the requirements while aiming for the best performance. Depending on the type of system and on the demand, the choice of solar modules and inverters varies. In this study, the system will be connected to the grid and the ground area in which it is to be installed is limited (explained in more detail in chapter 4). Therefore, both maximum installed power and specific area are given, being mandatory for the system to comply with these initial requirements. The undertaken steps aiming at the system sizing are presented ahead.

The power to be installed must be taken as a priority, since one has to make use of all of the installed capacity to achieve the maximum energy output. Thereby, when the solar park peak power ($P_{DC}$) to be installed is known as well as the power of the PV module ($P_{mod,\mathrm{STC}}$) to be used, one may compute the total number of required modules:

$$N_{mod} = \frac{P_{DC}}{P_{mod,\mathrm{STC}}} \tag{3.25}$$

Standard test conditions are a mean to measure the electric output performance of PV modules in a standardized way, enabling one to relatively compare every module between each other. Knowing the total capacity to be installed, the inverter to be employed can be sized, depending on the chosen DC/AC ratio, already stated in section 3.3.3.

The maximum and minimum operating module voltages are crucial to compute the number of modules in series in a system since, when connected in series, the voltage adds up (section 3.3.2).

The maximum and minimum voltages are attained at the minimum and maximum temperatures, respectively. The module maximum open circuit voltage ($V_{oc,\text{MAX}}$) and minimum maximum power point voltage ($V_{mp,\text{MAX}}$) are given by:

$$V_{oc,\text{MAX}} = V_{oc,\text{STC}} - \alpha(T_{min} - T_{ref,\text{STC}}) \tag{3.26}$$

$$V_{mp,\text{MIN}} = V_{mp,\text{STC}} - \alpha(T_{max} - T_{ref,\text{STC}}) \tag{3.27}$$

where $\alpha$ is the voltage temperature coefficient ($V_{oc}/^{\circ}C$), $V_{oc,\text{STC}}/V_{mp,\text{STC}}$ is the open circuit voltage/maximum power point voltage at standard test conditions, $T_{min}/T_{max}$ is the minimum/maximum (winter/summer) design cell temperature and $T_{ref,\text{STC}}$ is the reference temperature at STC (25$^{\circ}C$). For most European countries, the minimum and maximum temperatures typically used are -10$^{\circ}C$ and 60$^{\circ}C$, respectively. Using the maximum (3.26) and minimum (3.27) voltage together with the maximum and minimum inverter DC input voltage, one can compute the maximum ($N_{s,\text{MAX}}$) and minimum ($N_{s,\text{MIN}}$) number of modules in series:

$$N_{s,\text{MAX}} = \frac{V_{inv,\text{MAX}}}{V_{oc,\text{MAX}}} \tag{3.28}$$

$$N_{s,\text{MIN}} = \frac{V_{inv,\text{MIN}}}{V_{mp,\text{MIN}}} \tag{3.29}$$

where $V_{inv,\text{MAX}}$ is the inverter maximum DC input voltage and $V_{inv,\text{MIN}}$ the inverter minimum input voltage. As the current increases with solar modules connected in parallel, the same logic can be applied when computing the number of strings in parallel ($N_{p,\text{MAX}}$), bearing in mind that the maximum PV current must not exceed the maximum inverter input current. Hence, the expression that gives the number of strings in parallel to install is given by:

$$N_{p,\text{MAX}} = \frac{I_{inv,\text{MAX}}}{I_{mp,\text{STC}}} \tag{3.30}$$

Besides the module and inverter sizing, it is fundamental to size the cables connecting the components so that the system is able to stand the maximum currents and voltages.

## 3.6 Energy Yield Performance

### 3.6.1 Performance Analysis Parameters

In the majority of the cases, it is imperative that the system performs as planned in the design phase so that there is the maximum return on investment. One can draw upon specific standard measures to predict the performance of a solar PV park. Next, some of the used parameters also obtained through PVSyst software will be addressed [30], as they are significant for the analysis of the results presented ahead in this study.

- **Reference System Yield ($Y_r$)** - The reference yield is the total in-plane irradiation $H_t$ divided by the PV's STC irradiance $G_0$ [5].

$$Y_r = \frac{H_t(Wh/m^2)}{G_0(W/m^2)} \quad (h) \tag{3.31}$$

- **Array Yield ($Y_a$)** - It is given by the ratio of produced DC energy to the peak power of the PV array.

$$Y_a = \frac{E_{DC}}{P_{DC}} \quad (h) \tag{3.32}$$

- **Final System Yield ($Y_f$)** - It is defined as the ratio of AC energy output (inverter output) to the peak power of the PV array.

$$Y_f = \frac{E_{AC}}{P_{DC}} \quad (h) \tag{3.33}$$

- **Performance Ratio ($PR$)** - Evaluates the efficiency of a PV park and it is not directly dependent on the irradiation or plane orientation, wherefore it may be used to compare different installations at different sites. The PR is the ratio between the effectively produced energy and the energy that would be produced if the solar panel works at its nominal efficiency (STC).

$$PR = \frac{Y_f}{Y_r} = \frac{E_{grid}}{H_t \times A \times \eta} \tag{3.34}$$

where $\eta$ and A correspond to the efficiency under STC and panel area.

### 3.6.2 Losses

The conversion process from solar irradiation to available energy to be injected into the grid comprises several stages in which energy losses are inherent. This section presents the main losses along the process responsible for hindering the performance of the PV system. The losses can be divided in array capture losses and system losses, each one of them including different stages in the conversion process, as presented next in more detail.

#### 3.6.2.1 Array collection losses

Array collection losses refer to the sum of the losses since the energy in the irradiation is collected by the PV modules until it reaches the inverter. Consequently, it includes shading, non-ideal angle, irradiance loss, thermal behaviour, dirt (soiling), mismatching and DC cables losses. The thermal loss stems from the higher temperature at which the modules work when compared to STC conditions ($25°C$), which has a high influence in the voltage output as described in the section 3.3.2. Ahead in this section, the shading will be explained in more detail as well as the mismatching and cable losses. Array collection loss is given by the difference between the array and reference yield:

$$L_c = Y_r - Ya \tag{3.35}$$

- **Mismatch Losses** refers to the imbalance in current or voltage across modules in a string or between strings feeding into one MPPT. The connected modules might behave differently depending on the soiling, ageing or partial shadings, leading to a mismatch between their IV curves. The current output of a string is limited to the current of the lowest performing module and different strings connected in parallel may also have different voltages' outputs, which may arise, for instance, from diverse string wire length (specially in systems in which central inverters are employed). String inverters, on the other hand, only allow a few strings to be connected to one MPPT, which make them to stand out when compared to central inverters due to their ability of reducing this type of losses. Mismatch losses were considered while running the PVSyst simulations.

- **Array Incidence Loss**, also designated for IAM (incidence angle modifier), corresponds to the ratio of the irradiance reaching the PV cell's surface to the irradiance under normal incidence. Therefore, the bigger the incidence angle ($\theta$) the higher the losses will be due to reflections and absorptions on the solar panel's glass cover. The transmission loss stems from the reflections and transmissions of the Sun's ray through the various materials' interfaces (air-glass, glass-EVA and EVA-cell), as it is pictured in figure 3.16. This phenomenon obeys to Fresnel's Laws at the interface of two transparent materials of different refraction indexes n1 and n2 [24]. The Fresnel's laws are applied along the different materials' interfaces, allowing to calculate the irradiance effectively reaching the cell's surface.

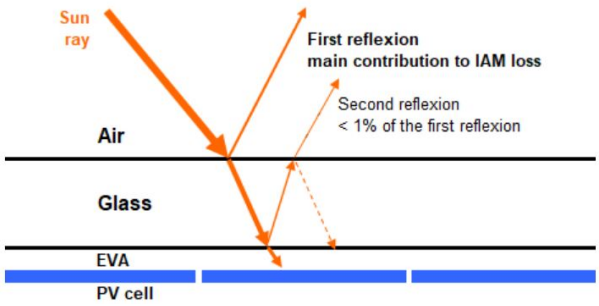


Figure 3.16: Solar panel layers' scheme and transmission loss

- **Soiling Losses** encompasses the dirt that accumulates on the solar panels, influencing the solar park performance. The degree of dirt depends on the site meteorological conditions and on the type of environment in which the system is included in. The accumulation of dust and other particles on the solar panels and frames represent one cause of a performance diminishing. In spite of not existing a definitive answer relative to dirt losses, a 3% loss was considered while performing all the simulations.

- **Shading** is one crucial factor to consider and foresee while designing the PV power plant, as it has a significant influence in the final annual energy yield. There exist two different types of shading: far shadings and near shadings. Far shadings refer to shadings produced by objects sufficiently far (ten times the PV park size) from the PV park as, for instance, the horizon line. Therefore, the shading impact that these objects create are considered to act in the PV park in a global way. On

the other hand, near shadings refer to shadings produced by near objects (buildings, trees). In this study, near shadings are meaningful for the optimization and design phase in the extent that in a utility-scale PV park, as there are many modules to be installed, the shading coming from adjacent rows (also called sheds) might have a significant effect. Consequently, the system has to be designed (ahead in the section 4) according to the location where it is inserted.

Shading losses stem from all the different types of incident radiation: beam, diffuse and albedo. For all the shading losses to be assessed during the simulation, each mentioned component has to be treated in a proper way. For the beam component, a shading factor is defined depending on the sun position. The shading factor is given as the shaded fraction of the PV array, ranging between 0 (no shading) to 1 (fully shaded). The shadows produced on the field (and the calculation of the shading factor) are computed geometrically and analytically, being this an exact calculation. PVSyst is able to build a shading factor table for different positions of the Sun (azimuth and height), from which every value can be obtained through an interpolation.

Concerning the diffuse component, a factor is defined as an integral over all sky directions, which will result in a shading factor for diffuse. This shading factor is only dependent on the geometry of the system, whereby it is calculated in the beginning of the simulation and subsequently applied at each time step. For tracking systems, the shading factor is recomputed for each position of the trackers. Even though there are no mutual shadings on the beam component when employing the backtracking strategy, the shading loss on the diffuse might be relevant. The diffuse component makes up approximately 50% of the yearly available incident irradiation in middle Europe and more than 30% in more sunny situations [25], contributing significantly for the shading factor on diffuse. Lastly, for the albedo component, an integral depending on the near obstacles on the ground is performed, which will also result in a shading factor (independent on the sun position). Hence, each component has an associated shading factor that contributes for a decrease in the irradiance that subsequently hits the collector plane.

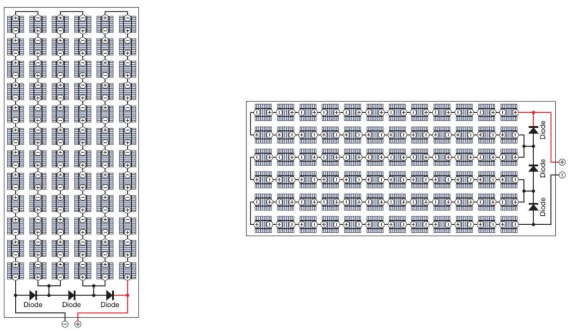


Figure 3.17: Portrait (Left) vs Landscape (Right) with 3 bypass diodes

As the modules inside are divided in strings of cells (connected through bypass diodes), its arrangement might significantly influence the final energy yield, as one will see ahead. In figure 5.3, 72-cells modules with 3 by-pass diodes (as the one used in this study) is presented as well as the two different possible arrangement of solar panels (portrait vs landscape).

Two different types of losses might be observed while designing a PV system: irradiance linear losses and electrical losses. Irradiance linear losses correspond to the linear shadings visible in the solar panel plane, with no influence in the system electrical circuit. On the other hand, electrical losses refer to the mismatch of electrical output from the modules connected in series and strings connected in parallel, since the total current in a string always corresponds to the module lowest produced current present in that string. According to Mermoud [25], when two or more strings are connected on the same MPPT (which is the case in a central inverter), the production of one string is almost completely lost if one third of the sub-modules gets shaded. As depicted in figure 3.18, if there exists only one string connected to the MPPT, the system takes advantage from the by-pass diodes (when disposed in landscape), limiting the losses only to approximately one third. However, from the moment when two or more strings are connected together in parallel, the losses increase significantly. From the chart, it is possible to conclude that 80% represent the diffuse part which is supposed not being affected by the shades on beam.

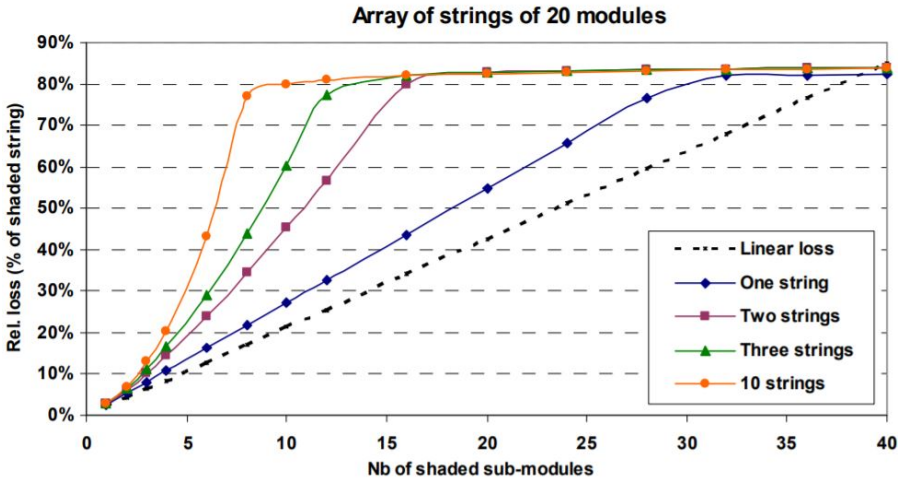


Figure 3.18: Relative loss for different number of strings connected to one MPPT [25]

- **DC Cables** should be sized so that in STC the voltage drop is as low as possible (typically in the order of 1% and 3% for DC and AC cables respectively, according to a German standard [10]). The larger the cable section, the lower the voltage drop will be. A high voltage drop would result in a possible mismatch between the PV modules voltage and the MPPT voltage range, which in turn could result in a poor performance of the latter one. Therefore, during the simulations, a 1% and 3% loss fraction was considered for DC and AC cables, respectively (at STC). Ahead in the study, the cable sizing will be carried out.

#### 3.6.2.2 System Losses

The inverter, as mentioned in section 3.3.3, is responsible for converting DC to AC power, adding losses to the system as well. It is represented by the difference of the array output energy and the useful system energy after having passed through the inverter:

$$L_s = Y_a - Y_f \tag{3.36}$$

- **Inverter and MPPT** account for a significant contribution of the overall losses of the system. As mentioned in section 3.3.3, the MPPT searches for the maximum power point present in the IV curve, which is constantly varying depending on external factors as the irradiance, temperature, shading, mismatch or ageing. Hence, as the MPPT is continuously iterating around the maximum power point, there exist time intervals in which this device is not working at its maximum efficiency, contributing for the overall losses. The losses stemming from the maximum power point tracking and from the DC/AC conversion are given by:

$$\eta_{tr} = \frac{P_{MPPT_{out}}}{P_{array_{out}}} \tag{3.37}$$

$$\eta_{conv} = \frac{P_{inverter_{out}}}{P_{MPPTout}} \tag{3.38}$$

where $P_{array_{out}}$, $P_{MPPT_{out}}$ and $P_{inverter_{out}}$ represent the maximum instantaneous power drawn from the array, the instantaneous real power and the AC output power, respectively. The static efficiency must take into account the both previous expressions:

$$\eta_{inv} = \eta_{tr} \times \eta_{conv} \tag{3.39}$$

## 3.7 Financial Performance

As there exist several stakeholders and substantial investments involved on this type of projects, the viability of a long-term solar PV plant must be evaluated based on its financial prospects. Project financing is only practicable when enough revenues capable of covering the costs are generated through electricity production. Hence, before proceeding towards further costly steps, a financial analysis must be carried out. Throughout this section, the main financial indicators will be introduced [20].

- **Levelized Cost of Energy (LCOE)** is the cost per unit of electricity produced during a given time period (hour, day, month, year or solar PV park lifetime):

$$LCOE = \frac{C_T}{E_a} = \frac{C_F + C_V}{E_a} = \frac{C_F + cE_a}{E_a} \quad (€/MWh) \tag{3.40}$$

where $C_T$ is the total annual cost (€) given by the sum of the current annual fixed cost ($C_F$) and annual variable cost ($C_V$). In a solar PV power plant, there is no variable cost, as there are no fuels involved. The fixed cost ($C_F$) include both the initial investment ($I_0$) and the fixed $O\&M$ costs over the power plant lifetime. The former one can be written in function of a constant annual payment over the project's lifetime ($A_T$):

$$I_0 = A_T \sum_{j=1}^{n} \frac{1}{(1+r)^j} = A_T \frac{(1+r)^n - 1}{r(1+r)^n} \quad (€) \tag{3.41}$$

In the previous equation (3.41), $r$ and $n$ are the minimum expected rate of return and the project's lifetime to be considered, respectively. Summing both the annuity payment (which can be easily written in function of the investment based on the equation 3.41) and the fixed $O\&M$ (which is assumed to be proportional to the investment per unit of power by a factor $\beta$), one can obtain the fixed annual generation cost per installed unit of power:

$$C_F = \left( \frac{r(1+r)^n}{(1+r)^n - 1} + \beta \right) I_0 \quad (€/MW) \tag{3.42}$$

- **Net Present Value (NPV)** criteria is used to evaluate the profitability of a project and it is defined by the difference between the discounted incomes and the discounted outcomes over the project lifetime:

$$NPV = \sum_{j=1}^{n} \frac{Inc_j}{(1+r)^j} - \sum_{j=0}^{n} \frac{Out_j}{(1+r)^j} \tag{3.43}$$

  where the incomes $(Inc)$ stem from the electricity sales and the outcomes $(Out)$ arise mainly from the investment and $O\&M$ costs. Drawing upon the obtained result stemming from the equation 3.44, different inferences might be obtained:

  - **NPV > 0** - Economically profitable project. The investment is recovered, the minimum rate of return is reached and a surplus is obtained.
  - **NPV = 0** - Feasible project. The investment is recovered and the minimum rate of return is achieved. However, the profitability is not clear.
  - **NPV < 0** - Not profitable project.

- **Internal Rate of Return (IRR)** is the discount rate that makes the net present value (NPV) equal to zero. Hence, if $IRR > r$, the project is economically viable. This criteria relies in the same formula as NPV, given by:

$$0 = \sum_{j=1}^{n} \frac{Inc_j}{(1+IRR)^j} - \sum_{j=0}^{n} \frac{Out_j}{(1+IRR)^j} \tag{3.44}$$

# Chapter 4

# Method

The developed method to analyze and solve the problem at stake will be outlined throughout this chapter. The method comprises different phases along which the different devices to employ and the chosen parameters will be tested. Initially, simulations are carried out to conclude about the modules and inverters to employ as well as the number of modules in series and strings in parallel. Afterwards, both fixed tilt and single-axis tracking systems will be optimized, which may be achieved through the variation of parameters that significantly influence the variable to study. Along the diverse simulations performed for fixed tilt and single-axis tracker, chosen parameters are varied within an interval range aiming at maximizing the energy yield. Additionally, the method includes an economical analysis, where every case will be compared based on the levelized cost of energy. The PV park layout is performed considering the constraints and terrain topography, which might have an influence in some parameters, as it is specified along the next chapter.

The main software used along the study was PVSyst as it possesses the features to develop PV solar parks' desktop studies. Thereby, PVSyst software is focused on the design, simulation, and data analysis of PV systems, allowing one to run several simulations while considering different parameters and compare the various results stemming from them. This software is capable of evaluating the performance of grid connected, stand-alone and pumping systems. Simulations were carried out for both fixed tilt and single axis-tracker systems (as well as portrait and landscape arrangement), having each one been tested while employing central and string inverters, as explained over this section in further detail.

Regarding the inverter selection, only central inverters were initially regarded as they influence the number of sub-arrays in which the solar PV park is divided due to their maximum allowed input power that must not be surpassed. After the system electrical connections and the solar panels disposition have been decided, the optimized energy yield was obtained and an economical comparison between the different cases (fixed tilt and single-axis with portrait and landscape configuration) was carried out to select the most profitable one. The string inverter was also subsequently tested for fixed tilt and single-axis as well, having the energy yield been obtained and compared relatively to the case of the central inverter. Lastly, AutoCAD was used to organize and dispose the solar modules throughout the available

area, complying with the plant restrictions and with the terrain topography. Thus, the terrain slope was taken into account, which might improve the sheds' organization and layout over the PV field.

As the simulation outputs strongly depend on external factors, PVSyst must use reliable meteorological data that is required to provide (at least) the horizontal global irradiation and average external temperature. The software has a built-in database holding a total of 8325 weather stations worldwide from Meteonorm 7.2. If the nearest site is more than 10km away (in Europe), a mixture of ground and satellite information is used. However, if ground measured radiation in not available in a range of 50km (Europe), only satellite data is used. Additionally, one can import data from external sources such as PVGIS (Photovoltaic Geographical Information System) and Nasa-SSE (Surface Meteorology and Solar Energy programme). PVGIS relies on data acquisition from different satellites (0.025º accuracy) covering Europe, Mediterranean basin, Africa and South-West Asia, while Nasa-SSE relies on satellite data (1º accuracy) covering all the world surface [3]. Meteonorm 7.2 was used to perform the simulations throughout the project as it is considered the most reliable source. All the three mentioned sources provide monthly data that must be converted to hourly meteorological data through stochastic models, as PVSyst operates only with hourly values. PVSyst also incorporates a 3D CAD design window to represent the near shading effects, which might be relevant to reckon with to obtain reliable simulation results.

## 4.1 PV Modules and Inverter Selection

In an early stage of this study, it is prominent to decide the main devices to employ so that the simulations may be performed with a particular type of configuration, which subsequently allows other parameters of interest to be tested. The next three sub-sections (4.1.1, 4.1.2 and 4.1.3) describe the path taken to select the central and string inverters to employ as well as the number of modules in series and strings in parallel able to provide the system with a higher performance capability. Besides the type of central and string inverter to employ, the quantity was also varied as it also influences the park performance as well as the investment and maintenance costs. Along this section, the system parameters (tilt angle, pitch and modules disposition) remain constant, as the goal is to carry out simulations combining all the initial considered devices to be possibly employed.

### 4.1.1 Central Inverter

Initially, the number of sub-arrays (number of arrays in which the total PV park is divided) must be chosen, which subsequently influences the type of module and inverter to select. The central inverter to be used hinges on the total power of each sub-array and on the deemed $P_{inv,ratio}$ interval (equation 3.24). The central inverter minimum and maximum power for each case may be found based on the inverter maximum and minimum $P_{inv,ratio}$ (equation 3.24) respectively, given by:

$$P_{min,inverter} = \frac{P_{subarray,\mathrm{STC}}}{P_{inv,max,ratio}} \tag{4.1}$$

$$P_{max,inverter} = \frac{P_{subarray,\text{STC}}}{P_{inv,min,ratio}} \tag{4.2}$$

where $P_{subarray,\text{STC}}$ (sub-array installed DC capacity in STC) varies depending on the number of sub-arrays. The $P_{inv,max,ratio}$ and $P_{inv,min,ratio}$ refer to the considered inverter maximum and minimum $P_{inv,ratio}$, respectively. If $P_{inv,ratio}$ is higher than the chosen $P_{inv,max,ratio}$ value for the project, the system is undersized since the inverter AC power would decrease, which in turn could lead to a premature power clipping. On the other hand, if $P_{inv,ratio}$ is lower than the chosen $P_{inv,min,ratio}$ value, the system would be oversized. As so, an interval between $P_{inv,min,ratio}$ and $P_{inv,max,ratio}$ is required for the inverter power intervals to be found, which in this study was decided to be within 1.1 and 1.3, respectively [19]. Once the number of sub-arrays to test is known and the $P_{inv,ratio}$ interval range is decided, the initial available central inverters can be selected. Hence, the number of sub-arrays and the $P_{inv,ratio}$ interval may be varied, leading to the choice of central inverters to use. Additionally, the maximum ground area of one sub-array for each case in which a different number of sub-arrays is considered can be easily obtained through the following equation:

$$A_{sub-array} = \frac{A_{ground}}{N_{sub-arrays}} \tag{4.3}$$

where $A_{ground}$ is the total available PV park area. This equation refers to the maximum area as it considers the total available area to be divided in equal parts, which may be not entirely true since each sub-array might occupy a smaller area depending on the values the parameters take as it will be shown ahead.

Once the PV modules and available central inverters are selected, the goal is to carry out several simulations in which all of these two types of devices are combined with each other, aiming at concluding regarding the performance of each combination. Thereby, for each case where a different number of sub-arrays is considered, all modules will be matched with all available inverters (already selected based on the inverter power ratio) under the same conditions, meaning that no other parameter is varied. The module/inverter combination to select depends on the selected variable to maximize or minimize, which should be identified in the beginning of the project.

### 4.1.2 Series/Parallel Connections

Similarly to the previous approach to select the best module/central inverter combination to be used, one must conclude about the number of modules and strings to connect in series and parallel, respectively. The minimum and maximum number of modules to connect in series hinges on the site maximum and minimum temperature as well as on the minimum and maximum inverter input voltage. If the minimum temperature is higher, the voltage output stemming from one string will be lower (section 3.3.2), which in turn will enable more modules to be connected in series for the same inverter maximum input voltage. For all the possibilities of modules in series and strings in parallel to be tested, several simulations need to be carried out. Once the possible interval of modules to connect in series is chosen

(based on the inverter voltage input interval), the number of strings to connect in parallel can also be deduced, always complying with the fact that the nominal power must not be surpassed and that the inverter power ratio must always be within the initial set interval. Additionally, the inverter maximum input current limits the maximum number of strings to connect in parallel.

### 4.1.3 String Inverter

As the power of a string inverter is much lower in comparison to a central inverter, the solar park does not need to be splited in several high power sub-arrays. In contrast, each string inverter is connected to a few strings over all the PV park, which will also result in many more inverters. Hence, the strategy to follow when selecting the string inverter to be used is slightly different from the one used for the central inverter. When employing string inverters, the maximum capacity to be installed as well as the $P_{inv,ratio}$ interval must be also taken into account.

In this case, simulations are also performed for every combination of module and string inverter. Furthermore, each of these combinations is simulated taking into account a different number of inverters (always complying with the $P_{inv,ratio}$ interval) to perceive the output difference, which is useful to conclude if the initial investment is worth the additional energy produced.

## 4.2 Fixed Tilt

Along this section, the undertaken stages related to the fixed tilt system analysis will be described. The fixed tilt layout may be presented in PVSyst software through the "unlimited sheds" feature, as in a utility-scale PV park the sheds are very long when compared to their width, which makes it possible to disregard the edge effects. The sheds arrangement are mainly characterized by the collector width (W), pitch (P) and tilt angle ($\beta$), being this nomenclature presented in figure 4.1. The pitch refers to the distance between sheds (rows) and the collector band width refers to the width of the shed (if two modules are in portrait configuration the width will be two times the length of the solar panel).

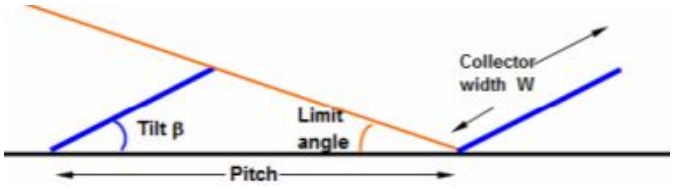


Figure 4.1: Sheds scheme [25]

The shading limit angle ($\theta$) is the angle from which shadow starts to be produced on the next shed (figure 4.1). There is no optimum value for this angle but often one considers the worst case scenario (December $22^{nd}$) for mutual shadings to be minimized. For a given shading limit angle, the pitch is computed by the software so that no shadings are produced on the solar panel plane, which may be calculated through the equation 4.4. The variables P, W, $\beta$ and $\theta$ represent the pitch (distance between sheds), width, plane tilt and shading limit angle, respectively. Ahead in the layout section (4.4), a more

detailed overview will be presented concerning the pitch calculation considering sloped terrain as well.

$$P = W\left(cos(\beta) + \frac{sin(\beta)}{tan(\theta)}\right) \tag{4.4}$$

The ground cover ratio (GCR) is one of the foremost parameters to regard while designing a PV park, being given by the ratio of the modules sensitive area to the ground total area occupied by the PV park. Considering the total available ground area and the total modules sensitive area, the minimum GCR can be computed through the equation 4.5.

$$GCR = \frac{A_{modules}}{A_{ground}} \tag{4.5}$$

As the ground area to be used must not be surpassed, the GCR to obtain must not be lower than the value stemming from the equation 4.5, if the available area is to be totally occupied. However, as mentioned, the goal is to occupy the area up to which there is no big variation in the energy yield, which might be smaller than the given initial area. The ground cover ratio may also be presented through the ratio of the width to the pitch (equation 4.6), which gives the "real" ground cover ratio used in the design of PV parks, as it is based on the shed parameters and not on the initial available area (as in the equation 4.5). Hence, based on the obtained ground cover ratio (equation 4.6), one might conclude about the initial area that will be definitely required to dispose all the solar modules.

$$GCR = \frac{Width}{Pitch} \tag{4.6}$$

In a fixed tilt system, if the tilt angle increases, the ground cover ratio decreases significantly (if the shading limit angle is considered to be constant). The mentioned relation (4.6) is also valid for single-axis tracking systems, as it will be presented in section 4.3.

### 4.2.1 Portrait vs Landscape

At first, the solar panels' disposition was studied taking into account two different possible solar panels' arrangement: portrait and landscape. It is important to highlight that shading is a factor to consider when optimizing a PV array, as the beam component has influence in the electrical shading part of the system. Thereby, the electrical effect hinges on the module arrangement (portrait vs landscape) and on the sub-modules (defined in section 3.6.2.1) of the employed solar panel (3 by-pass diodes in this case). Hence, several simulations were performed varying the plane tilt angle for these two different arrangements, allowing one to conclude about the shading impact on each case individually.

### 4.2.2 Plane Tilt and Pitch

When employing a fixed tilt system, the annual energy yield and performance ratio strongly depend on both pitch and plane tilt, as they influence the incident irradiation and shading in the collector plane. The figure 4.2 includes two different charts obtained through an initial sensibility analysis to

perceive the influence of the tilt angle and pitch on the grid energy and performance ratio. This figure presents the results in per unit scale. As aforementioned, the tilt angle that leads to the maximum energy yield is often not equal to the site latitude (as assumed in several studies) but lower than this value, due to the mutual shading effect. The nominal energy curve presented in the graphic depicts the energy that would be produced if the solar panel works at its nominal efficiency (STC).

As depicted in figure 4.2 (a) the angle that would lead to a maximum energy yield (without considering shading effects) is 34º whereas a plane tilt of 29º would lead to a maximum value of energy injected in the grid, supporting what was mentioned before. Regarding the performance ratio, one can see that the maximum value is given for the minimum tilt angle, which supports that the optimal system hinges on what is to be maximized. For this specific case, when there is an increase of the tilt angle, the global incident irradiation will increase significantly. As in the summer the sun is higher in the sky, the annual irradiance increases, which makes the grid energy to increase when there is decrease of the solar panel tilt angle. Thus, an increase of the tilt angle will cause the solar panels to receive a lower amount of annual irradiance and, consequently, a degrading of the performance ratio. Along this study, the grid energy was the foremost output to maximize and the costs were subsequently analyzed aiming at their reduction.

In figure 4.2 (b), the energy yield and performance ratio are presented in function of the pitch variation. As expected, the closer the sheds are placed, the lower the energy that is injected in the grid due to shading effects. However, after a certain pitch value, the $E_{grid}$ tends to become steady. In this case, as the global incident irradiation is accompanied by a shading decrease, the performance ratio has a similar behaviour to the grid energy variation.

If one wants to maintain a constant shading limit angle, both tilt angle and pitch are dependent on each other. Thereby, if the pitch increases, the plane tilt must also increase (up to a certain optimum). In this study, the limit angle was set to 18º for no shadings to occur approximately between 9h and 16h on the December 22nd (as will be shown ahead in the solar chart present in chapter 5). The combination of pitch and tilt angle that leads to the highest energy yield is associated with a specific ground cover ratio, which may be obtained based on the width and pitch (as given in equation 4.6). The GCR together with the modules area to be installed makes it possible to compute the needed ground area (equation 4.5) to place every module, allowing one to conclude about the initial available area that won't need to be occupied. Afterwards, several simulations have been performed considering a range of intervals for both tilt and pitch to verify that after the chosen optimal parameters' values, the energy yield percentage difference does not vary significantly (section 5).

### 4.2.3 Azimuth

In the northern hemisphere, it is common for the plane to face south (0º azimuth angle) to receive the maximum amount of irradiation. The azimuth angle is an important parameter to take into account in both fixed tilt and single-axis tracking systems. Simulations varying the azimuth angle were carried out to show and prove the best orientation the solar panels should face.

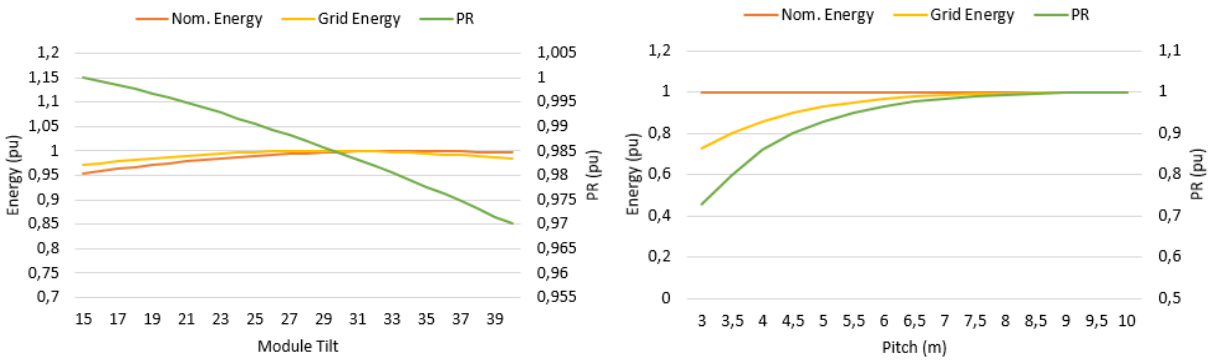


(a) Energy Yield/PR vs Tilt Angle

(b) Energy Yield/PR vs Pitch

Figure 4.2: Energy yield and PR variation with the tilt angle and pitch (Fixed tilt)

## 4.3 Single-Axis Tracker

The procedure followed for the energy yield maximization of the single axis-tracking system is introduced throughout this section. The trackers are aligned along the east-west direction (following the movement of the sun) and the axis of rotation is oriented along north-south direction. The influence of the backtracking strategy on the energy yield is tested as well as the effect of the pitch between rows.

### 4.3.1 Backtracking vs No Backtracking

When using single-axis trackers, near shadings have always to be considered when employing or not the backtracking strategy (section 3.4). In the former case (with backtracking), instead of tracking the sun aiming at decreasing the incidence angle (without backtracking), these will adopt a lower angle (in the morning and evening) to avoid beam mutual shadings, which also makes the incidence angle to increase. Thus, when making use of this strategy, the shading electrical loss effects are reduced but the losses stemming from mis-orientation increase. The factor that might lead one to adopt the backtracking strategy is the lower electrical shading effects (as when a part of a string gets shaded, the full production from that string is affected). Simulations considering both strategies were performed under the same conditions to draw results regarding the best one to employ.

### 4.3.2 Pitch

As in the fixed tilt configuration, the distance between trackers (pitch) highly influences the energy yield. As this is always a crucial parameter to consider in a PV park, simulations were also performed with its variation. After a certain pitch, the energy yield does not vary significantly and the ground cover ratio may be obtained as in the fixed tilt configuration through the equation 4.6. As so, if the width and pitch are known, the "real" ground cover ratio might be found as well as the required initial available area (equation 4.5).

## 4.4 Layout

The solar PV park layout and sub-arrays organization might be carried out using the AutoCAD software, after the simulations' results have been obtained and the main parameters have been defined. Consequently, this is one of the last steps of the study, as it can only be achieved when the option leading to the greater PV park performance has been found. Besides the disposition of the solar modules and inverters throughout the available ground area, electrical schemes including the connections between the different components were carried out for each case (central and string inverters).

Since the terrain topography was provided, a more thorough analysis regarding the sheds disposition was carried out. If the terrain is flat, the pitch might be computed based only on the panel tilt and shading limit angle (equation 4.4). On the other hand, if the sheds are placed on a sloped terrain, the pitch can be reduced for the shading limit angle to remain constant, which in turn makes the occupied area to decrease. In figure 4.3 a scheme including all the relevant dimensions is depicted, which through trigonometry calculations allowed one to find the relation between the sloped terrain angle and the pitch to adopt between sheds.

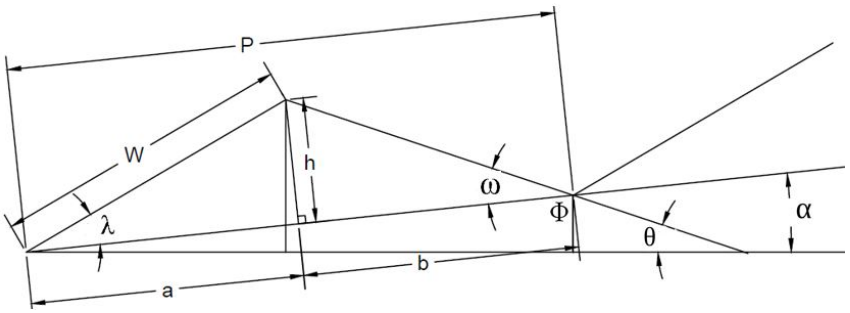


Figure 4.3: Sloped terrain scheme

Initially, both angles $\phi$ and $\omega$ can be written in function of both sloped terrain angle $\alpha$ (obtained through the topography) and shading limit angle $\theta$, as shown in equations 4.7 and 4.8.

$$\phi = 180 - \alpha - \theta \tag{4.7}$$

$$\omega = 180 - \phi \tag{4.8}$$

It is relevant to highlight that the angles $\beta$ and $\lambda$ are the tilt angles the sheds make with the horizontal and sloped plane, respectively. Through trigonometric operations, both dimensions a and b can be found:

$$sin(\lambda) = \frac{h}{W} \Leftrightarrow h = Wsin(\lambda) \tag{4.9}$$

$$cos(\lambda) = \frac{a}{W} \Leftrightarrow a = Wcos(\lambda) \tag{4.10}$$

$$tan(\omega) = \frac{h}{b} \Leftrightarrow b = \frac{h}{tan(\omega)} = \frac{Wsin(\lambda)}{tan(\omega)} \tag{4.11}$$

The pitch can subsequently be computed through the sum of both previously obtained dimensions,

being written as follows:

$$P = Wcos(\lambda) + \frac{Wsin(\lambda)}{tan(\omega)} \Leftrightarrow P = W\left(cos(\lambda) + \frac{sin(\lambda)}{tan(\alpha + \theta)}\right) \tag{4.12}$$

where $\lambda = \beta - \alpha$. As one can verify, if $\alpha$ is zero (flat terrain) and $\gamma = \beta$, the obtained expression is the same as the one presented in equation 4.4. The process of modifying the pitch is valuable when the slope is approximately even, which can also be achieved through construction works in which the soil can be adjusted.

## 4.5 Cable Sizing

Once the system sizing and park layout have been concluded, an estimate of the different cables' length may be performed using AutoCAD, which is relevant for the selection process of the most appropriate ones to employ. Once the cables' length have been estimated through the disposition of solar panels, inverters and transformers over the solar park, a different investment cost might be obtained for each case (central and string inverters with portrait/landscape disposition), which will be useful in the economical analysis presented ahead. The nominal voltage and maximum admissible current intensity in the cable are two crucial factors that must be considered during the cable sizing. In utility-scale PV parks, as the strings are composed by several PV modules in series, one has to ensure that the nominal cable voltage is not surpassed by the open circuit voltage when the system is operating at the site minimum temperature. Additionally, the cable cross section can be sized according to the maximum current intensity that might flow through the cable [10]. According to the European standard IEC 60364-7-712, the string cable must be capable of transporting a current ($I_s$) 1.25 times higher the PV module short circuit current ($I_{sc}$):

$$I_s = 1.25 I_{sc} \tag{4.13}$$

Next, one should size the cables so that the losses are minimized. The power and cross sectional area can be computed through the expressions presented in equations 4.14 and 4.15.

$$P_s = RI^2 \tag{4.14}$$

$$A_s = \frac{l}{R\kappa} \tag{4.15}$$

where $\kappa$, $l$ and R represent the material electrical conductivity, cable length and resistance, respectively. The former one varies depending on whether the cable is made of copper (56 $m/(\Omega.mm^2)$) or aluminum (34 $m/(\Omega.mm^2)$). Regarding the string cable sizing (that connect the solar panels to the string-box) and based on equations 4.14 and 4.15, its cross section area ($A_s$) can be found through the following equation:

$$A_s = \frac{2L_s I_s}{0.01 U_s \kappa} = \frac{2L_s I_s^2}{0.01 P_p \kappa} = \frac{2L_s P_s}{0.01 U_s^2 \kappa} \tag{4.16}$$

where $L_s$, $U_s$ and $P_s$ are the DC string cable length, maximum power string voltage (STC) and string power (STC), respectively. The obtained cross section value must be rounded up to the available standard cable size (2.5 $mm^2$, 4 $mm^2$, 6 $mm^2$). A voltage drop of 1% was considered for the cable sizing for it to be in line with the previously set simulations conditions.

Concerning the main DC cable (responsible for connecting the string-box to the inverter), one must adopt the same European standard as mentioned before, taking into consideration that the current stemming from the strings connected in parallel will be significantly higher. The main DC cable cross section ($A_{DC}$) can be found applying the following equation:

$$A_{DC} = \frac{2L_{DC} I_n^2}{0.01(P_{FV} - P_s)\kappa} \tag{4.17}$$

where $L_{DC}$, $I_n$ and $P_{FV}$ are the main DC cable length, string-box output current and power, respectively. The total line losses ($P_s$) can be calculated through:

$$P_s = \frac{2N L_s I_s^2}{A_s \kappa} \tag{4.18}$$

where N, $L_s$ and $A_s$ represent the number of strings, the string average cable length and the chosen cable cross sectional area. More specifically, each string cable length and cross sectional area can be considered, wherefore an equivalent equation to 4.18 can be written as follows:

$$P_s = \frac{2I_s^2}{\kappa}\left(\frac{L_1}{A_1} + \frac{L_2}{A_2} + \frac{L_3}{A_3} + ...\right) \tag{4.19}$$

The DC cables length should be minimized as the losses are greater when compared with the AC cables [41]. The AC cable establish the connection between the inverters and the transformation station and, for a three-phase system, assuming a maximum voltage of 3% relatively to the transformer input voltage [10], its cross sectional area may be computed through:

$$A_{AC} = \frac{\sqrt{3} L_{AC} I_{AC} cos(\phi)}{(0.03 U_n)\kappa} \tag{4.20}$$

where $L_{AC}$, $I_{AC}$, $cos(\phi)$ and $U_N$ are the AC cable length, the inverter AC nominal current, the power factor and the transformer input voltage (which varies on the type of transformer). Afterwards, the AC medium voltage cables (30kV) responsible for connecting the transformer stations to the sub-station also require to be sized, which can be carried out based on the equation 4.20.

## 4.6 Economic Analysis

Apart from the project technical analysis and optimization, an economical analysis is essential to opt for the most profitable alternative, as the best option is not always the one which provides the

largest amount of energy but the one able to provide the same energy at a cheaper price. The project's economic viability allows the prediction of the project's future success based on different results (mentioned in section 3.7), which need to be computed and analyzed so that a comparison can be carried out between each studied case. For the economical analysis to be correctly performed, it is required to know the cost of each solar PV park component, discount rate, project's lifetime, revenue, maintenance costs and energy produced over the project's lifetime.

As the solar modules do not hold the same performance along the years, the energy yield and consequently, the revenues, decrease over the project's lifetime. Hence, the economical analysis needs to be performed considering the ageing factor, as explained in more detail ahead in the next section (4.6). Over the years, there exists a degradation rate that needs to be taken into account when computing the grid energy in a long-term project for the estimate to be the most reliable as possible. In this case, the main parts subjected to ageing are the PV modules, which loose the energy production efficiency. The PV modules to be used must be analyzed and the expected lifetime as well as their degradation rate should be considered while carrying out the simulations that subsequently influence the economical analysis. Similarly, the inverters lifetime must be considered as it accounts for a significant part of the initial investment. Additionally, if the inverters lifetime does not correspond to the project's lifetime, a replacement is needed, which makes the costs and the LCOE to increase.

Over the years, there exists a degradation rate that needs to be considered when computing the grid energy in a long-term project for the estimate to be the most reliable as possible. In this case, the main parts subjected to ageing are the PV modules, which from time to time need to be repaired. The PV module to be used (Hanwha Qcells QPEAK 370W) is considered to possess 25 years of life span as it is specified in the data sheet presented in annex C, having its degradation been regarded. Both central and string inverters also have a lifetime of 25 years, having been confirmed by Sungrow and Huawei, respectively.

The PV module degradation incurs in an efficiency loss, leading to a decrease of the PV array yield. As shown in the module data-sheet (annex C), there is a graph depicting the relative efficiency of nominal power, which estimates a 83% efficiency after 25 years (which should be taken as a lower limit for an individual PV module [24]). This includes an initial loss of 3% (curve starts in 97%) from light incidence degradation (LID) caused by the presence of oxygen inside the molten silicon during its production process which, under the first hours of light exposition, may create complexes with boron acceptors. In turn, these complexes (boron-oxygen) create unwanted energy levels, which might capture electrons and holes that won't be used for the real PV effect. In addition to the LID, the annual degradation factor (assumed to be constant over the years) is estimated (by the manufacturer) to be 0.6%/year, given by the curve slope.

During the simulations, an average degradation rate for a set of modules was used, which (in accordance with information provided by the software) possess a significantly lower value (around 0.3% based on experimental studies with old technologies) than the degradation limit provided by the manufacturer for a single model (0.6%/year). As so, an average degradation factor of 0.4%/year was used while performing the simulation instead of the lower limit provided by the manufacturer. Besides the

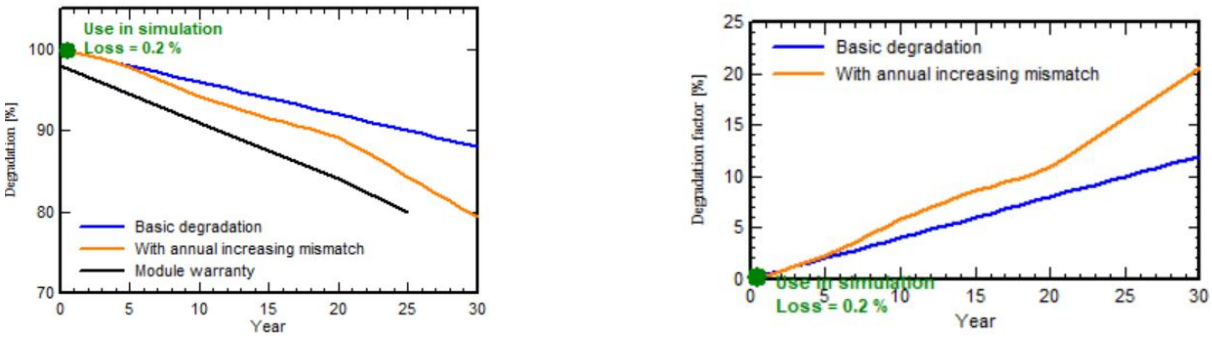


(a) Degradation

(b) Degradation factor

Figure 4.4: PV Modules Degradation and Degradation Factor [*Source: PVSyst*]

degradation rate, the losses arising from the mismatch between modules were estimated by PVSyst (through the Monte Carlo method), as they do not degrade at the same rate. In figure 4.4 (a) the linear module warranty (given by the manufacturer) is given in black and the aforementioned linear average degradation (0.4%/year) is given in blue. The orange non-linear curve (resulting from the Monte Carlo method) includes the mismatch losses that increase over the years, being the one used in the simulation.

# Chapter 5

# Results and Discussion

The present chapter provides an introduction to the case study proposed by Sotécnica, with whom this project is being developed with. In particular, an overview concerning the site features and project specifications provided by the company will be described. Sotécnica is a technological company that belongs to the VINCI-Energies group, possessing several other associated companies (Axians, Actemium, Omexom and VINCI Facilities). Sotécnica ensures the project and execution of electric installations, integrated security, surveillance systems, gases detection, transformation substations, integrated telecommunications and fluids networks as well as renewable energies installations. The present study is included in the scope of the latter one as it aims at the energy yield maximization of a utility-scale solar PV power plant.

Apart from the project description, the main technical and economical results obtained throughout the study will be presented. The project's technical part is based on simulations performed only for the first year of operation, as it provides satisfactory data to conclude about the optimal parameters' values. On the other hand, the economical results consider 25 years of project's lifetime, since the performance decreases throughout time, which in turn will produce an impact on the energy output.

The results of both fixed tilt and single-axis systems will be introduced in line with what was described over the chapter 4. The initial simulations were useful to conclude about the modules/inverters combinations leading to a greater energy yield performance. Once the inverters and modules to employ were defined, simulations (for fixed tilt and single-axis tracking systems) aiming at optimizing the parameters outlined in the previous chapter have been carried out. It is important to highlight that the parameters optimization was made while employing the selected central inverter. However, after the system has been optimized, simulations using the chosen string inverters have been performed (also for fixed and single axis tracker) to conclude about the energy yield drawn from the system in this case. In total, twelve different cases were analyzed since each type of inverter (three in total) has been analyzed with both portrait/landscape configuration and fixed tilt/single-axis tracking systems. Lastly, these twelve different cases will be economically assessed mainly through the levelized cost of energy, as it accounts for both energy yield as well as initial investment and O&M costs.

## 5.1 Project Description

The solar park is to be constructed at a given place in Portugal. There are 47.88 hectares (478 800 $m^2$) available to be preferably occupied. If needed, one can extend the aforementioned area up to 50.83 hectares (2.95 hectares represented in blue in the appendix A). The floor plan restrictions (cork oaks, stream) as well as the terrain topography are data with which the project has to comply with, being also presented in the appendix A. A total DC installed capacity of 24 $MW_p$ must be installed and the maximum allowed AC power to be injected into the grid must not surpass 20 $MW$.

It is important to point out that an optimized system is dependent on what is to be maximized. In this case, given the specific power to be installed and the available area, the project aims at giving priority to the former one. Thereby, the area to be occupied by the total capacity (24 $MW_p$) should be minimized in a way that the energy yield is maximized. As so, the solar panels should be disposed in a specific manner so that the grid energy does not vary significantly and the initial used area is minimized. The main goal of the study is to maximize the energy injected in the grid, finding the most appropriate parameter's values. All PV projects must go through several steps as the site identification, pre-feasibility study, feasibility study, financing, detailed design, construction and commissioning. The scope of this work is included in the detailed design phase as the goal is to find the most suitable design (layout and electrical) capable of maximizing the annual energy yield.

## 5.2 PV Module and Inverter Selection

Initially, as mentioned in section 4.1, the PV modules and inverters must be chosen so that other parameters can be analyzed with a particular configuration. Hence, this section presents the choice regarding the number of sub-arrays as well as the results obtained from the simulations in which every combination of module/inverter was tested under the same conditions. The list of modules and central inverters (from different manufacturers) initially considered was mostly obtained from the PVSyst database, being presented in the appendix B. In the same annex, the two used string inverters are also presented, having been provided by Huawei. Furthermore, information regarding the most recently used modules and inverters was provided by Sotécnica, which eased up the initial devices to select. Along this section (5.2), the solar modules were assumed to be disposed in portrait configuration and the pitch and tilt angle to possess a value of 9m and 30º, respectively.

### 5.2.1 Central Inverter

This sub-section presents the obtained results relatively to the number of sub-arrays as well as the choice of central inverter and PV module to employ ahead in this study. Relevant initial system data is depicted in table 5.1, where it is shown the considered $P_{inv,ratio}$ interval (mentioned in section 4.1.1), ranging between 1.1 and 1.3. Both minimum and maximum inverter's power thresholds are presented in table 5.2, which will enable one to select the central inverters that will suit each case where a different number of sub-arrays is considered. In this specific case, if $P_{inv,ratio}$ is higher than 1.3 or lower than 1.1,

the system would be undersized or oversized, respectively. As so, this range was deemed reasonable and will be considered henceforth.

Table 5.1: General System Data

| | |
|---|---|
| Total Installed DC Capacity ($kW_p$) | 24 000 |
| Max. Power Grid Connection ($kW$) | 20 000 |
| Inverter Max. $P_{nom}$ Ratio | 1.3 |
| Inverter Min. $P_{nom}$ Ratio | 1.1 |
| Total Available Ground Area ($m^2$) | 478 800 |

The obtained inverter power intervals (presented in table 5.2 for a different number of sub-arrays) allowed one to select, from the initial list (annex B), the central inverters that could possibly suit each different case (from 5 to 8 sub-arrays).

Table 5.2: Data for a different number of sub-arrays

| Nº Sub-Arrays | 5 | 6 | 7 | 8 |
|---|---|---|---|---|
| Installed DC Capacity ($kW_p$) | 4800 | 4000 | 3428.6 | 3000 |
| Inverter Min. Power ($kW$) | 3692.3 | 3076.9 | 2637.4 | 2307.7 |
| Inverter Max. Power ($kW$) | 4363.6 | 3636.4 | 3116.9 | 2727.3 |
| Sub-Array Max. Area ($m^2$) | 95760 | 79800 | 68400 | 59850 |

Based on these power intervals calculated for all the different cases, the available central inverters were selected, being these presented in table 5.3. After the possible group of central inverters has been selected for each different case, several simulations were carried out to match all possible module/inverter combinations. All the remaining parameters were kept constant for one to identify the combination that would lead to a greater performance. As one can see from the table 5.3, only Siemens inverters are available if one desires to divide the solar park in five or six sub-arrays. Both these situations were disregarded, as one big damaged inverter, combined with the fact that the replacement needs specialized personnel, would lead to large yield losses (section 3.3.3).

All the possible module-inverter combinations for seven and eight sub-arrays were simulated under the same conditions and the three best alternatives for each case are presented in table 5.4, having this selection been based on the annual energy yield ($E_{grid}$). The values of annual energy are presented for an individual sub-array (column $E_{grid}$/SA) and for all the PV park (column $E_{tot}$). Both modules from Open Renewables (annex B) didn't prove to be among the best modules to employ due to their lower power value. Hence, many more modules would be needed to attain the required power, resulting also in a higher maximum voltage (section 3.3.2), which surpasses the maximum inverter acceptable input voltage under certain conditions (lower temperatures).

As one may conclude from the table 5.4, the 370W module (Hanwha Qcells) combined with the central inverters SG3000HV and SG2500HV manufactured by SunGrow make up the best case scenarios for 7 and 8 sub-arrays, respectively. As one could expect, when employing seven inverters, the energy per sub-array will be higher due to the greater inverter AC nominal power. However, the total

Table 5.3: Available central inverters according to the number of sub-arrays

| | Inverters | |
|---|---|---|
| SA | Manufacturer | Model |
| 5 | Siemens | Sinacon PV3750<br>Sinacon PV4000<br>Sinacon PV4180<br>Sinacon PV4360 |
| 6 | Siemens | Sinacon PV3420<br>Sinacon PV3600 |
| 7 | SunGrow<br>SMA<br>Siemens | SG3000HV<br>Sunny Central 2750-EV<br>Sinacon PV3000 |
| 8 | SunGrow | SG2500HV<br>SG2500 |
| 8 | SMA | Sunny Central 2500-EV<br>Sunny Central 2750-EV |

annual produced energy is similar in both cases. Following the reasoning related with the redundancy factor and since the maximum power to inject in the grid must not surpass 20MW, the combination leading to a greater grid energy (SunGrow SG2500HV) corresponding to the case of 8 sub-arrays was selected to proceed with, being used hereafter in the next simulations.

Table 5.4: Best module/central inverter combinations (7 and 8 sub-arrays)

| Nº Sub-Arrays | Module | Inverter | $E_{grid}$/SA (kWh) | $E_{tot}$ (kWh) |
|---|---|---|---|---|
| 7 | Hanwha Qcells 365W | SunGrow SG3000HV | 5,362,425 | 37,536,975 |
| | Hanwha Qcells 370W | SMA Central 2750 | 5,399,701 | 37,797,907 |
| | Hanwha Qcells 370W | SunGrow SG3000HV | 5,441,810 | **38,092,670** |
| 8 | Hanwha Qcells 370W | SMA Central 2750 | 4,730,099 | 37,840,792 |
| | Hanwha Qcells 370W | SMA Central 2500 | 4,739,968 | 37,919,744 |
| | Hanwha Qcells 370W | SunGrow SG2500HV | 4,760,757 | **38,086,056** |

### 5.2.2 Series/Parallel Connections

This sub-section presents the results that led to the PV park arrangement selection. More specifically, the number of modules connected in series and strings connected in parallel were chosen based on the energy yield performance. In figure 5.1 the global horizontal irradiation and the temperature over one year are presented for the specific site to be analyzed. The minimum temperature was set for 5ºC in the PVSyst software, since after an hourly analysis over the years, it was verified that at the project's site it is rare for the temperature to fall below this value (fig. 5.1). Hence, the inverters were concluded to stand between 24 and 29 modules in series (due to its minimum and maximum input voltage) and, for each one of these cases, the number of strings was varied, always complying with the fact that the maximum installed power for one sub-array must not surpass $3000kW_p$ and that the power ratio interval

should always be within the interval 1.1 and 1.3 (table 5.1). As the selected central inverter's AC power is 2500kW and the maximum capacity to install per sub-array is 3000kW, the $P_{inv,ratio}$ will not be higher than 1.2.

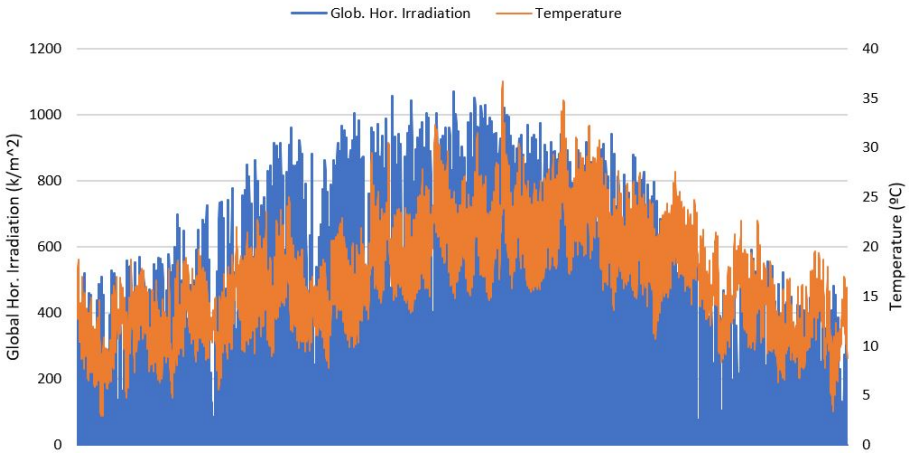


Figure 5.1: Global horizontal irradiation and temperature

The best results stemming from these simulations are presented in table 5.5, which led one to conclude that the best alternative is to opt for 29 modules in series. Despite both cases with 28 and 29 modules in series have led to the same energy yield, the latter one was chosen since the voltage will be higher, causing a decrease in the voltage drop along the string cables. Thus, for the installed power to remain the same, a smaller number of strings need to be connected in parallel, which decreases the DC cable length responsible for connecting the string to the string-box (specified ahead). Additionally, the mismatch that might stem from different strings connected in parallel to the same MPPT input decreases.

For each case, the interval range of possible strings' parallel connections are presented between brackets (table 5.5). The highest value of grid energy is presented in the same table for each case, corresponding always to the maximum value of strings' parallel connections, which is depicted in the chart presented in figure 5.2 for 28 modules in series. Based on the above-mentioned data, the chosen combination to be used henceforth was 29 series/280 parallel. Based on both modules and central inverter data sheets (Appendix C), data relative to the system was obtained from the PVSyst (according to section 3.5), being presented in table 5.6.

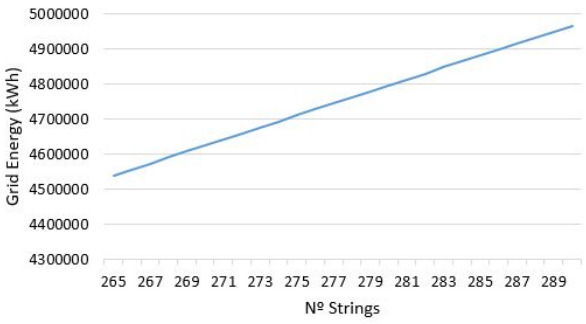


Figure 5.2: Grid Energy vs Number of Strings

| NºSeries | NºParallel | $E_{grid}$ (kWh) |
|---|---|---|
| 24 | 338(310-338) | 4,998,974 |
| 25 | 324(298-324) | 4,991,871 |
| 26 | 312(285-312) | 4,999,143 |
| 27 | 300(275-300) | 4,991,871 |
| 28 | 290(265-290) | 5,003,987 |
| 29 | 280(256-280) | 5,003,987 |

Table 5.5: Series/Parallel Combinations

Table 5.6: Initial data for one sub-array and for all the PV park (8 sub-arrays included)

| | Sub-Array | PV Park |
|---|---|---|
| Nº Modules | 8120 | 64960 |
| Module Area ($m^2$) | 16191 | 129528 |
| Nominal PV Power ($kW_p$) | 3004 | 24032 |
| Maximum PV Power ($KW$) | 2834 | 22672 |
| Nominal AC Power ($KW$) | 2500 | 20000 |
| $V_{mp}$ ($60°C$) | 987 V | - |
| $V_{oc}$ ($5°C$) | 1488 V | - |
| $I_{mp}$ (STC) | 2624 A | - |
| $I_{sc}$ (STC) | 2769 A | - |

### 5.2.3 String Inverter

The strategy followed to select the string inverter to be used was slightly different from the one used for the central inverter. Although there is no need to divide the park according to the number of inverters, one amongst the eight aforementioned sub-arrays was also used to perform the simulations with the string inverters. As the total capacity to be installed is the priority, the simulations were undertaken considering a maximum power of $3000kW_p$ and the same $P_{inv,ratio}$ interval (table 5.1).

Huawei Technologies is one of the leading companies in the string inverter world market and provided data regarding the most recent manufactured inverters, which were included in the simulations. Hence, both Huawei string inverters' PVSyst files (presented in appendix B) containing data according to what is specified in their data sheets (appendix C) were made available.

Table 5.7: Module/String inverter combinations

| Module | Inverter | Nº of Inverters | $E_{grid}$ (kWh) | AC Power (kW) | $P_{inv,ratio}$ |
|---|---|---|---|---|---|
| Hanwha Qcells 370W | SUN2000-105KTL | 26 | 5,010,423 | 2730 | 1.10 |
| | | 25 | 5,010,356 | 2625 | 1.14 |
| | | 24 | 5,010,244 | 2520 | 1.19 |
| | | 23 | 5,009,724 | 2415 | 1.24 |
| | | 22 | 5,008,389 | 2310 | 1.3 |
| Hanwha Qcells 370W | SUN2000-185KTL | 15 | 5,002,248 | 2625 | 1.14 |
| | | 14 | 5,001,644 | 2450 | 1.23 |

These simulations were carried out considering a configuration of 29 modules in series and 280 strings in parallel, whose best results are depicted in table 5.7. Both string inverters manufactured by Huawei proved to comply with the system features. As one may notice, a decrease in the number of inverters causes a decrease in the AC output power, which in turn is associated with a higher $P_{inv,ratio}$. The choice between the number of inverters hinges on a trade-off between the energy produced and the price of each inverter, being associated with the levelized cost of energy. From the table 5.4, one may conclude that in both cases an increase in the number of inverters leads to a higher energy yield. However, the energy yield difference between using 22 or 26 SUN2000-105KTL inverters is only 0.04%,

which is not enough to offset the initial investment of four string inverters. As so, the simulations carried out henceforth considered 22 inverters of this type, which results in 176 string inverters to be used in the entire PV park (8 sub-arrays). Since the energy yield difference between using both SUN2000-185KTL string inverters makes up only 0.012%, 14 string inverters of this type will be considered. Ahead in the economical analysis, both strings inverters will be analyzed and conclusions will be drawn from the LCOE.

## 5.3 Fixed Tilt System

### 5.3.1 Portrait vs Landscape

Firstly, the solar modules disposition was studied since it influences the way in which the shadings impact the energy yield (section 4.2) due to the solar panel's electrical components. The project site receives on average 68% of horizontal beam irradiation (PVSyst), which proves to be a considerable part of the total irradiation. The portrait and landscape dispositions (figure 5.3) used in the following simulations were considered to have two modules vertically oriented and four modules horizontally oriented along the shed's width, respectively. The graphic 5.3 a) and b) depict, respectively, the electrical loss due to shadings and the energy injected in the grid, having been obtained through the variation of the tilt angle. When the tilt angle increases, more shadings will be produced in the collector plane, increasing the electrical losses (figure 5.3 a) and decreasing the energy injected into the grid (5.3 b). After a specific angle (29º in this case) has been attained, the losses' difference between the two cases start to increase significantly (5.3 a), which can also be noticed through the difference concerning the energy injected into the grid (5.3 b). Thus, landscape configuration will be employed henceforth to analyze the other different parameters while seeking the maximization of the energy yield.

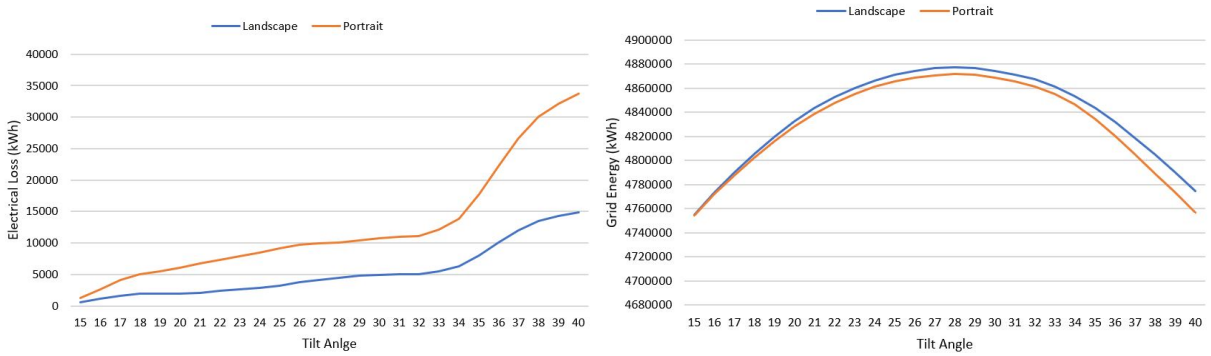


(a) Electrical Loss (b) Grid Energy

Figure 5.3: Portrait vs Landscape

However, different string cables' length are required depending on whether the panels are disposed in portrait or landscape. Thus, no conclusions can be drawn from this analysis regarding the most economical viable configuration to employ, as different dispositions lead to different energy values but also to different initial investments. Along this section, even though the goal is to maximize the energy

yield, an economical analysis (5.8) will also be carried out, which will consider both portrait/landscape configurations.

### 5.3.2 Plane Tilt and Pitch

After having obtained results regarding the solar modules disposition, simulations have been carried out aiming at finding the most suitable angle and pitch for this specific location. As there are no moving parts capable of employing the backtracking strategy, one must ensure that the shadings stemming from adjacent rows are minimized as much as possible. A limit angle of 18º was set for no shadings to be produced between 9h and 16h on the December $22^{nd}$, approximately. The solar chart corresponding to the location at stake is presented in figure 5.4, depicting the limit (upper dashed curve) from which shading starts to be produced, complying to what was mentioned before.

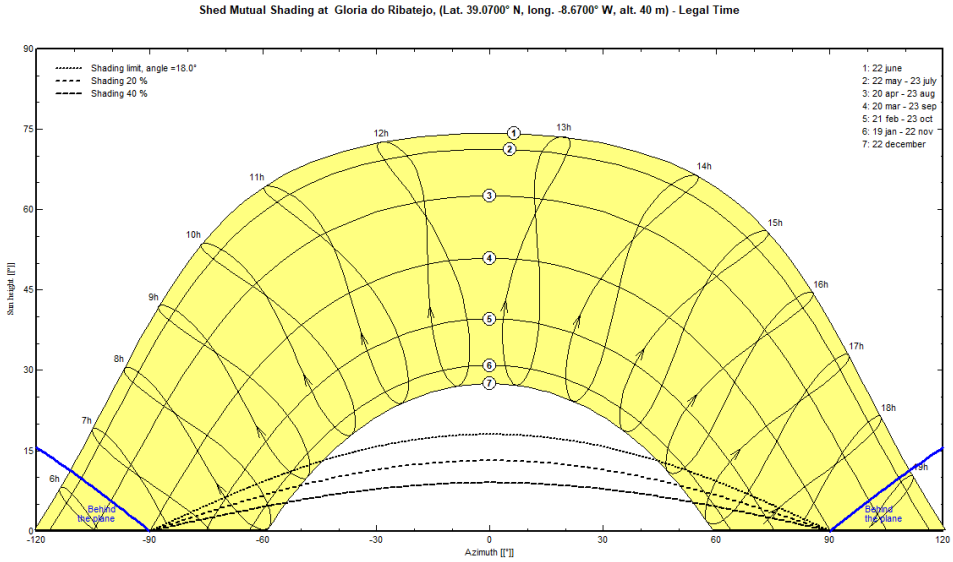


Figure 5.4: Solar Chart *[Source:PVSyst]*

If the shading limit angle is to be kept constant, the pitch and tilt angle are dependent on each other (as one can see in figure 4.1). As so, a tilt angle increase will be followed by a pitch increase (figure 5.5) for the shading limit angle to remain constant. As pictured in figure 5.5, there exists a maximum of produced energy corresponding to a specific pitch and tilt angle. Below and above 30º, the beam and diffuse irradiance hitting the solar modules decrease, leading to the shape of the blue curve. The exact values leading to the maximum energy yield (for one sub-array) are presented in table 5.8.

The ground cover ratio (table 5.8) was calculated through the relation presented in equation 4.6, in which the width and the pitch were considered to be 4m and 9.65m, respectively. As the total sensible area to be occupied by the solar panels is known (table 5.6), the needed ground area can be calculated through the equation 4.5. Bearing in mind that the solar panels will only make use of the area corresponding to this specific ground cover ratio, one can compute the percentage of the initial ground available area that will be indeed occupied. These values for both one single sub-array and all the PV park are presented in table 5.9. As one can see, the percentage of initial available area really needed

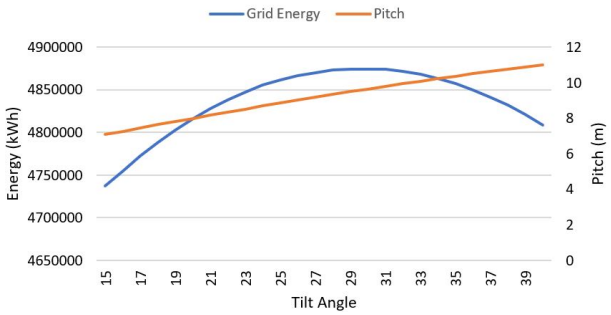


Figure 5.5: Grid Energy and Pitch Variation

| | |
|---|---|
| Limit Angle | 18º |
| Maximum Energy | 4874.6 MWh |
| Tilt Angle | 30º |
| Pitch | 9,65m |
| GCR | 41.45% |

Table 5.8: Optimal Values

to place the solar modules arranged like was mentioned before is approximately 65%, which still makes some available space to be used for other purposes.

Table 5.9: Sub-Array and PV Park Area

| | Sub-Array | PV Park |
|---|---|---|
| Module Area ($m^2$) | 16,191 | 129,528 |
| Needed Ground Area ($m^2$) | 39,062 | 312,492 |
| Total Available Area ($m^2$) | 59,850 | 478,800 |
| Used Area ($\%$) | 65 | 65 |

Simulations for all possible combinations of pitch and tilt angle (within a specific interval range) were carried out to conclude about their influence on the final output. The pitch and tilt angle were varied within intervals ranging from 6m to 12m and from 15º to 40º, respectively. These range intervals were chosen based on the previous obtained values (table 5.8), having been considered reasonable to study the output that would be achieved under other different conditions.

Initially, the tilt angle was individually varied for every pitch value, being the results stemming from these simulations presented in figure 5.6 a). From a certain pitch value (around 9m), the shading effects start to decrease and its weight on the final output proves to be negligible. Hence, as it is pictured, an increase of the pitch is related to a lower grid energy output difference, which was expected. Consequently, values of pitch greater than 10m (which corresponds approximately to the value of pitch obtained for the shading limit angle simulation) cause the grid energy output to differ less, which may be understood through the difference in the shape of the obtained curves that start to be closer to each other (figure 5.6). For instance, if the pitch between rows is 6m, the tilt angle leading to the highest energy yield proves to be the lowest one (15º), as an increase of this parameter would induce an increase of the produced near shadings and consequently a decrease of the energy injected into the grid.

In line with what was already mentioned, the chart presented in figure 5.6 b) depicts the result stemming from a set of simulations in which both parameters tilt and pitch were varied within the same range interval as specified above. Besides the result of energy yield for every single combination of both parameters, it also shows the "combination path" (green line) that leads to the maximum energy yield. As can be seen, both pitch and tilt angle start to increase initially for the energy yield to be maximized. However, the tilt angle tends to become steady after the pitch has reached a certain value, after which

the grid energy (scale presented on the right side of the chart) does not vary significantly as well.

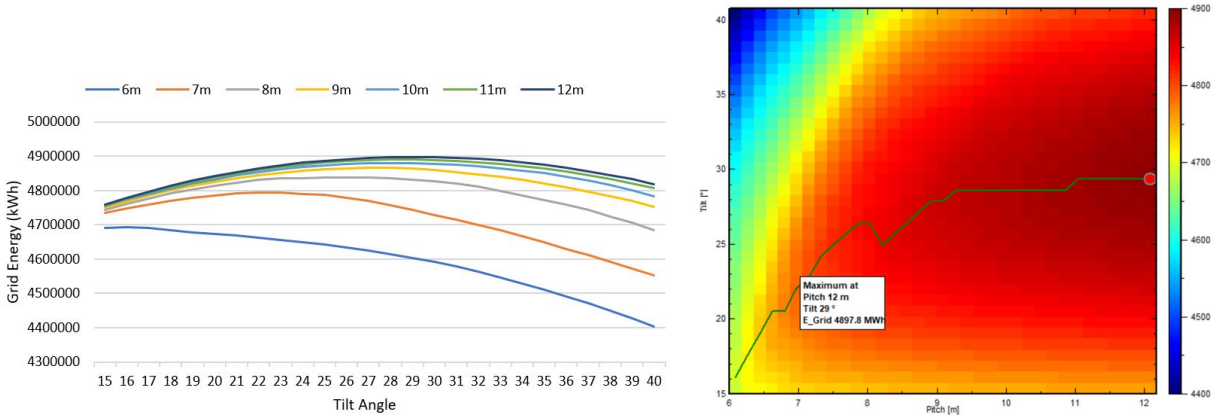


(a) Pitch/Tilt Variation (b) Pitch/Tilt Variation

Figure 5.6: Grid Energy for variable pitch and tilt angle

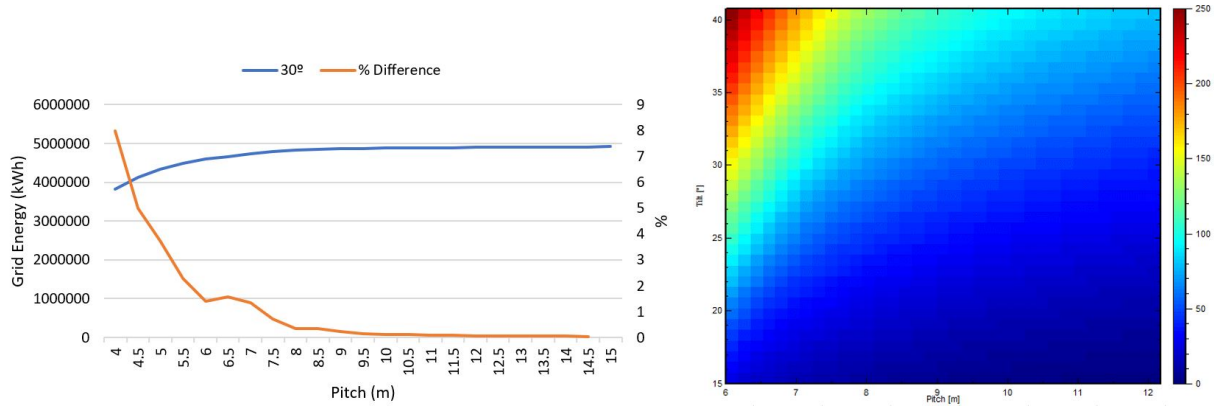


(a) Grid energy difference with pitch variation for 30º tilt angle (b) Shading Loss

Figure 5.7: Energy grid percentual difference vs pitch variation and shading loss

In figure 5.7 a), the grid energy output as well as its percentage difference variation along the pitch are presented for a fixed tilt angle of 30º (corresponding to the optimal value according to the previous obtained result). As shown in the chart, the grid energy variation (presented in percentage) decreases with the increase of the pitch. After a pitch of approximately 9m has been attained, the percentage difference variation stays below 0.13%, which is already considered negligible. Complementing the previous results, figure 5.7 b) pictures the electrical shading effects according to the variation of the pitch and tilt angle as well. The maximum losses due to electrical shadings, as expected, correspond to the minimum and maximum values of pitch and tilt angle, respectively.

### 5.3.3 Azimuth

Lastly, the azimuth angle was varied from -15º to 15º to perceive the direction the solar modules should face to maximize the energy yield. Throughout this set of simulations, the pitch and tilt angle were set for 9.65m and 30º, respectively. As depicted in figure 5.8 a), the greatest values of energy were obtained when the azimuth angle takes the value of approximately 0º, as the solar park is located

in the north hemisphere. A graph depicting the grid energy in function of both azimuth and tilt angle is shown in figure 5.8 b). The lowest values of energy (represented in blue), as expected, were obtained when the azimuth and tilt angles took extreme values. On the other hand, the maximum values of produced energy were obtained for an angle of approximately 30º and for an azimuth angle of zero degrees (southern orientation).

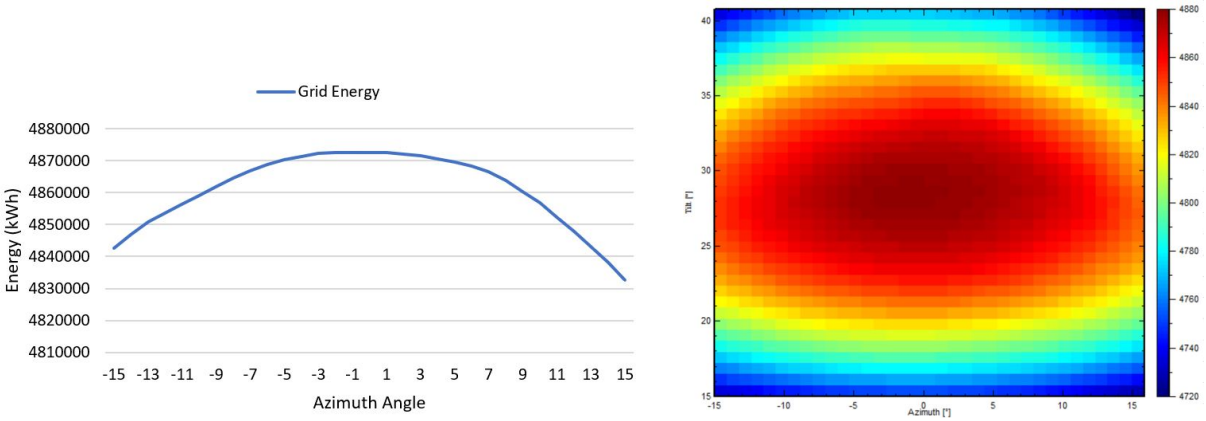


(a) Grid energy vs Azimuth Angle

(b) Grid Energy vs Azimuth and Tilt Angle

Figure 5.8: Grid Energy vs Azimuth/Tilt Angle

## 5.4 Single-Axis Tracking System

The solar modules disposition and azimuth angle already found while studying the fixed tilt system were taken as an assumption for the following simulations, since in the case of the single axis-tracking system these values will also lead to greater values of energy yield. Hence, the solar modules disposition and azimuth angle were henceforth considered to be in landscape and 0º, respectively.

### 5.4.1 Backtracking Strategy and Pitch

Initially, simulations were carried out considering a single-axis tracking system with and without the employment of the backtracking strategy (3.14). Hence, the influence of this strategy was assessed, being the grid energy output and shading losses arising from each case presented in figure 5.9 a), which vary depending on the pitch between rows as well. As one may notice, the backtracking strategy (orange) shows to be more advantageous in relation to the case in which it is not employed (blue), leading to slightly greater values of grid energy yield output. The grid energy scale corresponding to the two mentioned curves is presented on the left side of the graph.

The shading losses per unit area associated with each one of these cases are included in the same graph, being the scale presented on the right side of the figure. A smaller value of pitch, together with the non-implementation of the backtracking strategy (grey) leads to greater shading losses' values, stemming mainly from the the lack of incident beam component on the collector plane (visible shades). On the other hand, when the backtracking strategy is employed, there are no beam shading losses,

since the collector plane constantly modifies the angle depending on the sun height (section 3.4). In this latter case, the shading losses (yellow) arise mainly due to the diffuse and albedo component, which do not vary significantly along the pitch.

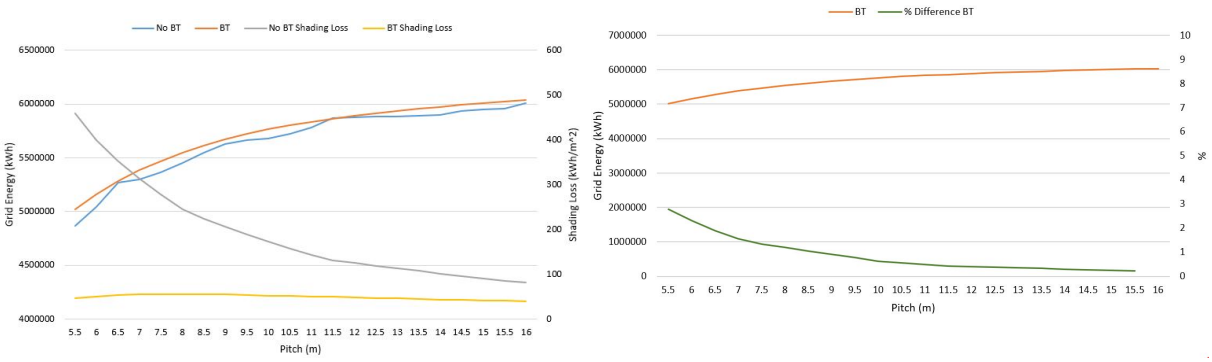


(a) Backtracking vs No Backtracking

(b) Grid energy percentual difference variation

Figure 5.9: Energy grid percentual difference with pitch variation and shading loss

Stemming from the results presented before, one may conclude that the backtracking strategy represents an added value to the single-axis tracking system. However, for the pitch between rows to be set, the grid energy percentual difference variation was also obtained along the pitch (considering an interval ranging from 5.5m to 16m). The chart presented in figure 5.9 b) depicts the grid energy percentual difference variation (green curve), which is always decreasing along the pitch (considering a constant increment of 0.5m), similarly to the fixed system behaviour. For a pitch between 9.5m and 10m, a difference of 0.7% was obtained, which was deemed reasonable. As so, the same pitch as the one used for the fixed tilt system was considered henceforth for the performance of the next simulations.

Table 5.11: Sub-Array and PV Park Area

| | |
|---|---|
| Max. Rotation Angle (E-W) | -55º 55º |
| Tilt Angle (N-S) | 0º |
| Maximum Energy | 5721.4MWh |
| Pitch | 9.65m |
| GCR | 45% |

| | Sub-Array | PV Park |
|---|---|---|
| Module Area ($m^2$) | 16,191 | 129,528 |
| Needed Ground Area ($m^2$) | 39,061 | 312,492 |
| Total Available Area ($m^2$) | 59,850 | 478,800 |
| Used Area ($\%$) | 65 | 65 |

In table 5.11, the "real" GCR corresponding to the aforementioned pitch (9.65m) is presented (equation 4.6), which shows to be equal relatively to the fixed tilt system. Consequently, the available initial area percentage to be occupied by all the PV modules (equation 4.5) is 65% in this case (table 5.11). The amount of annual grid energy drawn from the single-axis tracking system proved to be significantly greater in comparison with the fixed tilt system (table 5.8), reaching a value of 5721.4MWh/sub-array.

## 5.5 Systems' Performance Comparison

Along the previous sections (5.3 and 5.4) both fixed tilt and single-axis tracking systems' performances were improved in the extent that relevant parameters were varied aiming at maximizing the

energy yield. The previous simulations were carried out considering the central inverter, which was suitable to initially test the energy output depending on the parameters' variation. However, both systems were also simulated with the already mentioned string inverters (present in annex B) to conclude about their effect in the final output. During these simulations, every previously optimized parameter remained the same, as it has been already concluded that they lead to the maximum energy yield. The results concerning the energy yield stemming from both systems over the 25 years with the employment of both central and string inverters are depicted in the chart presented in figure 5.10. This chart provides an overview of the six different cases corresponding to the landscape configuration. As one may notice, the single-axis tracking system proves to clearly generate a greater amount of energy in comparison with the fixed tilt system. More specifically, when employing the central and string inverter, the single-axis tracking system produces 15% and 14.3% more energy than the fixed tilt one, respectively. Furthermore, the string inverters led to 3.5% and 2.7% higher energy yields when employed in the fixed tilt and single-axis tracking system, respectively. The higher energy yield difference obtained in the fixed tilt system (3.5%) compared to the single-axis tracking one might be explained due to the beam shading, which is responsible for the strings' mismatch connected to the same MPPT (section 3.6.2.1). As a string inverter possesses many more available MPPT inputs than a central inverter, the beam shading (and consequently the mismatch) is better circumvented.

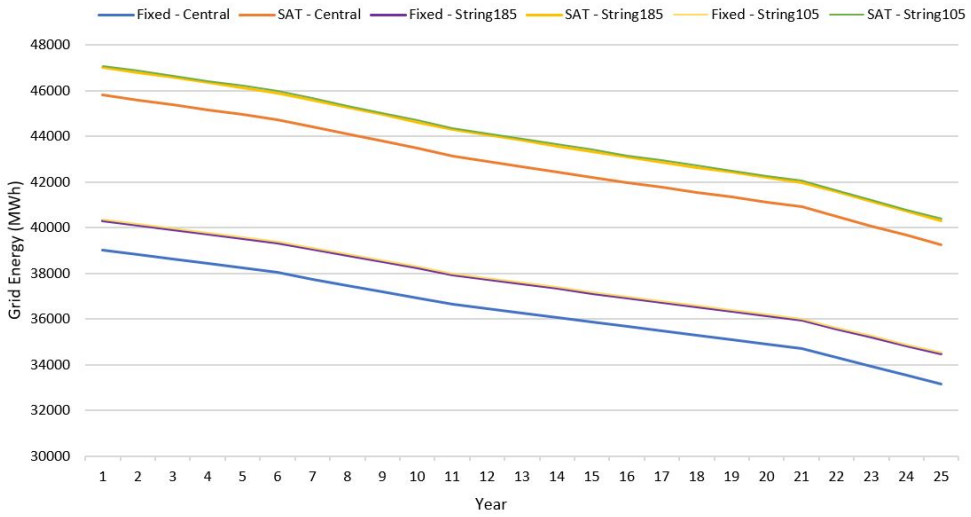


Figure 5.10: Performance comparison (Landscape)

Table 5.12: Fixed and Single-Axis systems' energy yield (Landscape and Portrait)

| System | Inverter | $E_{grid}$ (kWh) Landscape | $E_{grid}$ (kWh) Portrait |
|---|---|---|---|
| Fixed | Central | 472720.2 | 472176.2 |
| | String105 | 490048.9 | 489491.1 |
| | String 185 | 489293.6 | 488734.8 |
| Single-Axis | Central | 556386.2 | 557429.4 |
| | String105 | 572056.3 | 572547.6 |
| | String 185 | 571129.8 | 571617.5 |

A summary of data obtained for the twelve different cases employing both central and string inverters is presented in table 5.12. The shown grid energy corresponds to the sum of the discounted energy for every year over the project's lifetime. Furthermore, the table provides the energy values corresponding to portrait and landscape configuration. From the table, one can conclude that the fixed tilt system provides slightly higher values of energy when employing the landscape configuration, which was expected due to the near shading effect along with the solar panel electrical circuit. On the other hand, the opposite was verified in the case of the single axis system. However, it is important to highlight that, for this specific pitch, the percentual difference between these two types of configuration makes up only 0.1%, which might be considered negligible.

## 5.6 Layout

The solar PV park layout is a crucial task that must be undertaken, having been divided in two different parts. Firstly, it allows the different components to be distributed over the available area while considering the diverse plant restrictions as, for instance, the ground slope, trees and stream. Thus, the solar panels' disposition corresponding to both systems (fixed tilt and single-axis tracking) were distributed always complying with the initial restrictions as well as with every parameter previously defined. The components' disposition over the available area provides relevant information concerning each case cables' length, which depends on the type of employed inverter. Thus, an estimate of all DC and AC cables was carried out taking into account the three different type of inverters as well as the solar panels' disposition (portrait/landscape). This procedure shows to be relevant as the cables' sizing (section 5.7) depends on their length, which subsequently also influences the initial investment.

Table 5.13: System data corresponding to different inverters

| | Central SG2500HV | String SUN2000-105KTL | String SUN2000-185KTL |
|---|---|---|---|
| Nºstrings/sub-array | 280 | 280 | 280 |
| Nºstrings/shed | 4 | 4 | 4 |
| Nº inverters/sub-array | 1 | 22 | 14 |
| Nºtotal inverters | 8 | 176 | 112 |
| NºDC inputs/inverter | 18 | 12 | 18 |
| NºMPPT/inverter | 2 | 6 | 9 |
| NºDC inputs/sub-array | 18 | 264 | 252 |
| Nºstrings/string-box | 28 | - | - |
| Nºstring-boxes/sub-array | 10 | - | - |
| Nºsheds/string-box | 7 | - | - |
| Nºstrings for Y connector | - | 16 | 28 |

Additionally, it is fundamental to undertake the strings' distribution over the three different inverters, based on these components' technical specifications. In table 5.13, obtained system data is presented for the three situations in which different inverters are employed. In the case of the central inverter, all strings are firstly connected to the string-boxes (ten/sub-array), which in turn are connected

to the inverter's available inputs. On the other hand, only a few strings can be connected in the case of the string inverters. As one can see in table 5.13, the 280 strings (existent in one sub-array) must be connected onto the 264 and 252 string inverters' available inputs. More specifically, in the case of the string inverter SUN2000-185KTL, there exist 28 strings that require a Y connector so that these can be equally distributed over the 14 inverters. The Y connector allows two different strings to be connected to the same inverter's input, enabling one to circumvent the fact of having more strings than available inputs. Thus, in this specific case, each inverter would have two extra strings connected through two Y connectors plugged into two different inputs. The appendix D depicts the single-line diagrams for the three systems (central inverter and both string inverters), representing the strings' distribution as well as the other required main devices.

## 5.7 Cable Sizing

This section refers to the cables' sizing results, according to what was mentioned in section 4.5. The cables' sizing depends on various parameters and it will be presented for both central and string inverters as well as for portrait/landscape solar module configuration, leading to twelve different situations. The tables presented in the appendix E provide data used to size the cables as well as available cables' sections and their respective prices (provided by Sotécnica), which are useful for the economic study (section 5.8).

In the case of the central inverter, the string cable (table E.1), main DC cable (table E.2) and low voltage AC cable (table E.3) were sized depending on the aforementioned variables. The string cable (made of copper) is responsible for connecting the solar panels between each other and to make up the connection until the string-box, which is responsible to group different strings. Hence, the string length was firstly calculated (through AutoCAD), which varies depending on the selected configuration (portrait/landscape). As expected, the landscape string length is relatively greater when compared to the portrait one (table E.1), as the solar panels are horizontally distributed. Afterwards, the distance between each string and the stringbox was measured and an average value was found, which summed with the string length enable one to calculate each string average cable length. Even though different distances from each string to its respective stringbox make the cable's section to vary, an average was assumed since the same cable's section is to be used in all strings. Therefore, even though some string cables undergo a voltage drop higher than 1%, there also exist other strings with a voltage drop much lower than this value.

The table E.1 also presents some data relative to the next stages until the transformer station is reached. The second stage (main DC cable) makes up the connection between the different string-boxes (10/sub-array) and their respective inverter. As each cable responsible for this connection has a different length and the current to transport is much higher than in the strings' cables, two different cross-sectional areas were chosen (table E.2). Regarding the cables aiming at connecting the inverter to the transformer station (third stage in table E.1), only one section was adopted as these two devices are close to each other. The same process was undertaken for the situations in which the string invert-

ers were used. However, as a different layout and number of inverters is employed, diverse values were obtained relatively to the previous ones.

In table E.4, the results stemming from the SUN2000-105KTL cables' length estimate are presented. The string cable (copper) length shows to be smaller, differing from the previous one due to the distance between the strings and the inverter. As shown in the layout section, the string inverter SUN2000-105KTL requires to be connected to the AC combiner (two inverters to one AC combiner) and subsequently to the transformer station. As there exist 22 inverters connected to 11 AC combiners, the table E.5 provides the distance from the latter ones towards the transformer station as well as each cable section assuming the voltage drop to be 1%. The available standard cables were chosen according to the previous obtained values, having been chosen two different cross-sectional areas.

## 5.8 Economic Analysis

Over this section, relevant topics for a reliable economical analysis will be outlined. All costs (investment and $O\&M$) will be outlined, as they are of great importance to subsequently proceed towards a thorough economical viability analysis.

According to Sotécnica, the project's lifetime and the initial discount rate were considered to be 25 years and 6%, respectively. Additionally, the initial energy selling price was assumed to take the value of 40 €/$MWh$. As the discount rate and energy selling price are volatile values, a sensibility analysis was carried out to perceive their influence in the economic outputs. Thus, different results of levelized cost of energy (LCOE) and net present value (NPV) were obtained while considering different input values.

### 5.8.1 Costs

The cost estimates were initially based on data provided by Sotécnica, being each component's cost contribution presented in table 5.14. This table includes the values relative to a fixed tilt system employing a central inverter as well as with the modules oriented vertically (portrait). Based on the installed power ($24MW_p$) and considering a price of 600 €/$kW_p$ for this type of system, each individual component cost was computed, which summed gives the initial investment value (table 5.14) for this specific type of system (with the specifications mentioned above). From the table 5.14, one can conclude that the PV modules are the most expensive system's component, making up half of the initial investment value.

The present work aims at assessing all the possible alternatives and select the best case scenario from the economical point of view (LCOE), which requires each particular case initial investment to be computed based on the diverse components. The two main components responsible for the system's initial investment variation are the inverters and cables. Thus, this two components' costs have been computed for each different situation in which different inverters and configuration (portrait/landscape) were employed.

The table 5.15 presents the price of the needed components (provided by Sotécnica) to install

Table 5.14: Fixed Tilt components' cost (central inverter and portrait configuration)

| | % | €/$W_p$ | Price (€) |
|---|---|---|---|
| PV Modules | 51 | 0.306 | 7,354,771 |
| Support Structures | 7 | 0.042 | 1,009,478 |
| Accessories | 16 | 0.096 | 2,307,379 |
| Central Inverters | 9 | 0.054 | 1,297,901 |
| Elect. and Mech. Installation | 15 | 0.090 | 2,163,168 |
| Project and Commissioning | 1 | 0.006 | 144,211 |
| SCADA | 1 | 0.006 | 144,211 |

the Huawei string inverter (SUN2000-105KTL) as well as the total cost of both string inverters, which show to be slightly more expensive than the value presented for the central inverter (table 5.14). The SUN2000-185KTL string inverter's price has been computed based on the assumption that it is 50% more expensive than the SUN2000-105KTL (according to Huawei). This string inverter is similar to the SUN2000-105KTL with the exception that it does not require the AC combiner before the transformer station.

Table 5.15: SUN2000-105KTL components' costs and both string inverters' total cost

| | Quantity | Unit Price | Price (€) |
|---|---|---|---|
| SUN2000-105KTL | 176 | 4000 | 704,000 |
| AC Combiner | 88 | 250 | 22,000 |
| STS-2500 | 8 | 78,000 | 624,000 |
| SmartACU2000B-D-PID/PLC | 8 | 3000 | 24,000 |
| One time discount | 1 | 320,000 | 320,000 |
| **Total Cost (SUN2000-105KTL)** | | | 1,694,000 |
| **Total Cost (SUN2000-185KTL)** | 112 | 14437.5 | 1,617,000 |

As mentioned before, the cables' cost is one amongst the two factors that mostly influence the initial investment. Thus, different DC and AC cables' length are needed when employing different type of inverters as well as when employing portrait/landscape configuration. As one might expect, the landscape configuration requires a longer DC string cable, which in a utility-scale park shows to be significant in terms of cost difference. Based on the cables' length estimate as well as on their sizing (section 5.7), the total costs corresponding to each different system have been obtained. The prices of the cables are presented in the appendix E. It is important to emphasize that the presented prices are merely indicative. A summary of the cables' costs for these six different cases is presented in table 5.16.

Over the project's lifetime, operation and maintenance costs will contribute to the constant yearly expenses, which were considered to be 7€/$kW_p$ for fixed tilt configuration (table 5.17) when using central inverters. However, a different O&M cost (OPEX costs) must be attributed to the system when string inverters are employed, as this is one of the main advantages of this type of devices. According to previous studies, the string inverters' O&M costs are approximately 6.9% cheaper than the central inverter ones (table 5.17).

Table 5.16: Cables' total costs

| Inverter | Disposition | Price (€) |
|---|---|---|
| Central | Landscape | 134,600 |
| | Portrait | 122,504 |
| String 105 | Landscape | 262,790 |
| | Portrait | 250,694 |
| String 185 | Landscape | 307,251 |
| | Portrait | 295,155 |

Table 5.17: Fixed Tilt and Single-Axis System Operation and Maintenance Costs

| System | Inverter | €/$W_p(Annual)$ | Price (€)/Year |
|---|---|---|---|
| Fixed | Central | 0.007 | 168,246 |
| | String | 0.00652 | 156,637 |
| Single-Axis | Central | 0.00714 | 171,611 |
| | String | 0.00665 | 159,770 |

According to Sotécnica, the initial investment and O&M of a single-axis tracking system are 10% and 2% more costly relatively to a fixed tilt system, respectively. Thus, these values have been assumed and the single-axis tracking system initial investments were obtained based on it. In table 5.18 the initial investment for the twelve different cases are depicted, which will be relevant to proceed the economic viability study (5.8.2).

Table 5.18: Systems' initial investment

| Inverter | Disposition | System | Investment (€) | Cost (€/$kW_p$) |
|---|---|---|---|---|
| Central SG2500HV | Portrait | Fixed Tilt | 14,409,956 | 600 |
| | | Single-Axis | 15,850,952 | 660 |
| | Landscape | Fixed Tilt | 14,422,052 | 601 |
| | | Single-Axis | 15,864,257 | 661 |
| String SUN2000-105KTL | Portrait | Fixed Tilt | 14,923,702 | 622 |
| | | Single-Axis | 16,416,072 | 684 |
| | Landscape | Fixed Tilt | 14,935,798 | 622 |
| | | Single-Axis | 16,429,377 | 685 |
| String SUN2000-185KTL | Portrait | Fixed Tilt | 14,891,163 | 620 |
| | | Single-Axis | 16,380,279 | 683 |
| | Landscape | Fixed Tilt | 14,903,259 | 621 |
| | | Single-Axis | 16,393,585 | 683 |

### 5.8.2 Economic Viability

The previously computed costs as well as the obtained energy along the project's lifetime are useful to carry out the economic viability study, which allows one to predict how successful the project might be in the long run. The levelized cost of energy for both studied systems (fixed tilt and single-axis)

Table 5.19: LCOE and NPV values

| | | LCOE (€/MWh) | | NPV (k€) | |
|---|---|---|---|---|---|
| | | Landscape | Portrait | Landscape | Portrait |
| Fixed Tilt | Central Inverter | 35.06 | 35.07 | 2336 | 2326.3 |
| | String Inverter 185 | 34.55 | 34.57 | 2666.1 | 2655.9 |
| | String Inverter 105 | 34.56 | 34.58 | 2663.8 | 2653.6 |
| Single Axis | Central Inverter | 32.38 | 32.29 | 4240.4 | 4295.5 |
| | String Inverter 185 | 32.28 | **32.23** | 4409.2 | 4442 |
| | String Inverter 105 | 32.29 | 32.24 | 4410.5 | 4443.4 |

was calculated while employing the three different types of inverters. As stated in the section 3.7, this variable is the ratio between the costs and the annual energy. It is relevant to emphasize that both costs and energy need to be discounted to the present, which hinges on the discount rate and on the project's lifetime.

Initially, the LCOE and NPV have been computed considering a discount rate of 6% and an electricity selling price of 40 €/MWh, being the results depicted in table 5.19. As can be seen, the single-axis tracking system LCOE shows to be significantly lower relatively to the fixed tilted one regardless of the configuration type (portrait/landscape). Thus, even though the tracking system is more expensive than the fixed tilt one, the energy produced is significantly higher to offset the initial investment.

From the table, one can perceive that in the fixed tilt system the landscape configuration leads to slightly better results. As so, in this case, the higher energy produced is sufficient to compensate the greater cables' initial investment. On the other hand, the portrait configuration has shown to be slightly cheaper in the case of the single-axis tracking system. The difference between these two systems might be justified due to the near shadings, which hinge on both solar panels' configuration and tracking system. In addition, for both type of systems, the string inverters have proved to perform slightly better, leading to lower values of LCOE. More specifically, the SUN2000-185KTL string inverter has proved to achieve the lowest values, being 1.4% and 0.24% lower than when using the central inverter for fixed tilt and single-axis tracking system, respectively. Hence, one might conclude that the string inverter stands out relatively to the central inverter mainly when used in the fixed tilt system.

In figure 5.11, both net present value and LCOE are depicted, representing the six different cases combining both type of system employed (fixed tilt or SAT) and type of inverter. As the net present value is positive in every case, the project is said to be economically profitable whichever used system or inverter. Between both string inverters, the LCOE difference might be considered negligible, as it accounts only for 0.03%. Through the obtained results, one can conclude that the most suitable solution is the single-axis tracking system together with the employment of the string inverter SUN2000-185KTL and portrait configuration.

#### 5.8.2.1 Sensibility Analysis

In the previous section, both levelized cost of energy and net present value were found for specific values of discount rate and electricity selling price. However, the discount rate depends on both time value of money and uncertainty risk and the selling price depends on the type of contract.The different

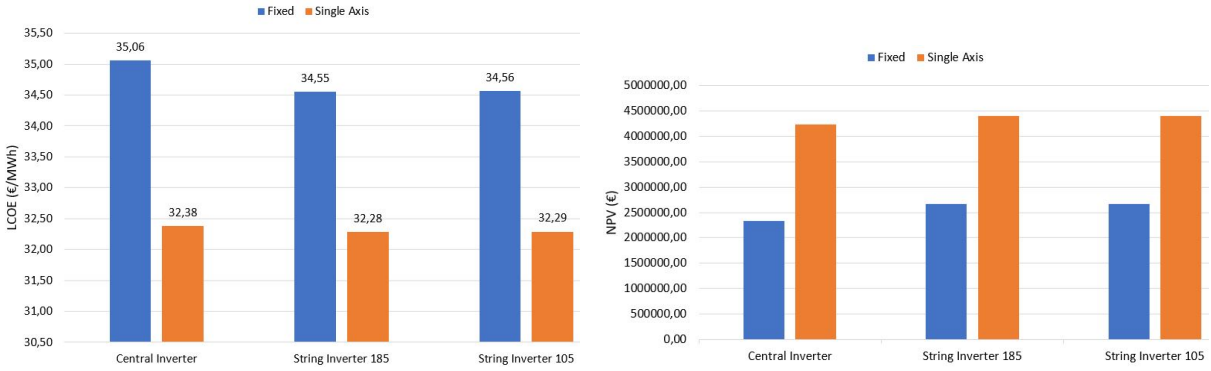


(a) LCOE (b) NPV

Figure 5.11: LCOE and NPV (Fixed tilt and Single-axis)

project's outcomes significantly depend on these values, which have been varied for the already chosen case (section 5.8.2). Results corresponding to different case scenarios were obtained through a sensibility analysis, in which both discount rate and electricity selling price were varied. In figure 5.12 a), the levelized cost of energy is depicted for a variation of the discount rate from 2% to 6%.

As shown in the chart, the higher the discount rate, the more expensive the system will be in the future. The figure 5.12 b), on the other hand, presents the variation of the net present value according to specific values of both discount rate and electricity selling price, which vary within an interval range of 2%-6% and 30€-50€, respectively. As shown in figure, a greater net present value stems from a lower discount rate as well as a higher electricity selling price.

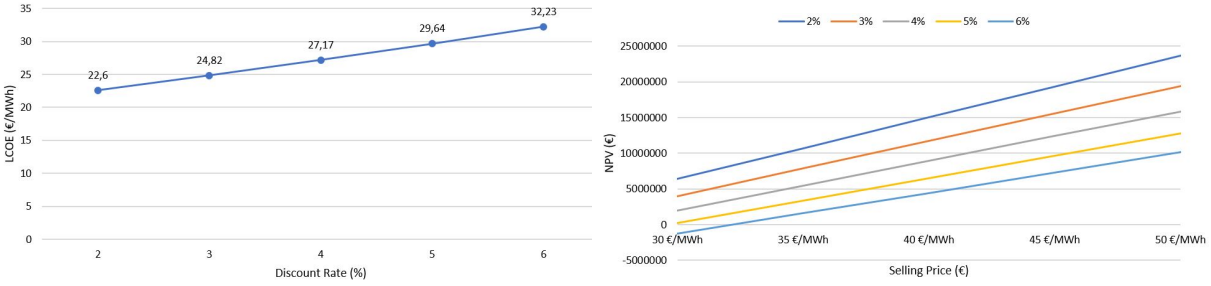


(a) LCOE (b) NPV

Figure 5.12: LCOE and NPV sensibility analysis

#### 5.8.2.2 Recommendations

Throughout the present study, the maximization of the energy yield to inject into the grid has been achieved through successive simulations automatically performed by the PVSyst software. These simulations have been carried out aiming at maximizing the energy yield generated by the solar PV park under analysis, which was undertaken through the choice of the most suitable equipments (solar modules and inverters) as well as the best parameters' values. Furthermore, an economic analysis (section 5.8) has been carried out, which allowed one to conclude regarding the most cost-effective solution. After a thorough analysis and concluding based on the presented findings, all solar park

equipments as well as its features might be summarized as follows:

- String inverter SUN2000-185KTL (Appendix C);
- Solar module Hanwha QCells 370W (Appendix C);
- 8 sub-arrays composed by 280 strings of 29 modules in series each;
- Single-axis tracking system;
- 9.65m pitch;
- Backtracking strategy;
- Portrait configuration;

# Chapter 6

# Conclusions

## 6.1 Achievements

The main goal of this dissertation was to maximize the energy output stemming from a $24MW_p$ grid connected solar PV park, having PVSyst software been chosen as the decision support tool software. PVSyst was a crucial tool as it allowed one to run successive simulations for each considered parameter, enabling them to be individually varied. Hence, through an automatic trial-error method, one could perform a sensibility analysis and perceive the influence of each parameter on the energy yield maximization. Additionally, an economical analysis was carried out so that each case scenario viability could be evaluated in a long term period. Initially, all available PV modules were combined with each central inverter so that the most suitable combination module/inverter could be selected based on the energy output. Moreover, two different string inverters (manufactured by Huawei) were also included in the study to assess their possible advantage relatively to the central inverter. According to the devices' data sheets, the number of modules in series and strings in parallel as well as the number of inverters was selected.

After the modules and inverters have been chosen, two different types of system (fixed tilt and single-axis tracking) were considered and significant parameters were varied to perceive how differently each one of them influences the energy output. Regarding the fixed tilt system, the module configuration (portrait/landscape) was analyzed, which allowed one to conclude that, due to the module electric circuit, the landscape configuration leads to slightly greater energy yields on account of near shadings. Additionally, the parameters' optimal values accountable for the energy yield were individually varied through a sensibility analysis as aforementioned. The shading limit angle was initially set ($18^o$) and the maximum energy yield was obtained for a specific pitch and tilt angle. Concerning the single-axis tracking system, the backtracking strategy was assessed and concluded to be slightly advantageous. The grid energy was obtained for the project's lifetime and it was concluded that, when employing the central inverter and string inverter, the single-axis tracking system produces 15% and 14.3% more energy relatively to the fixed tilt one, respectively. Furthermore, the string inverters led to 3.5% and 2.7% higher energy yields when employed in the fixed tilt and single-axis tracking system, respectively.

The PV park layout was carried out in two different phases. At first, the devices' distribution and connections were undertaken based on the respective modules and inverters' data sheets, which was crucial to properly decide regarding the required equipments' quantity. Secondly, the different equipments were disposed over the available area (AutoCAD), allowing the different cables' lengths to be estimated for each different case scenario. Finally, the cables' sizing was undertaken as well as their prices' estimates, having been prominent for a subsequent economic analysis. The LCOE was obtained for twelve different cases in which, for both types of system (fixed tilt and single-axis tracking), all inverters and portrait/landscape configuration were considered.

Throughout this study, a generic method to approach the problem related with the optimization of a utility-scale solar PV park was developed. Specifically, this method was applied to the case study provided by Sotécnica, contributing for its performance improvement as well as the choice of the most suitable devices and parameters to employ. Based on the obtained results and among the wide range of possibilities through which this study has came across, one may conclude that the most viable solution is the one employing a single-axis tracking system together with backtracking strategy as well as with the modules disposed in portrait configuration. A comparison between the considered central/string inverters together with an economic analysis has shown that the string inverter (SUN2000-185KTL) is the best alternative to employ as it does not just provide a better price per unit of energy as well as it allows to be easily replaced whenever it is needed.

## 6.2 Future Work

The optimization of a solar PV park is a multi-variable problem. Along the present dissertation, the goal was to maximize the energy injected into the grid which, at the same time, could have hindered other important variables. As the economic assessment is becoming an increasingly important factor to invest on utility-scale projects, a tool that relates relevant parameters directly with economic variables could be developed, so that the impact of the former ones could be assessed in a different manner. Thus, the diverse economic variables (investment, LCOE, NPV) could be maximized or minimized aiming at finding the most suitable parameters' values.

# Bibliography


[1] Al-Khazzar, Akram. A comprehensive solar angles simulation and calculation using matlab. *International Journal of Energy and Environment*, 6:367–376, June 2015.

[2] Alberto Dolara, Francesco Grimaccia, Sonia Leva, Marco Mussetta, Roberto Faranda, Moris Gualdoni. Performance analysis of a single-axis tracking pv system. *IEEE Journal of Photovoltaics*, 2 (4):524–531, Oct 2012.

[3] André Mermoud, Bruno Wittmer. Pvsyst tutorial, May 2017.

[4] Ashish Raj, Manoj Gupta, Sampurna Panda. Design simulation and performance assessment of yield and loss forecasting for 100 $kw_p$ grid connected solar pv system. *2nd International Conference on Next Generation Computing Technologies*, Oct. 2016.

[5] B. Shiva Kumar, K. Sudhakar. Performance evaluation of 10 MW grid connected solar photovoltaic power plant in india. *Energy Reports*, pages 184–192, Dec 2015.

[6] P. A. Basha. Performance analysis of horizontal single-axis tracker vs. fixed tilt solar pv plants in southern states of india, Apr 2016.

[7] Bruno Nascimento, Daniel Albuquerque, Miguel Lima, Pedro Sousa. Backtracking algorithm for single-axis solar trackers installed in a sloping field. *Journal of Engineering Research and Applications*, 5:100–103, Dec 2015.

[8] C. Kandasamy, P. Prabu and K. Niruba. Solar potential assessment using pvsyst software. In *2013 International Conference on Green Computing, Communication and Conservation of Energy (ICGCE)*, pages 667–672, Dec 2013.

[9] Department of Economic and Social Affairs, Population Division. World population prospects: The 2017 revision, key findings and advance tables. working paper no. esa/p/wp/248. Technical report, United Nations, 2017.

[10] *Energia Fotovoltaica. Manual sobre tecnologias, projecto e instalação*. European Commission, Jan 2004. GREENPRO Project.

[11] Gairaa, Kacem and Khellaf, Abdallah and Chellali, Farouk and Benkaciali, Said and Bakelli, Yahia and Bezari, Salah. *Maximisation and Optimisation of the Total Solar Radiation Reaching the Solar Collector Surfaces*, pages 873–886. 01 2015. doi: 10.1007/978-3-319-17031-2_57.

[12] B. Goss. *Design process optimization of solar photovoltaic systems*. PhD thesis, Loughborough University, Centre for Renewable Energy Systems Technology (CREST), Oct 2015.

[13] IFC, Technical Report. Utility-scale solar photovoltaic power plants - a project's developer's guide. Technical report, International Finance Corporation - World Bank Group, 2015.

[14] International Energy Agency. *Renewables 2018, Market Analysis and forecast from 2018 to 2023*, October 2018.

[15] International Energy Agency. Renewables information: Overview, 2018. Manual.

[16] International Energy Agency. World energy balances: Overview, 2018. Manual.

[17] International Energy Agency. Photovoltaic power systems programme - 2017 Annual Report. Technical report, May 2018.

[18] Irfan Jamil, Jinquan Zhao, Li Zhang, Rehan Jamil, Syed Furqan Rafique3. Evaluation of energy production and energy yield assessment based on feasibility, design, and execution of 150MW grid-connected solar pv pilot project in nooriabad. *International Journal of Photoenergy*, Nov 2017.

[19] Jayanta Deb Mondol, Brian Norton. Optimal sizing of array and inverter for grid-connected photovoltaic systems. *Solar Energy*, 80:1517–1539, Apr 2016.

[20] João Santana, Rui Castro. Basics on the economic assessment of the power system. Volume 1, September 2016.

[21] Kathie Zipp. Why array oversizing makes financial sense, Feb 2018.

[22] L. El Chaar, L.Lamont, N. El Zein. Review of photovoltaic technologies. *Renewable and Sustainable Energy Reviews*, 15:2165–2175, Jan 2011.

[23] Lo Chin Kim, Yun-Seng Lim, Kee Shin Yiing. Improvement of bifacial solar panel efficiency using passive concentrator and reflector system. *International Journal of the Institute of Materials Malaysia*, 1:91–106, Oct. 2013.

[24] A. Mermoud. Pvsyst help contents. PVSyst Version 6.7.9.

[25] A. Mermoud. Optimization of row-arrangement in pv systems, shading loss evaluations according to module positioning and connections. 27th European Photovoltaic Solar Energy Conference – Frankfurt, Germany, Sep 2012.

[26] A. Mermoud. A tool to optimize the layout of ground-based pv installations taking into account the economic boundary conditions. 29th European Photovoltaic Solar Energy Conference – Amsterdam, Netherlands, Sep 2014.

[27] Michael Mendelsohn, Travis Lowder, and Brendan Canavan. *Utility-Scale Concentrating Solar Power and Photovoltaics Projects: A Technology and Market Overview*. NREL - National Renewable Energy Laboratory, April 2012.

[28] Mohammad Hejri, Hossein Mokhtari, Mohammad Reza Azizian Lennart Söder. An analytical-numerical approach for parameter determination of a five-parameter single-diode model of photovoltaic cells and modules. *International Journal of Sustainable Energy, http://dx.doi.org/10.1080/14786451.2013.863886*, Dec. 2013.

[29] Muhammad Z. B. Rosselan, Shahril Irwan Sulaiman, Ismail Musirin. Sizing optimization of large-scale grid-connected photovoltaic system using cuckoo search. *Indonesian Journal of Electrical Engineering and Computer Science*, 8(1):169–176, Oct 2017.

[30] Nallapaneni Manoj Kumar, M. Rohit Kumar, P. Ruth Rejoice, Mobi Mathew. Performance analysis of 100 k$W_p$ grid connected si-poly photovoltaic system using pvsyst simulation tool. *Energy Procedia*, pages 180–189, 2017.

[31] Patrick Donnelly-Shores. What does 'utility-scale solar' really mean?, July 2013.

[32] Priya Yadav, Nitin Kumar, S.S Chandel. Simulation and performance analysis of a 1kwp photovoltaic system using pvsyst, 2015. International Conference on Computation of Power, Energy, Information and Communication.

[33] Remus Teodorescu, Marco Liserre, Pedro Rodríguez. *Grid Converters for Photovoltaic and Wind Power Systems*. John Wiley Sons, Ltd, 2011.

[34] G. V. Research. Solar cell market analysis by product (silicon wafer, monocrystalline, multicrystalline, cadmium telluride, copper indium galium selenide, amorphous silica), and segment forecasts to 2022. Technical report, Grand View Research, 2016.

[35] Richard Perez, Robert Seals, Pierre Ineichen, Ronald Stewart, David Menicucci. A new simplified version of the perez diffuse irradiance model for tilted surfaces. *Solar Enegy*, 39(3):221–231, 1987.

[36] Rui Castro. Data-driven pv modules modelling: Comparison between equivalent electric circuit and artificial intelligence based models. *Sustainable Energy Technologies and Assessments*, 30: 230–238, Oct 2018.

[37] Sun-Hong Mina, Ohjoon Kwon, Matlabjon Sattorov, Hoechun Jung. Effects on electronics exposed to high-power microwaves on the basis of a relativistic backward-wave oscillator operating on the x-band. *Journal of Electromagnetic Waves and Applications*, Jun 2017.

[38] Tamas Kerekes, Eftichis Koutroulis, Dezso Sera, Remus Teodorescu, Markos Katsanevakis. An optimization method for designing large pv plants. *IEEE Journal of Photovoltaics*, 3(2):814–822, Apr 2013.

[39] A. E. Tutorials. Solar cell iv characteristic and solar cell iv curve, 2019.

[40] V. Tyagi, Nurul Rahim, N. Rahim, Jeyraj, Selvaraj. Progress in solar pv technology: Research and achievement. *Renewable Sustainable Energy Reviews*, 20(1):443–461, Jan 2013.

[41] A. Verma and S. Singhal. Solar pv performance parameter and recommendation for optimization of performance in large scale grid connected solar pv plant - case study. *J. Energy Power Sources*, 2(1):40–53, Jan 2015.

[42] W. Shockley. The theory of p-n junctions in semiconductors and p-n junction transistors. *Bell System Technical Journal*, pages 435–489, 1949.

# Appendix A

# Plant Restrictions

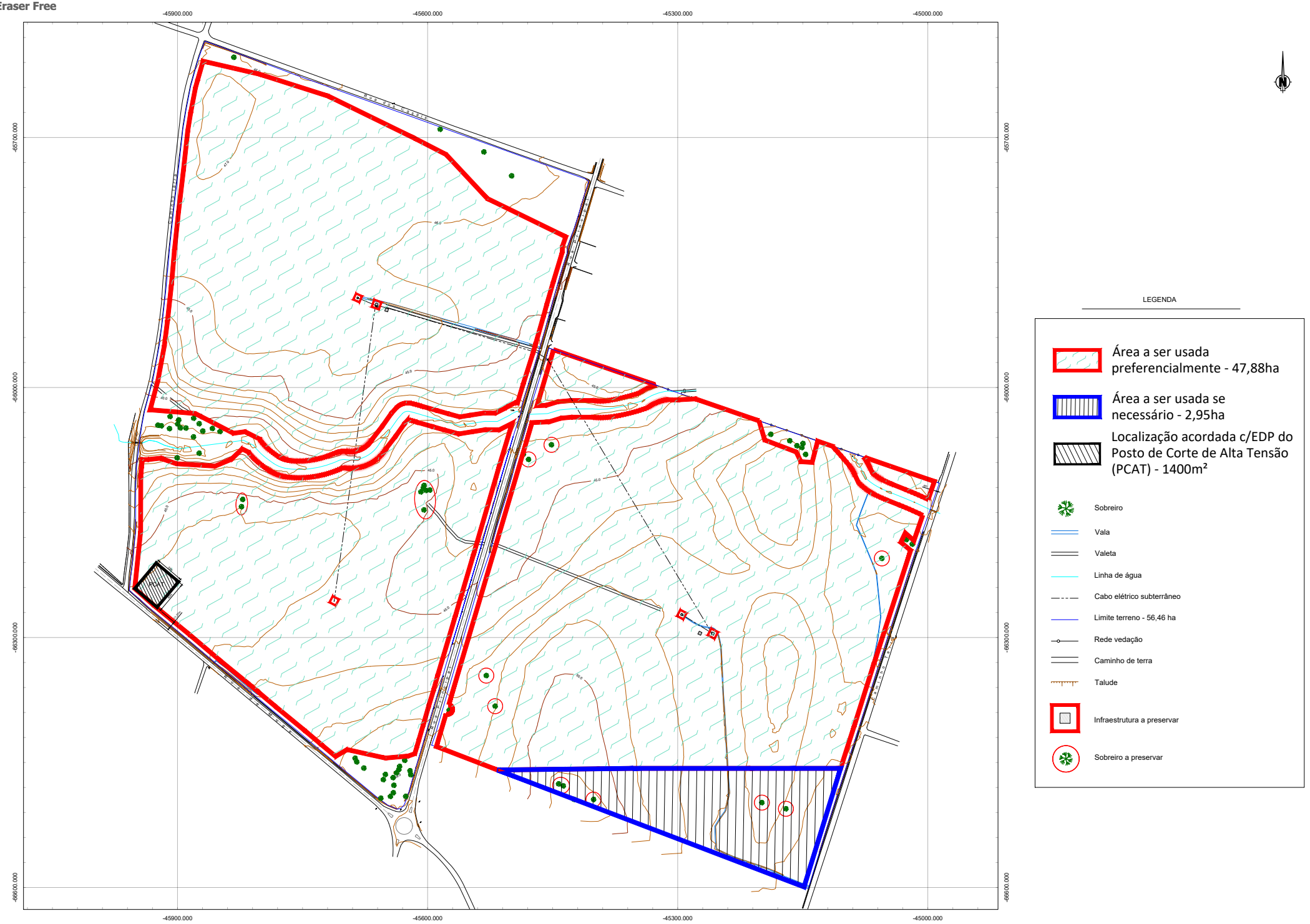

# Appendix B

# List of Modules and Inverters

Table B.1: List of central/string inverters

| Inverters | | | |
|---|---|---|---|
| | Manufacturer | Model | File PVSyst |
| Central | Sungrow | SG2500HV | Sungrow_SG2500HV.OND |
| | | SG2500 | Sungrow_SG2500.OND |
| | | SG3000HV | Sungrow_SG3000HV.OND |
| | SMA | Sunny Central 2500-EV | SMA_Central_2500.OND |
| | | Sunny Central 2750-EV | SMA_Central_2750.OND |
| | Siemens | Sinacon PV2500 | Siemens_Sinacon_PV2500.OND |
| | | Sinvert PVS 2520 US | Sinvert_PVS2520_60Hz.OND |
| | | Sinvert PVS 2520 | Sinvert_PVS2520_50Hz.OND |
| | | Sinacon PV3000 | Siemens_Sinacon_PV3000.OND |
| | | Sinacon PV3135 | Siemens_Sinacon_PV3135.OND |
| | | Sinacon PV3270 | Siemens_Sinacon_PV3270.OND |
| | | Sinacon PV3420 | Siemens_Sinacon_PV3420.OND |
| | | Sinacon PV3600 | Siemens_Sinacon_PV3600.OND |
| | | Sinacon PV3750 | Siemens_Sinacon_PV3750.OND |
| | | Sinacon PV4000 | Siemens_Sinacon_PV4000.OND |
| | | Sinacon PV4180 | Siemens_Sinacon_PV4180.OND |
| | | Sinacon PV4360 | Siemens_Sinacon_PV4360.OND |
| String | Huawei | SUN2000-105KTL-H1 | SUN2000-105KTL-H1 - (20180706).OND |
| | | SUN2000-185KTL-H1 | SUN2000-185KTL-H1-Preliminary-v0.1.OND |

Table B.2: List of modules

| Modules | | |
|---|---|---|
| Manufacturer | Model | File PVSyst |
| Hanwha Q Cells | Q.PLUS L-G4.2 345 | Hanwha_Qcells_QPLUS_L_G4_2_345.PAN |
| | Q.PLUS L-G4.2 350 | Hanwha_Qcells_QPLUS_L_G4_2_350.PAN |
| | Q.PEAK L-G4.2 360 | Hanwha_Qcells_QPEAK_L_G4_2_360.PAN |
| | Q.PEAK L-G4.2 365 | Hanwha_Qcells_QPEAK_L_G4_2_365.PAN |
| | Q.PEAK L-G4.2 370 | Hanwha_Qcells_QPEAK_L_G4_2_370.PAN |
| Open Renewables | Open 250-PQ60 | Open_Renewables_250-PQ60.PAN |
| | Open 255-PQ60 | Open_Renewables_255-PQ60.PAN |

# Appendix C

# Module and Inverters' Data Sheets

## MECHANICAL SPECIFICATION

| | |
|---|---|
| **Format** | 1960 mm × 991 mm × 35 mm (including frame) |
| **Weight** | 22.5 kg ±5 % |
| **Front Cover** | 3.2 mm thermally pre-stressed glass with anti-reflection technology |
| **Back Cover** | Composite film |
| **Frame** | Anodised aluminium |
| **Cell** | 6 × 12 monocrystalline Q.ANTUM solar cells |
| **Junction box** | 66-77 × 90-115 × 15-20 mm, Protection class ≥ IP67, with bypass diodes |
| **Cable** | 4 mm² Solar cable; (+) ≥ 1200 mm, (–) ≥ 1200 mm |
| **Connector** | HQC4, IP68 |

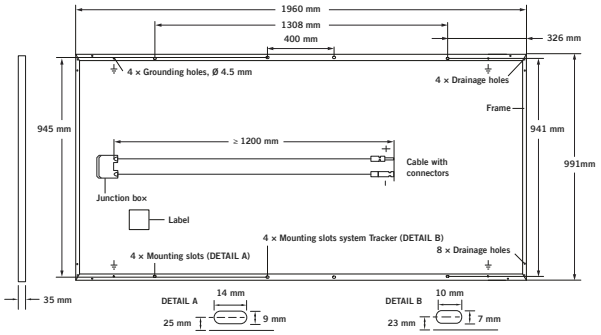


## ELECTRICAL CHARACTERISTICS

| POWER CLASS | | | 355 | 360 | 365 | 370 |
|---|---|---|---|---|---|---|
| **MINIMUM PERFORMANCE AT STANDARD TEST CONDITIONS, STC[1] (POWER TOLERANCE +5 W / –0 W)** | | | | | | |
| Minimum | Power at MPP[2] | $P_{MPP}$ | 355 | 360 | 365 | 370 |
| | Short Circuit Current* | $I_{SC}$ | 9.63 | 9.69 | 9.75 | 9.81 |
| | Open Circuit Voltage* | $V_{OC}$ | 47.58 | 47.87 | 48.16 | 48.45 |
| | Current at MPP* | $I_{MPP}$ | 9.12 | 9.19 | 9.27 | 9.35 |
| | Voltage at MPP* | $V_{MPP}$ | 38.94 | 39.16 | 39.38 | 39.59 |
| | Efficiency[2] | η | ≥ 18.3 | ≥ 18.5 | ≥ 18.8 | ≥ 19.0 |
| **MINIMUM PERFORMANCE AT NORMAL OPERATING CONDITIONS, NOC[3]** | | | | | | |
| Minimum | Power at MPP[2] | $P_{MPP}$ | 262.7 | 266.4 | 270.1 | 273.8 |
| | Short Circuit Current* | $I_{SC}$ | 7.77 | 7.81 | 7.86 | 7.91 |
| | Open Circuit Voltage* | $V_{OC}$ | 44.51 | 44.78 | 45.05 | 45.32 |
| | Current at MPP* | $I_{MPP}$ | 7.16 | 7.23 | 7.29 | 7.36 |
| | Voltage at MPP* | $V_{MPP}$ | 36.68 | 36.86 | 37.04 | 37.22 |

[1] 1000 W/m², 25 °C, spectrum AM 1.5 G  [2] Measurement tolerances STC ±3%; NOC ±5%  [3] 800 W/m², NOCT, spectrum AM 1.5 G  * typical values, actual values may differ

### Q CELLS PERFORMANCE WARRANTY

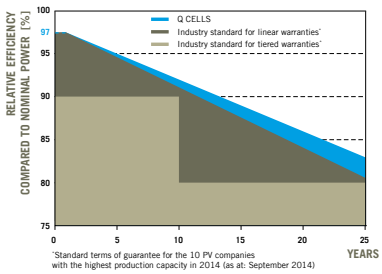


At least 97 % of nominal power during first year. Thereafter max. 0.6 % degradation per year.
At least 92 % of nominal power up to 10 years.
At least 83 % of nominal power up to 25 years.

All data within measurement tolerances. Full warranties in accordance with the warranty terms of the Q CELLS sales organisation of your respective country.

### PERFORMANCE AT LOW IRRADIANCE

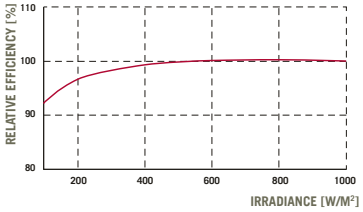


Typical module performance under low irradiance conditions in comparison to STC conditions (25 °C, 1000 W/m²).

### TEMPERATURE COEFFICIENTS

| | | | | | | | |
|---|---|---|---|---|---|---|---|
| **Temperature Coefficient of $I_{SC}$** | α | [%/K] | +0.04 | **Temperature Coefficient of $V_{OC}$** | β | [%/K] | –0.28 |
| **Temperature Coefficient of $P_{MPP}$** | γ | [%/K] | –0.39 | **Normal Operating Cell Temperature** | NOCT | [°C] | 45 ±3 |

## PROPERTIES FOR SYSTEM DESIGN

| | | | | | |
|---|---|---|---|---|---|
| **Maximum System Voltage** | $V_{SYS}$ | [V] | 1500 | **Safety Class** | II |
| **Maximum Reverse Current** | $I_R$ | [A] | 20 | **Fire Rating** | C / TYPE 1 |
| **Push/Pull Load (in accordance with IEC 61215)** | | [Pa] | 5400 / 2400 | **Permitted Module Temperature On Continuous Duty** | –40 °C up to +85 °C |

## QUALIFICATIONS AND CERTIFICATES

IEC 61215 (Ed. 2); IEC 61730 (Ed. 1), Application class A
This data sheet complies with DIN EN 50380.

## PACKAGING INFORMATION

| | |
|---|---|
| **Number of Modules per Pallet** | 30 |
| **Number of Pallets per 40' High Cube Container** | 22 |
| **Number of Modules per 40' High Cube Container** | 660 |

**NOTE:** Installation instructions must be followed. See the installation and operating manual or contact our technical service department for further information on approved installation and use of this product.

**Made in China**

**Hanwha Q CELLS Australia Pty Ltd**
Suite 1, Level 1, 15 Blue Street, Sydney, NSW 2060, Australia | **TEL** +61 (2) 9016 3033 | **FAX** +61 (0)2 9455 0873 | **EMAIL** q-cells-australia@q-cells.com | **WEB** www.q-cells.com/au



Engineered in **Germany**

# SG2500HV-MV-20

| Input (DC) | SG2500HV-MV-20 |
|---|---|
| Max. PV input voltage | 1500V |
| Min. PV input voltage / Startup input voltage | 800 V / 840 V |
| MPP voltage range for nominal power | 800 – 1300 V |
| No. of independent MPP inputs | 1 |
| No. of DC inputs | 18 |
| Max. PV input current | 3508 A |
| Max. DC short-circuit current | 4210 A |
| PV array configuration | Negative grounding or floating |

| Output (AC) | |
|---|---|
| AC output power | 2750 kVA@ 45 ˚C / 2500 kVA@ 50 ˚C |
| Max. inverter output current | 2886 A |
| AC voltage range | 10 – 35 kV |
| Nominal grid frequency / Grid frequency range | 50 Hz / 45 – 55 Hz, 60 Hz / 55 – 65 Hz |
| THD | < 3 % (at nominal power) |
| DC current injection | < 0.5 % In |
| Power factor at nominal power / Adjustable power factor | > 0.99 / 0.8 leading to 0.8 lagging |
| Feed-in phases / Connection phases | 3 / 3 |

| Efficiency | |
|---|---|
| Inverter max. efficiency / Inverter Euro. efficiency | 99.0 % / 98.7 % |

| Transformer | |
|---|---|
| Transformer rated power | 2500 kVA |
| Transformer max. power | 2750 kVA |
| LV / MV voltage | 0.55 kV / 10 – 35 kV |
| Transformer vector | Dy11 |
| Transformer cooling type | ONAN (Oil Natural Air Natural) |
| Oil type | Mineral oil (PCB free) or degradable oil on request |

| Protection | |
|---|---|
| DC input protection | Load break switch + fuse |
| Inverter output protection | Circuit breaker |
| AC MV output protection | Circuit breaker |
| Overvoltage protection | DC Type I+II / AC Type II |
| Grid monitoring / Ground fault monitoring | Yes / Yes |
| Insulation monitoring | Yes |
| Overheat protection | Yes |
| Nigtht SVG function | Yes |

| General Data | |
|---|---|
| Dimensions (W*H*D) | 6058*2896*2438 mm |
| Weight | 18 T |
| Degree of protection | IP54 |
| Auxiliary power supply | Optional: Max. 40 kVA |
| Operating ambient temperature range | -35 to 60 ℃ (> 50 ℃ derating) |
| Allowable relative humidity range (non-condensing) | 0 – 95 % |
| Cooling method | Temperature controlled forced air cooling |
| Max. operating altitude | 1000 m (standard) / > 1000 m (optional) |
| Display | Touch screen |
| Communication | Standard: RS485, Ethernet; Optional: optical fiber |
| Compliance | CE, IEC 62109, IEC 61727, IEC 62116 |
| Grid support | Night SVG function , L/HVRT, active & reactive power control and power ramp rate control |
| Type designation | SG2500HV-MV-20 |

# Smart String Inverter (SUN2000-105KTL-H1)

| Technical Specifications | SUN2000-105KTL-H1 |
|---|---|
| | **Efficiency** |
| Max. Efficiency | 99.0% |
| European Efficiency | 98.8% |
| | **Input** |
| Max. Input Voltage | 1,500 V |
| Max. Current per MPPT | 25 A |
| Max. Short Circuit Current per MPPT | 33 A |
| Start Voltage | 650 V |
| MPPT Operating Voltage Range | 600 V ~ 1,500 V |
| Rated Input Voltage | 1,080 V |
| Number of Inputs | 12 |
| Number of MPP Trackers | 6 |
| | **Output** |
| Rated AC Active Power | 105,000 W @40°C |
| Max. AC Apparent Power | 116,000 VA @25°C |
| Max. AC Active Power (cosϕ=1) | 116,000 W @25°C |
| Rated Output Voltage | 800 V, 3W + PE |
| Rated AC Grid Frequency | 50 Hz / 60 Hz |
| Rated Output Current | 75.8 A |
| Max. Output Current | 84.6 A |
| Adjustable Power Factor Range | 0.8 LG ... 0.8 LD |
| Max. Total Harmonic Distortion | < 3% |
| | **Protection** |
| Input-side Disconnection Device | Yes |
| Anti-islanding Protection | Yes |
| AC Overcurrent Protection | Yes |
| DC Reverse-polarity Protection | Yes |
| PV-array String Fault Monitoring | Yes |
| DC Surge Arrester | Type II |
| AC Surge Arrester | Type II |
| DC Insulation Resistance Detection | Yes |
| Residual Current Monitoring Unit | Yes |
| | **Communication** |
| Display | LED Indicators, Bluetooth + APP |
| RS485 | Yes |
| USB | Yes |
| Power Line Communication (PLC) | Yes |
| | **General** |
| Dimensions (W x H x D) | 1,075 x 605 x 310 mm (42.3 x 23.8 x 12.2 inch) |
| Weight (with mounting plate) | 79 kg (174.2 lb.) |
| Operating Temperature Range | -25°C ~ 60°C (-13°F ~ 140°F) |
| Cooling Method | Natural Convection |
| Max. Operating Altitude | 4,000 m (13,123 ft.) |
| Relative Humidity | 0 ~ 100% |
| DC Connector | Amphenol UTX |
| AC Connector | Waterproof PG Terminal + Terminal Clamps |
| Protection Degree | IP65 |
| Topology | Transformerless |

## Efficiency Curve

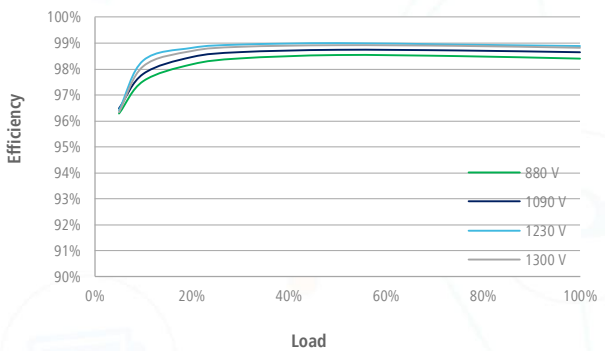


## Circuit Diagram

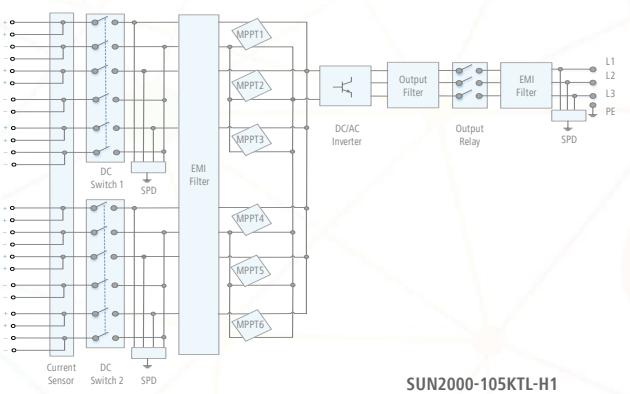


SUN2000-105KTL-H1

# Smart String Inverter (SUN2000-185KTL-H1) – Preliminary Version

| Technical Specifications | SUN2000-185KTL-H1 |
|---|---|
| | **Efficiency** |
| Max. Efficiency | 99.0% |
| European Efficiency | 98.6% |
| | **Input** |
| Max. Input Voltage | 1,500 V |
| Max. Current per MPPT | 26 A |
| Max. Short Circuit Current per MPPT | 40 A |
| Start Voltage | 550 V |
| MPPT Operating Voltage Range | 500 V ~ 1,500 V |
| Nominal Input Voltage | 1,080 V |
| Number of Inputs | 18 |
| Number of MPP Trackers | 9 |
| | **Output** |
| Nominal AC Active Power | 175,000 W @40°C, 168,000 W @45°C, 150,000 W @50°C |
| Max. AC Apparent Power | 185,000 VA |
| Max. AC Active Power (cosϕ=1) | 185,000 W |
| Nominal Output Voltage | 800 V, 3W + PE |
| AC Grid Frequency | 50 Hz / 60 Hz |
| Nominal Output Current | 126.3 A @40°C, 121.3 A @45°C, 108.3 A @50°C |
| Max. Output Current | 134.9 A |
| Adjustable Power Factor Range | 0.8 LG ... 0.8 LD |
| Max. Total Harmonic Distortion | < 3% |
| | **Protection** |
| Input-side Disconnection Device | Yes |
| Anti-islanding Protection | Yes |
| AC Overcurrent Protection | Yes |
| DC Reverse-polarity Protection | Yes |
| PV-array String Fault Monitoring | Yes |
| DC Surge Arrester | Type II |
| AC Surge Arrester | Type II |
| Insulation Detection | Yes |
| Residual Current Monitoring Unit | Yes |
| | **Communication** |
| Display | LED Indicators, Bluetooth + APP |
| RS485 | Yes |
| USB | Yes |
| MBUS | Yes |
| | **General** |
| Dimensions (W x H x D) | 1,035 x 700 x 365 mm (40.7 x 27.6 x 14.4 inch) |
| Weight (with mounting plate) | 84 kg (185.2 lb.) |
| Operating Temperature Range | -25°C ~ 60°C (-13°F ~ 140°F) |
| Cooling Method | Smart Air Cooling |
| Max. Operating Altitude without Derating | 4,000 m (13,123 ft.) |
| Relative Humidity | 0 ~ 100% |
| DC Connector | MC4 EVO2 |
| AC Connector | OT Connector |
| Protection Degree | IP65 |
| Topology | Transformerless |

## Efficiency Curve

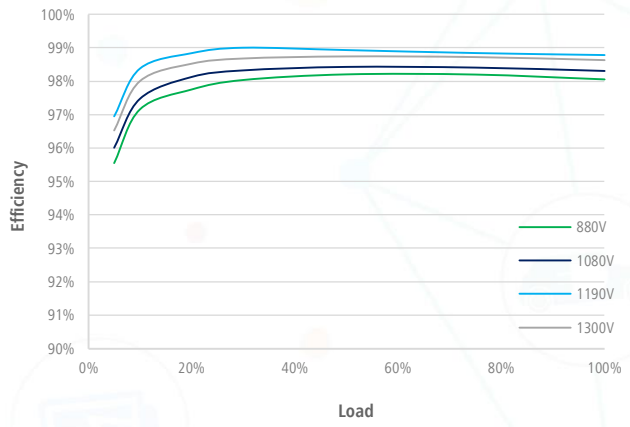


## Circuit Diagram

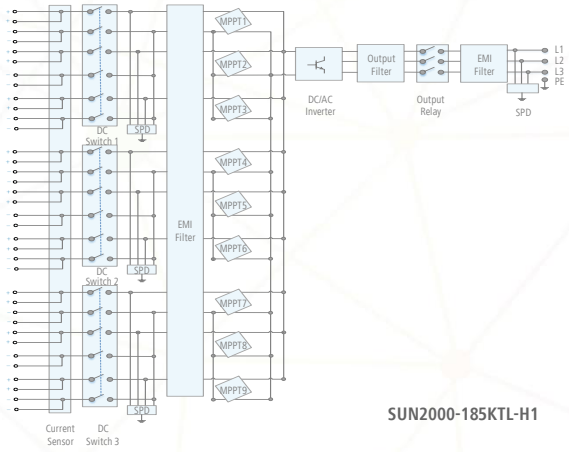


SUN2000-185KTL-H1

# Appendix D

# Electrical Schematic

# Central Inverter

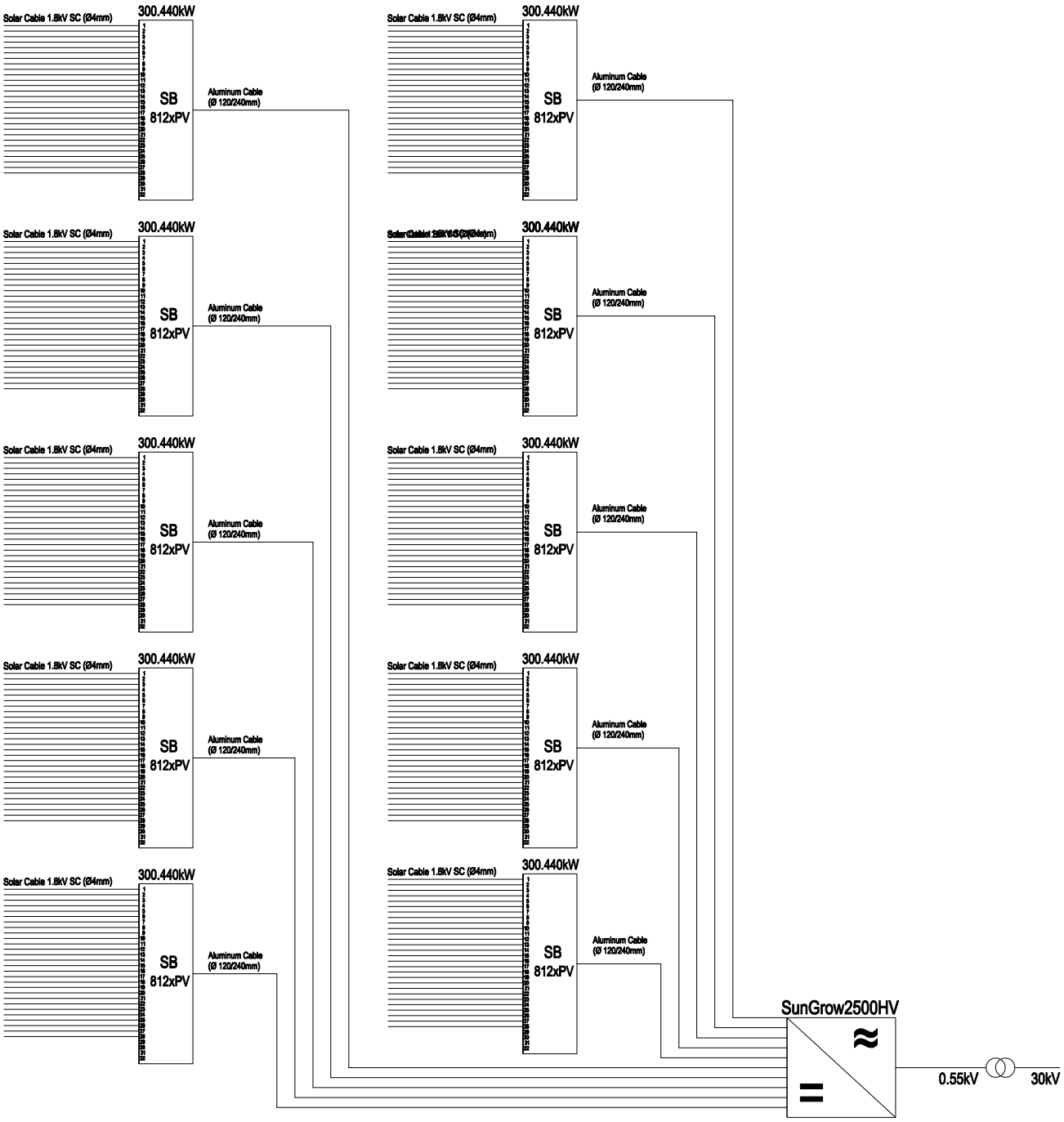

# String Inverter SUN2000-KTL105

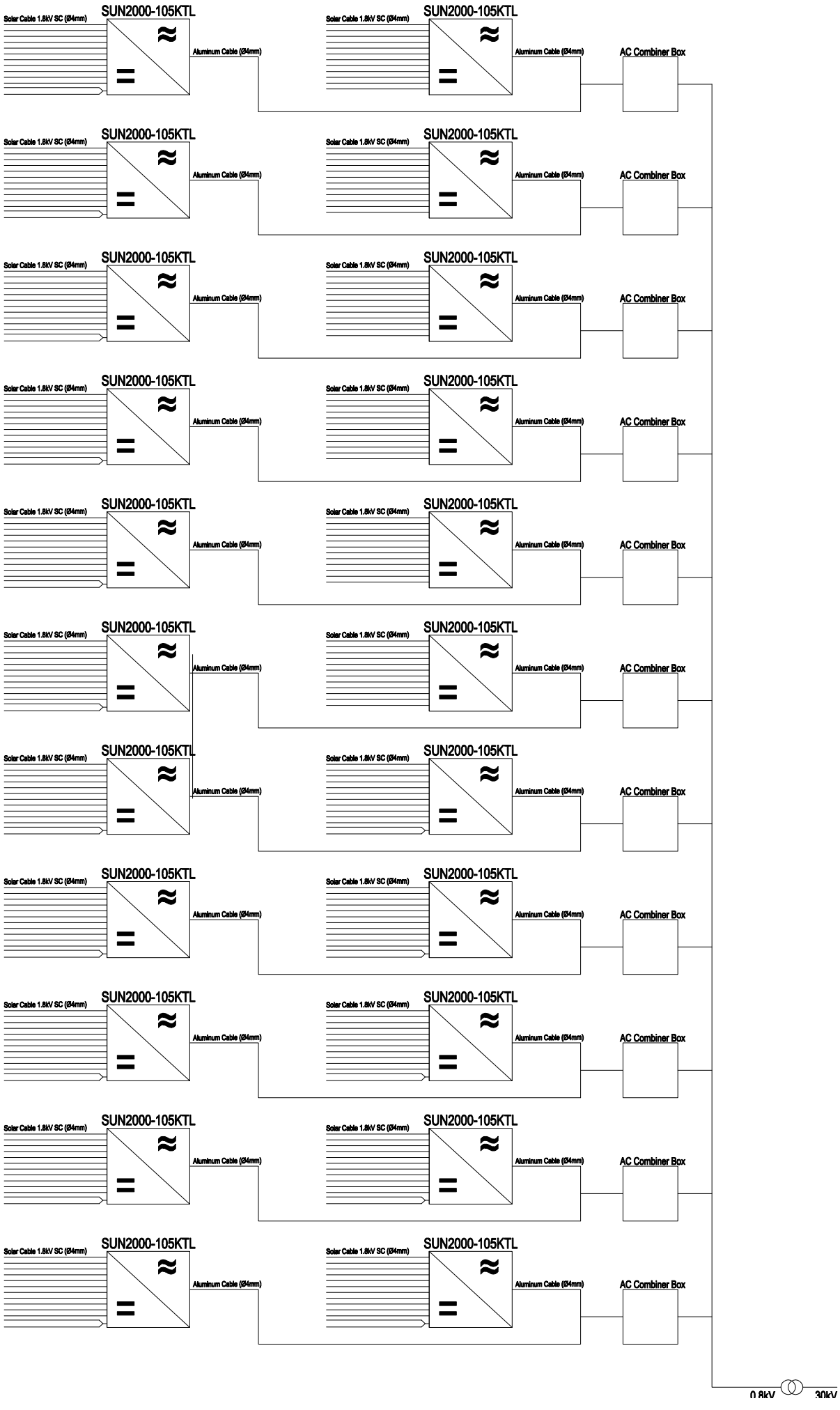

# String Inverter SUN2000-KTL185

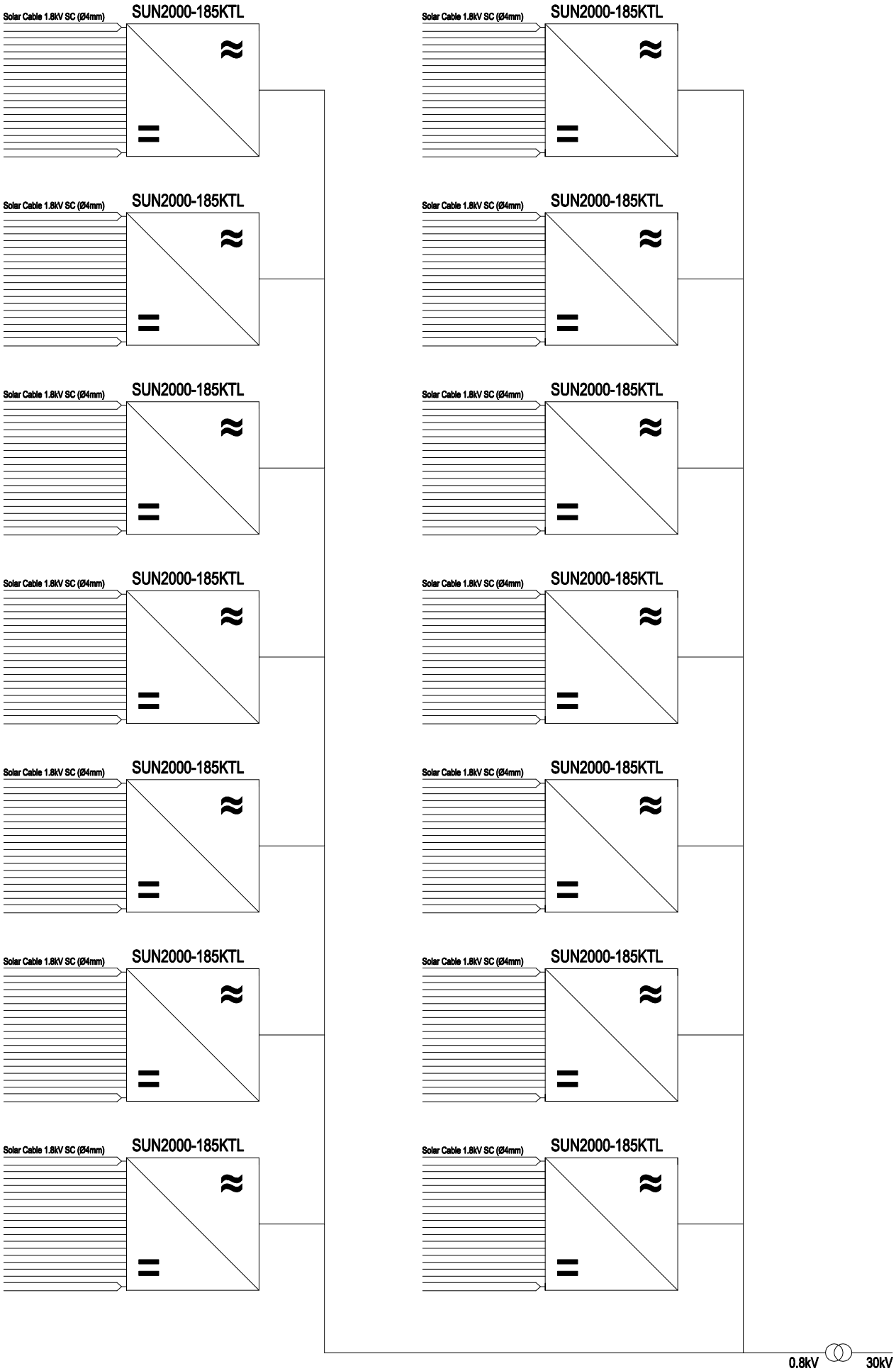

# Appendix E

# Cables' Sizing and Prices

Table E.1: Cables' sizing (Central Inverter)

| | Central Inverter | Landscape | Portrait |
|---|---|---|---|
| String Cable - Copper | String cable max. current (A) | 12.26 | 12.26 |
| | String length (m) | 60 | 45 |
| | Avg. distance from the string to the SB (m) | 50 | 50 |
| | String avg. cable length (m) | 110 | 95 |
| | Total string cable/sub-array (m) | 30,736 | 26,536 |
| | System total string cable (m) | **245,891** | **212,291** |
| | String power (W) | 10,730 | 10,730 |
| | String voltage (V) | 1148.11 | 1148.11 |
| | String current (A) | 9.35 | 9.35 |
| | Cross-sectional area ($mm^2$) | 3,19 | 2,76 |
| | Available cable cross-sectional area ($mm^2$) | 4 | 4 |
| | Power line losses/SB (W) | 2399.15 | 2071.32 |
| Main DC Cable - Aluminum | Short circuit current/SB (A) | 274.68 | |
| | Cable maximum current (A) | 343.35 | |
| | DC Cable length (m) | Varies - Table E.2 | |
| | Inverter total input power (W) | 3,004,400 | |
| | Stringbox output power (W) | 300,440 | |
| | Inverter DC input voltage (V) | 1148.11 | |
| | Stringbox output current (A) | 261.8 | |
| | Inverter output voltage (V) | 550 | |
| | Cross-sectional area ($mm^2$) | Varies - Table E.2 | |
| | Available cable cross-sectional area ($mm^2$) | Table E.2 | |
| AC Cable - Aluminum | Inverter output current (A) | 5462.5 | |
| | Inverter input current (A) | 2618 | |
| | AC Cable length (m) | Varies - Table E.3 | |
| | Cross-sectional area ($mm^2$) | Varies - Table E.3 | |
| | Available cable cross-sectional area ($mm^2$) | Table E.3 | |
| | Power factor | 0.95 | |

Table E.2: Main DC cables' sizing and prices (Central Inverter)

| Main DC cable (One sub-array) - Stringbox to inverter | | | | | |
|---|---|---|---|---|---|
| Stringbox | Length (m) | Section ($mm^2$) | Cable ($mm^2$) | Price (€/m) | Price (€) |
| 1 | 16.2 | 21.91 | 120 | 2.16 | 35 |
| 2 | 46 | 62.23 | 120 | 2.16 | 99.4 |
| 3 | 55 | 74.40 | 120 | 2.16 | 118.8 |
| 4 | 75 | 101.46 | 120 | 2.16 | 162 |
| 5 | 123 | 166.39 | 240 | 3.42 | 420.7 |
| 6 | 123 | 166.39 | 240 | 3.42 | 420.7 |
| 7 | 167 | 225.91 | 240 | 3.42 | 571.1 |
| 8 | 256 | 346.3 | 240 | 3.42 | 875.5 |
| 9 | 293 | 396.35 | 240 | 3.42 | 1002.1 |
| 10 | 341 | 461.28 | 240 | 3.42 | 1166.2 |
| Total | 1495.2 | | | Total cost | 4871.4 |

Table E.3: Low voltage AC cables' sizing and prices (Central Inverter)

| LV AC cable length (One sub-array) - Inverter to transformer station | | | | | |
|---|---|---|---|---|---|
| Inverter | Length (m) | Section ($mm^2$) | Cable ($mm^2$) | Price (€/m) | Price (€) |
| 1 | 10 | 240.33 | 240 | 27.58 | 275.8 |
| 2 | 10 | 240.33 | 240 | 27.58 | 275.8 |
| 3 | 10 | 240.33 | 240 | 27.58 | 275.8 |
| 4 | 10 | 240.33 | 240 | 27.58 | 275.8 |
| 5 | 10 | 240.33 | 240 | 27.58 | 275.8 |
| 6 | 10 | 240.33 | 240 | 27.58 | 275.8 |
| 7 | 10 | 240.33 | 240 | 27.58 | 275.8 |
| 8 | 10 | 240.33 | 240 | 27.58 | 275.8 |
| Total | 80 | | | Total cost | 2206.4 |

Table E.4: Cables' sizing (String Inverter SUN2000-105KTL)

| String Inverter SUN2000-105KTL | | Landscape | Portrait |
|---|---|---|---|
| String Cable - Copper | String cable current (A) | 12.26 | 12.26 |
| | String length (m) | 59.5 | 45 |
| | Avg. distance from the string to the inverter (m) | 30.7 | 30.7 |
| | String avg cable length (m) | 90.2 | 75.2 |
| | Total string cable/sub-array (m) | 25,247 | 21,047 |
| | System total string cable (m) | **201,973** | **168,373** |
| | String power (W) | 10,730 | 10,730 |
| | String voltage (V) | 1148.11 | 1148.11 |
| | String current (A) | 9.35 | 9.35 |
| | Cross-sectional area ($mm^2$) | 2.62 | 2.19 |
| | Available cable cross-sectional area ($mm^2$) | 4 | 4 |
| | Power line losses/SB (W) | 1970.65 | 1642.81 |
| AC Cable - Aluminum | Inverter max. output current (A) | 84.6 | |
| | Cable max. current (A) | 105.75 | |
| | AC Cable length (m) | **13.5** | |
| | Cable length/sub-array (m) | 297 | |
| | System total cable length (m) | 2376 | |
| | Inverter max. output power (W) | 105000 | |
| | Inverter output voltage (V) | 800 | |
| | Current (A) | 75.8 | |
| | Cross-sectional area ($mm^2$) | 3.10 | |
| | Available cable cross-sectional area ($mm^2$) | 4 | |
| | Power line losses (W) | 938.46 | |
| LV AC Cable - Aluminum | AC Combiner output current (A) | 151.6 | |
| | Maximum admissible current | 211.5 | |
| | AC Cable length (m) | Varies - Table E.5 | |
| | Cross-sectional area ($mm^2$) | Varies - Table E.5 | |
| | Available cable cross-sectional area ($mm^2$) | Table E.5 | |
| | Power factor | 0.95 | |

Table E.5: AC cables' sizing and prices (String Inverter SUN2000-105KTL)

| AC Cable length (One sub-array) - AC combiner to transformer station | | | | | |
|---|---|---|---|---|---|
| AC Combiner | Length (m) | Section ($mm^2$) | Available cable ($mm^2$) | Price (€/m) | Price (€) |
| 1 | 16 | 4.89 | 70 | 7.63 | 122.1 |
| 2 | 55 | 16.81 | 70 | 7.63 | 419.7 |
| 3 | 97 | 29.65 | 70 | 7.63 | 740.1 |
| 4 | 124 | 37.91 | 70 | 7.63 | 946.1 |
| 5 | 154 | 47.08 | 70 | 7.63 | 1175.0 |
| 6 | 188 | 57.47 | 70 | 7.63 | 1434.4 |
| 7 | 227 | 69.39 | 70 | 7.63 | 1732 |
| 8 | 266 | 81.32 | 120 | 13.26 | 3527.2 |
| 9 | 308 | 94.16 | 120 | 13.26 | 4084.1 |
| 10 | 338 | 103.33 | 120 | 13.26 | 4481.9 |
| 11 | 374 | 114.33 | 120 | 13.26 | 4959.2 |
| Total | 2147 | | | Total cost | 23621.8 |

Table E.6: Cables' sizing (String Inverter SUN2000-185KTL)

| String Inverter SUN2000-185KTL | | Landscape | Portrait |
|---|---|---|---|
| String Cable Sizing - Copper | String cable max. current (A) | 12.26 | 12.26 |
| | String length (m) | 60 | 45 |
| | Avg. distance from the string to the inverter (m) | 39.6 | 39.6 |
| | String avg. cable length (m) | 99 | 84 |
| | Total string cable/sub-array (m) | 27,748 | 23,548 |
| | System total string cable (m) | **221,984** | **188,384** |
| | String power (W) | 10,730 | 10,730 |
| | String voltage (V) | 1148.11 | 1148.11 |
| | String current (A) | 9.35 | 9.35 |
| | Cross-sectional area ($mm^2$) | 2.88 | 2.44 |
| | Available cable cross-sectional area ($mm^2$) | 4 | 4 |
| | Power line losses /SB (W) | 2165.89 | 1838.06 |
| LV AC Cable Sizing - Aluminum | Inverter max. output current (A) | 134.9 | |
| | Maximum admissible current (A) | 168.6 | |
| | Inverter max. output power (W) | 185000 | |
| | Inverter output voltage (V) | 800 | |
| | Current (A) | 121.3 | |
| | AC Cable length (m) | Varies - Table E.7 | |
| | Cross-sectional area ($mm^2$) | Varies - Table E.7 | |
| | Available cable cross-sectional area ($mm^2$) | Table E.7 | |
| | Power factor | 0.95 | |

Table E.7: AC cables' sizing and prices (String Inverter SUN2000-185KTL)

| AC Cable length (One sub-array) - Inverter to transformer station | | | | | |
|---|---|---|---|---|---|
| Inverter | Length (m) | Section ($mm^2$) | Available cable ($mm^2$) | Price (€/m) | Price (€) |
| 1 | 10 | 2.45 | 70 | 7.63 | 76.3 |
| 2 | 39 | 9.54 | 70 | 7.63 | 297.6 |
| 3 | 72,7 | 17.78 | 70 | 7.63 | 554.7 |
| 4 | 93.6 | 22.89 | 70 | 7.63 | 714.2 |
| 5 | 120.97 | 29.59 | 70 | 7.63 | 923 |
| 6 | 139 | 34 | 70 | 7.63 | 1060,6 |
| 7 | 175 | 42.80 | 70 | 7.63 | 1335.3 |
| 8 | 197.3 | 48.26 | 70 | 7,63 | 1505.4 |
| 9 | 244.5 | 59.80 | 70 | 7.63 | 1865,5 |
| 10 | 258.9 | 63.33 | 70 | 7.63 | 1975.4 |
| 11 | 297 | 72.65 | 120 | 13.26 | 3938.2 |
| 12 | 324.5 | 79.37 | 120 | 13,26 | 4302.9 |
| 13 | 359 | 87.81 | 120 | 13.26 | 4760.3 |
| 14 | 385.2 | 94.22 | 120 | 13.26 | 5107.8 |
| Total | 2716.67 | | | Total cost | 28417.1 |